Physics – Uspekhi **57** (5) 421 – 452 (2014)

REVIEWS OF TOPICAL PROBLEMS PACS numbers: 47.27.E –, 47.27.ep, 47.27.Gs, 52.35.Ra, 52.65.Kj

Subgrid-scale modeling for the study of compressible magnetohydrodynamic turbulence in space plasmas

A A Chernyshov, K V Karelsky, A S Petrosyan

DOI: 10.3367/UFNe.0184.201405a.0457

Contents

Abstract. A state-of-the-art review is given of research by computing physics methods on compressible magnetohydrodynamic turbulence in space plasmas. The presence of magnetic fields and compressibility in this case makes space plasma turbulence much less amenable to direct numerical simulations than a neutral incompressible fluid. The large eddy simulation method is discussed, which was developed as an alternative to direct modeling and which filters the initial magnetohydrodynamic equations and uses the subgrid-scale modeling of universal small-scale turbulence. A detailed analysis is made of both the method itself and different subgrid-scale parametrizations for compressible magnetohydrodynamic turbulent flows in polytropic and heat-conducting plasmas. The application of subgrid-scale modeling to study turbulence in the local interstellar medium and the scale-invariant spectra of magnetohydrodynamic turbulence are discussed.

A A Chernyshov, K V Karelsky Space Research Institute, Russian Academy of Sciences, ul. Profsoyuznaya 84/32, 117997 Moscow, Russian Federation
E-mail: achernyshov@iki.rssi.ru, kkarelsk@iki.rssi.ru
A S Petrosyan Space Research Institute, Russian Academy of Sciences, ul. Profsoyuznaya 84/32, 117997 Moscow, Russian Federation; Moscow Institute of Physics and Technology (State University), Institutskii per. 9, 141700 Dolgoprudnyi, Moscow region, Russian Federation
E-mail: apetrosy@iki.rssi.ru

Received 28 March 2013, revised 13 September 2013
Uspekhi Fizicheskikh Nauk **184** (5) 457 – 492 (2014)
DOI: 10.3367/UFNr.0184.201405a.0457
Translated by K A Postnov; edited by A Radzig

1. Introduction

Compressible magnetohydrodynamic (MHD) turbulence is a widespread state of space plasma in a variety of astrophysical, heliophysical, and geophysical processes. For example, MHD turbulence in accretion disks originates from a magnetorotational instability (MRI) [1–3]. Stellar clouds are formed due to magnetic field effects and gravitation under turbulent conditions [4–6]. The dynamics of the interstellar and interplanetary medium are also turbulent in character [7–9]. Most turbulent phenomena in solar physics are described by MHD equations, including the solar wind, solar corona expansion, convective zone, photosphere, and solar tachocline [10–14]. Turbulent phenomena are observed in the near-Earth space both in the solar wind and in different zones of Earth's magnetosphere. In particular, properties of space plasma probed by satellites in the geomagnetic tail region can be adequately explained only in the framework of turbulence theory and models [15–19]. MHD turbulence plays an important role in originating the dynamo processes and space magnetic field generation [20–24]. Turbulent flows in the magnetic field are also widespread in applied fields. Engineering applications include the possibility of controling the boundary layer and a flow resistance decrease [25, 26], as

well as MHD flows in channels [27] in the processes of steel casting and in tubes for thermonuclear reactor cooling [28].

The turbulence originates from an instability of the initial state of space plasmas. The instability enhances the amplitude of oscillations in electrically conducting plasma to the nonlinear level, where complex processes of interaction and mutual transformation of the oscillations become significant. At large flow velocities, i.e., at large Reynolds numbers Re (Re characterizes the relation between the inertial and viscous forces), the flow becomes unstable and fragments into large-scale eddies. Nonlinear interaction between the eddies leads to their permanent splitting down to small scales at which viscous damping due to molecular viscosity comes into prominence. The scale fragmentation of eddies corresponds to turbulent motion energy transfer from the long-wave to short-wave parts of the spectrum. As a result, irregular eddies of different sizes emerge in the flow, and the flow velocity at each point changes chaotically. The most important feature of the space turbulence is the presence of random magnetic fields along with random velocity variations. In such flows, the nonlinearity, viscosity, diffusion, anisotropy, and compressibility effects play a significant part. The turbulence is three-dimensional; therefore, the numerical modeling of the compressible MHD turbulence is an important tool for the study of charged fluid in such MHD flows. In addition, space plasma, as a rule, cannot be directly probed in experiments.

Developing efficient numerical methods and enhancing modern computational capacity, which allow MHD simulations of compressible turbulent flows with realistic similarity numbers, are important tasks for computational physics. These simulations are extremely important for understanding the complicated physics, especially when the object studied is beyond direct experimental reach. Notice that MHD problems are differed from those of neutral fluid dynamics. MHD equations contain two fields that introduce many more degrees of freedom into the system's dynamics; for example, both direct and inverse spectral cascades are possible [29]. Additionally, self-organization processes emerge in MHD turbulence that have no analogs in usual hydrodynamics, namely, cross-helicity conservation [30], which leads to the appearance of a high correlation between the magnetic field and the flow velocity, whereas conservation of the magnetic helicity may result in the formation of force-free magnetic configurations [31].

Direct numerical simulations (DNSs) provide the most complete information on turbulent flows in a fluid [32]. DNS approach assumes a numerical solution to the complete system of nonstationary MHD equations. This approach resolves all scales of the charged fluid motion. DNSs do not require a special closure of MHD equations. Direct numerical calculations of MHD turbulence encounter fundamental difficulties caused by large hydrodynamic and magnetic Reynolds numbers, which are typical of space plasmas. In this case, the number of degrees of freedom of the turbulent motion is high, and, consequently, the minimal number of nodes on the numerical grid must be restrictively large for direct numerical simulations of realistic turbulent flows with high Reynolds numbers.

The statistical approach to studying turbulent flows [33] based on averaging the equations of motion (RANS — Reynolds averaged Navier–Stokes) is an alternative to direct numerical simulations. In the RANS method, all parameters of the fluid motion are resolved into the mean and turbulent

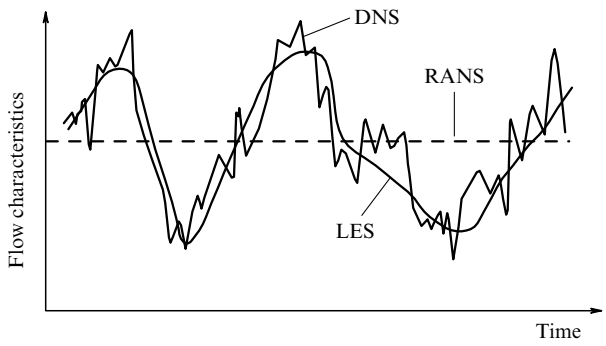

Figure 1. Comparison of DNS, RANS, and LES calculated results.

components. Reynolds stresses therewith arise in the equations of motion that need to be closed. Thus, all the turbulence is modeled (for example, in the $k-\varepsilon$ model [34]) and not calculated, as in the DNS method. The RANS method is commonly applied for theoretical studies of averaged flows [35]. This approach does not contain information about the turbulence dynamics.

The large eddy simulation (LES) method describes the approximate turbulence dynamics, in which the large-scale part of the turbulent flow is directly calculated, while the small-scale part of the flow is modeled, i.e., LES is the intermediate approach for turbulence studies between DNS and RANS. This is illustrated in Fig. 1 which shows the differences between the three methods of calculations used in turbulence studies.

The LES method invokes a filtering operation to resolve the turbulent motion characteristic into the large-scale and small-scale parts, which is related to isotropy, homogeneity, and the universality of small scales of the turbulent motion. Small-scale motions are eliminated from the original system of equations by the filtering procedure, and later their influence on the motion is simulated using subgrid-scale (SGS) model (or, in other words, SFS — subfilter scale), expressed through the filtered parameters of turbulent flows. The large-scale turbulent flow is calculated by solving filtered nonstationary MHD equations. LES is commonly applied to model flows with high Reynolds numbers, since this method assumes that the energy is transferred from large scales to small scales only inside the inertial interval. As the number of degrees of freedom in LES is lower than in DNS, the former requires much less computational capacity than DNS.

Originally, the large eddy simulation method was developed to model flows of a neutral fluid [36–41] in meteorology and oceanology. Most of the simulations were conducted for incompressible fluids. For compressible media, however, LES is applied much more rarely due to the increased complexity of the problem, which requires solving an energy equation. In the filtered energy equation, several subgrid-scale additional terms simultaneously emerge that need to be parametrized. LES was first developed and used for a compressible neutral fluid by Speziale et al. [42]. In the early applications of LES to compressible flows, transport equations for the internal energy per unit mass [43, 44], pressure [45], or specific enthalpy [42, 46] were considered. Papers [47, 48] proposed using the total energy equation to close the system of hydrodynamic equations for a neutral compressible fluid, with some of the subgrid-scale terms being identical to those in the internal energy equation or enthalpy equation. Detailed

information on different subgrid-scale models of the large eddy simulation method for a compressible fluid can be found in Ref. [49]. The authors of this paper consider and test parametrizations for various forms of the energy equation: the internal energy, enthalpy, and total energy.

In electrically conducting plasma flows, the LES method has been applied and explored in extremely rare occasions. All previous studies of this topic mainly used the incompressible fluid approximation and treated engineering applications. Papers [50–55] invoked LES to study incompressible MHD turbulence, while paper [56] considered the effect of a magnetic field in the LES method on the flow of an incompressible electrically conducting fluid at low magnetic Reynolds numbers without use of the magnetic induction equation. In all the papers mentioned above, the system of equations for incompressible MHD turbulence was analyzed without employment of the energy equation.

Significant progress in studies of three-dimensional compressible MHD flows was achieved in a series of papers [57–68]. To close the system of MHD equations, either a polytropic (or adiabatic) process was assumed, or pressure was only treated as a passive scalar that provided the MHD turbulence incompressibility [57, 59–61, 63–68]. However, many plasma flows cannot be described by an incompressible medium approximation or by equations for compressible fluid in the polytropic approximation, and what is needed involves considering a heat-conducting fluid with the aid of the energy equation. The application of LES to a compressible heat-conducting MHD fluid is significantly complicated by the need to solve the energy equation in which terms due to the magnetic field appear. Furthermore, additional, fundamentally new subgrid-scale terms arise after the filtration, thus requiring a new theory for their parametrization [58, 59, 62, 65]. The study of the applicability of the various subgrid-scale models is mainly performed by comparing the LES and DNS results. As a rule, the comparison of modeled results is made for moderate values of the similarity parameters, which can still be directly calculated; here, the developed parametrizations of the subgrid-scale terms are assumed to correctly reproduce the turbulent flow for large similarity numbers as well.

Full nonlinear three-dimensional MHD equations including dissipation, thermal, diffusion, and compressibility effects are so complicated that they are amenable only to approximate numerical solution. However, as space MHD flows are characterized by large Reynolds numbers and Mach numbers are nonzero, studies of the compressible MHD turbulence are constrained by computational capacities and have been carried out in much rarer cases than for incompressible media. In such cases, therefore, one relies on simplified models ignoring some effects. For example, in ideal MHD flow simulations, one usually neglects dissipation and heat conductivity and assumes infinite plasma electrical conductivity [69]. Here, the system of MHD equations becomes hyperbolic and not parabolic, as for the dissipative system of equations, which facilitates numerical solutions, since it becomes possible to use the well-developed Godunov schemes of a different order of accuracy (as a result, the solution of the three-dimensional problem is reduced to solving a series of one-dimensional problems; numerical fluxes in each space direction are calculated from the corresponding one-dimensional Riemann problem for arbitrary discontinuity decay [70]).

Several studies use TVD (total variation diminishing), ENO/WENO (essentially nonoscillatory, weighted ENO) calculation schemes and schemes based on the minimal derivative value principle, etc., to solve the viscous compressible gas equations in the MHD case [71] by adding numerical viscous flows to the corresponding inviscid flows. However, this frequently violates the monotonicity of the difference scheme and can lead to incorrect results; usually, this approach is commonly applied to inviscid fluids. When using grids, such methods can also be considered as a large eddy simulation method with implicit filtering and numerical viscosity which can play the role of 'subgrid closure'. Sometimes, the anelastic approximation [72–74] is used in MHD simulations, when acoustic wave modes are assumed to be absent or stationary; however, such an approximation is mainly applied only for modeling convective zones in the Sun and stars. Frequently, the interstellar and interplanetary media, as well as the solar wind, are considered by assuming a polytropic (or adiabatic) relationship between the density and pressure to close the system of equations; in this case, the temperature of the process plays a secondary role, and the system of equations for compressible MHD turbulence is solved without the energy equation [9, 75–79]. Another simplification consists in the study of two-dimensional compressible MHD turbulence [80–83]. In papers [80, 81], the initial conditions for the velocity and magnetic field were taken in the form of a deterministic, nonrandom distribution (the so-called Orszag–Tang eddy [84, 85]); however, random distributions of the initial velocities and magnetic fields seem to be more appropriate for MHD simulations of space plasmas. The influence of the magnetic Reynolds number on two-dimensional MHD flows for different initial conditions is considered in more detail in paper [83]. Two-dimensional MHD turbulence is substantially different from three-dimensional turbulence, because the mean vorticity in a two-dimensional flow (ignoring the viscosity) is conserved, whereas the vortex tubes in a three-dimensional flow are deformed, and the vorticity is not an invariant of motion. In addition, turbulent dynamos and the generation of large-scale magnetic fields are only possible in the presence of three-dimensional MHD turbulence [86]. Sometimes, the plasma beta-parameter (the ratio of the plasma pressure to the magnetic field energy) is assumed in space flow studies so high that the magnetic field can be neglected; thus, the problem is reduced to the hydrodynamic one, and the system of equations for a neutral fluid motion is solved [87–89].

The study of compressible turbulence in the framework of both neutral fluid dynamics and magnetic hydrodynamics is a challenging problem, since there is no analytical or approximate theory of such phenomena. However, despite the significant role of the compressibility in space plasmas, a variety of observations suggest the Kolmogorov spectrum of density fluctuations [90, 91]. To interpret these observations, the last-cited two papers proposed a theory of a 'nearly incompressible' medium that describes density fluctuations of neutral [92] and magnetic [93] gases in the passive scalar transfer regime. In paper [88], the analytical theory for a compressible neutral gas was confirmed by direct numerical simulations only for the two-dimensional case. In paper [79], direct numerical modeling demonstrated that in compressible MHD turbulence there occurs a similar effect of decreasing the local turbulent Mach number from supersonic to subsonic values, which corresponds to the transformation of super-

sonic turbulence fluctuations to subsonic ones. However, the density and kinetic energy spectra were not obtained in that paper due to constraints of the direct numerical simulation method, and their coincidence and the realization of the passive regime for density in compressible MHD turbulence were not demonstrated. In spite of this fact, the authors of Ref. [79] utilized these results in interpreting data of satellite observations in the solar wind and the local interstellar medium.

Significant progress in understanding the local interstellar medium turbulence was achieved in papers [64, 94–96]. These papers reported on the density and energy fluctuation spectra, properties of plasma magnetization, and anisotropy, which were obtained for the first time from three-dimensional LES computations using MHD equations for compressible plasma.

In the present paper, we discuss the state-of-the-art of subgrid-scale simulation methods for studying compressible MHD turbulence of space plasmas; its layout is as follows. In Section 2, the large eddy simulation method, as applied to polytropic and heat-conducting plasmas, is formulated, filtered MHD equations for both cases are derived, and subgrid-scale tensors to be parametrized are analyzed in detail. In Section 3, we discuss various subgrid-scale models proposed for compressible MHD turbulence. We also discuss the prospects of the proposed models by comparing LES and DNS results. Applications of LES to some important problems of space physics, including turbulence in the local interstellar medium, are considered in Section 4. Section 5 is concerned with the investigation of scale-invariant spectra of compressible MHD turbulence in the inertial interval using a driving force. We discuss in detail different representations of the driving force to obtain the clearly determined inertial turbulence interval and analyze the advantages of the proposed linear driving force representation in studies of compressible MHD turbulence. In conclusion, we formulate the main results of the discussed line of investigation into computational physics of turbulent flows.

2. Large eddy simulation method for magnetohydrodynamic plasma flows

2.1 Magnetohydrodynamic equations for compressible plasma

The MHD equations were first considered by H Alfvén, who combined the Maxwell equations with equations of ordinary fluid dynamics. The governing system of equations for a compressible electrically conducting fluid is written out as follows:

continuity equation

$$\frac{\partial \rho}{\partial t} + \frac{\partial \rho u_j}{\partial x_j} = 0\,; \tag{1}$$

momentum equation

$$\frac{\partial \rho u_i}{\partial t} + \frac{\partial}{\partial x_j}(\rho u_i u_j + p\delta_{ij} - \sigma_{ij}) - \frac{1}{c}\,\varepsilon_{ijk}\, j_j B_k = 0\,; \tag{2}$$

energy equation

$$\frac{\partial \rho E}{\partial t} + \frac{\partial}{\partial x_j}\left[(\rho E + p)\, u_j + q_j - \sigma_{ij} u_i\right] - \Xi\, j = 0\,, \tag{3}$$

and *magnetic induction equation*

$$\frac{\partial B_i}{\partial t} = \varepsilon_{ijk}\,\frac{\partial}{\partial x_j}\,\varepsilon_{klm}(B_l u_m) + \eta\,\frac{\partial^2 B_i}{\partial x_j^2}\,, \tag{4}$$

$$\frac{\partial B_i}{\partial x_i} = 0\,. \tag{5}$$

Here, the following notations are utilized: ρ is the density; p is the pressure; u_j is the velocity component in the x_j direction; $\sigma_{ij} = 2\mu S_{ij} - (2/3)\mu S_{kk}\delta_{ij} + \zeta S_{kk}\delta_{ij}$ is the viscous stress tensor; $S_{ij} = (\partial u_i/\partial x_j + \partial u_j/\partial x_i)/2$ is the strain rate tensor; μ is the dynamical (molecular) viscosity coefficient; ζ is the volume viscosity coefficient; $p = \rho RT$ is the equation of state for an ideal gas, where R is the molar gas constant; $q_j = -\psi(\partial T/\partial x_j)$ is the dissipation due to heat conduction (the Fourier law), where ψ is the heat conductivity coefficient; $E = \epsilon + u_i u_i/2$ is the energy, including the internal energy $\epsilon = C_v T$ and kinetic energy $u_i u_i/2$, where C_v is the heat capacity at constant volume; $\eta = c^2/4\pi\sigma$ is the magnetic diffusion coefficient; σ is the electric conductivity; $F_l = (1/c)\varepsilon_{ijk}\, j_j B_k$ is the Lorentz force; B_j is the magnetic induction in the x_j direction; j is the electric current density; Ξ is the electric field strength; δ_{ij} is the Kronecker symbol, and ε_{ijk} is the Levi-Civita tensor.

Let us transform the system of MHD equations (1)–(5) using the Maxwell equations, and reduce it to the dimensionless form. The MHD approximation assumes that the electric field energy is much smaller than the magnetic field energy. In this case, all electromagnetic characteristics can be expressed through the magnetic field quantities. As a result, it is possible to consider and study only the interaction between the magnetic and hydrodynamic fields. To render equations dimensionless, the standard procedure of normalization to the characteristic values is used: u_0 — velocity, ρ_0 — density, L_0/U_0 — time, B_0 — magnetic field, p_0 — pressure, μ_0 — dynamic viscosity, η_0 — magnetic diffusion, ψ_0 — heat conductivity, and L_0 — length scale. Then it follows:

$$\frac{\partial \rho}{\partial t} + \frac{\partial \rho u_j}{\partial x_j} = 0\,, \tag{6}$$

$$\frac{\partial \rho u_i}{\partial t} + \frac{\partial}{\partial x_j}\left(\rho u_i u_j + p\delta_{ij} - \frac{1}{\mathrm{Re}}\,\sigma_{ij} + \frac{B^2}{2\mathrm{M}_\mathrm{a}^2}\,\delta_{ij} - \frac{1}{\mathrm{M}_\mathrm{a}^2}\,B_j B_i\right) = 0\,, \tag{7}$$

$$\frac{\partial B_i}{\partial t} + \frac{\partial}{\partial x_j}(u_j B_i - u_i B_j) - \frac{1}{\mathrm{Re}_\mathrm{m}}\,\frac{\partial^2 B_i}{\partial x_j^2} = 0\,, \tag{8}$$

$$\frac{\partial B_i}{\partial x_i} = 0\,, \tag{9}$$

$$\begin{aligned}\frac{\partial}{\partial t}\left(\rho E + \frac{B^2}{2\mathrm{M}_\mathrm{a}^2}\right) &+ \frac{\partial}{\partial x_j}\Bigg((\rho E + P)\,\tilde{u}_j \\ &+ \frac{1}{\mathrm{Pr}\,\mathrm{Re}\,\mathrm{M}_\mathrm{s}^2(\gamma - 1)}\,q_j - \frac{1}{\mathrm{Re}}\,\sigma_{ij} u_i - \frac{1}{\mathrm{M}_\mathrm{a}^2}\,B_j B_i u_i\Bigg) \\ &- \frac{\partial}{\partial x_j}\left[\frac{\eta}{\mathrm{Re}_\mathrm{m}\,\mathrm{M}_\mathrm{a}^2}\,B_i\left(\frac{\partial B_i}{\partial x_j} - \frac{\partial B_j}{\partial x_i}\right)\right] = 0\,.\end{aligned} \tag{10}$$

In equations (6)–(10), the following dimensionless similarity parameters are used [29]: $\mathrm{Re} = \rho_0 u_0 L_0/\mu_0$ is the hydrodynamic Reynolds number, $\mathrm{Re}_\mathrm{m} = u_0 L_0/\eta_0$ is the magnetic Reynolds number, $\mathrm{M}_\mathrm{s} = u_0/c_\mathrm{s}$ is the (acoustic) Mach number, and where c_s is the speed of sound defined as $c_\mathrm{s} = \sqrt{\gamma p_0/\rho_0}$, $\mathrm{M}_\mathrm{a} = u_0/u_\mathrm{a}$ is the magnetic (or Alfvén) Mach

number, where $u_a = B_0/\sqrt{4\pi\rho_0}$ is the Alfvén velocity, $\mathrm{Pr} = C_p\mu_0/\varphi_0$ is the Prandtl number, with C_p being the heat capacity at constant pressure.

2.2 Filtering of magnetic hydrodynamic equations in the large eddy simulation method

In the LES method, the original equations undergo filtering, as proposed in paper [97]. Each physical quantity is resolved into large-scale (filtered) and small-scale components. Then, the large-scale effects are directly computed, while small-scale effects are modeled. In other words, the information on turbulent structures with sizes smaller than the filter width is lost during the filtering operation, so, to close the filtered system of equations, various subgrid-scale models are utilized. To arrive at filtered equations of motion, filtering operators can be introduced in explicit and implicit forms. In the implicit approach, the filtering operator is represented by difference discretization, and in this case the filtering scales are smaller than the grid step [98]. Shortcomings of implicit filtering are related to difficulties in comparing the results obtained with direct numerical simulations and experimental data. Additionally, implicit filtering does not allow a control over the high-frequency spectral range, which may lead to numerical errors. Therefore, explicit filtering is preferable in the LES method.

For explicit filtering of MHD equations in the LES method one can invoke a low-pass filter ξ satisfying the normalization condition

$$\int_a^b \xi(x_j - \acute{x}_j, \bar{\Delta}_j)\,\mathrm{d}\acute{x}_j = 1\,. \tag{11}$$

Here, $\xi(x_j - \acute{x}_j, \bar{\Delta}_j)$ is the filter, and $\bar{\Delta}$ is the filter band. Then, for example, the filtered velocity is expressed as

$$\bar{u}_j = \int_a^b u(\acute{x}_j)\,\xi(x_j - \acute{x}_j, \bar{\Delta}_j)\,\mathrm{d}\acute{x}_j\,, \tag{12}$$

where $a = x_j - \bar{\Delta}_j/2$, $b = x_j + \bar{\Delta}_j/2$, $\bar{\Delta}_j = (\bar{\Delta}_x, \bar{\Delta}_y, \bar{\Delta}_z)$, and $x_j = (x, y, z)$ are the axes of a Cartesian coordinate system.

Other flow characteristics are determined in a similar way.

Let us represent all variables of the problem as the sum of filtered (corresponding to large scales) and unfiltered (corresponding to small scales) parts: $u = \bar{u} + u'$, $B = \bar{B} + B'$, $p = \bar{p} + p'$, etc.

Notice that, unlike statistical Reynolds averaging, this resolution possesses more complicated properties:

$$\begin{aligned} &\bar{\bar{f}} \neq \bar{f}, \\ &\bar{f}' \neq 0\,, \\ &\overline{\frac{\partial f}{\partial x_k}} = \frac{\partial \bar{f}}{\partial x_k}\,, \\ &\overline{\frac{\partial f}{\partial t}} = \frac{\partial \bar{f}}{\partial t}\,, \end{aligned} \tag{13}$$

where f is one of the characteristics of motion. The first two properties in formulas (13) are fundamentally different from those in the statistical approach [99].

To simplify equations describing turbulent MHD variable-density flows, it is convenient to utilize Favre filtering [100] (or density-weighted filter) in order to avoid the appearance of additional SGS terms. Density-weighted filtering is applied to all characteristics of the charged fluid flow but pressure and the magnetic field, and is defined as

$$\tilde{f} = \frac{\overline{\rho f}}{\bar{\rho}}\,. \tag{14}$$

To specify filtering operation, two symbols are used in formula (14): the bar corresponds to the usual filtering, and the tilde stands for the density-weighted filtering.

Thus, the Favre-filtered velocity takes the form

$$\tilde{u}_j = \frac{\overline{\rho u_j}}{\bar{\rho}} = \frac{\int_a^b \rho u_j\,\xi(x_j - \acute{x}_j, \bar{\Delta}_j)\,\mathrm{d}\acute{x}_j}{\int_a^b \rho(\acute{x}_j)\,\xi(x_j - \acute{x}_j, \bar{\Delta}_j)\,\mathrm{d}\acute{x}_j}\,. \tag{15}$$

Favre-averaged quantities can also be represented as a sum; for example, the velocity is written down as $u = \tilde{u} + u''$. Here, the double prime is used to denote the small-scale part of the Favre-filtered quantity.

The properties of the density-weighted filtering can then be expressed as follows:

$$\begin{aligned} &\overline{\rho u''} \neq 0\,, \\ &\tilde{\tilde{u}} \neq \tilde{u}\,, \\ &\tilde{u}'' \neq 0\,. \end{aligned} \tag{16}$$

It is important to note that there is no simple relationship between the Favre-filtered and conventionally filtered variables. To obtain $\bar{u}$ from $\tilde{u}$, the density pulsations must be known.

The magnetic field, like density and pressure, is filtered using a conventional means in order not to complicate calculations, since MHD equations do not contain products of density and magnetic field induction.

Traditionally, a cylinder (box) filter, a Gaussian filter and a spectral (Fourier) filter are utilized in the LES method [36].

The cylinder filter assumes the form

$$\xi(x, \acute{x}) = \begin{cases} \dfrac{1}{\bar{\Delta}}\,, & \text{if } |x - \acute{x}| \leqslant \dfrac{\bar{\Delta}}{2}\,, \\ 0\,, & \text{if } |x - \acute{x}| > \dfrac{\bar{\Delta}}{2}\,, \end{cases} \tag{17}$$

the Gaussian filter takes the form

$$\xi(x, \acute{x}) = \left(\frac{6}{\pi\bar{\Delta}^2}\right)^{1/2} \exp\left(-\frac{6|x - \acute{x}|^2}{\bar{\Delta}^2}\right)^{1/2}, \tag{18}$$

and the Fourier filter has the form

$$\xi(x, \acute{x}) = \frac{\sin\left[k_c(x - \acute{x})\right]}{k_c(x - \acute{x})}\,, \quad \text{where} \quad k_c = \frac{\pi}{\bar{\Delta}}\,. \tag{19}$$

The Gaussian filter is smooth in both physical and spectral spaces. The cylinder filter represents essentially a step in the physical space, while the Fourier filter represents a step in the spectral space. The Fourier filter is usually applied to discretize the original fluid equations of motion using the spectral approach.

In real physical problems, three-dimensional compressible turbulent flows are frequently considered, so it is necessary to apply a three-dimensional filter (multidimensional in the general case). The multidimensional filter can be designed by two different means. In the first case, it can be

represented as a linear combination of one-dimensional filters, i.e., any physical parameter is filtered independently along each direction [101]:

$$\xi^n = \frac{1}{n}\sum_{i=1}^{n} \xi^i\,, \tag{20}$$

where ξ^i is the one-dimensional filter in the i direction, and n is the dimensionality of the space considered. The linear combination signifies the simultaneous application of all one-dimensional filters along each spatial direction. The second means assumes consecutive multiplication of one-dimensional filters, which can be expressed as

$$\xi^n = \prod_{i=1}^{n} \xi^i\,. \tag{21}$$

Such a definition of the multidimensional filter ξ^n, unlike the first case, represents not simultaneous, but consecutive application of one-dimensional filters. The accuracy of the multidimensional filters constructed by two different methods is studied in depth and tested in paper [101], where the consecutive multiplication of filters was shown to produce more accurate results than the linear combination of one-dimensional filters. Therefore, we used formula (21) in our papers [57–68, 94–96] for executing three-dimensional filtering in simulations of compressible MHD flows.

2.3 Filtered equations of magnetic hydrodynamics for a polytropic plasma

Polytropic processes are assumed in many problems of space physics. Such a model is effectively applied to study and simulate compressible turbulence in neutral [102] and magnetized [82] fluids, solar wind turbulence [75, 76], interstellar gas turbulence [9], and other problems of astrophysical turbulence [77, 103]. This allows the polytropic relation $p = \rho^\gamma$ between the pressure and density, where γ is the polytrope index, to be used instead of the cumbersome and complicated energy conservation equation to close the system of equations. In this case, the system of compressible MHD equations is reduced to a simpler form. After performing the density-weighted filtering operation, we can write down the system of MHD equations in the following form [60, 63]:

filtered continuity equation

$$\frac{\partial\bar\rho}{\partial t} + \frac{\partial\bar\rho\tilde u_j}{\partial x_j} = 0\,; \tag{22}$$

filtered momentum equation

$$\frac{\partial\bar\rho\tilde u_j}{\partial t} + \frac{\partial}{\partial x_j}\left(\bar\rho\tilde u_i\tilde u_j + \bar p\delta_{ij} - \frac{1}{\mathrm{Re}}\,\tilde\sigma_{ij} + \frac{\bar B^2}{2\mathrm{M}_\mathrm{a}^2}\,\delta_{ij} - \frac{1}{2\mathrm{M}_\mathrm{a}^2}\,\bar B_j\bar B_i\right) = -\frac{\partial}{\partial x_j}\left(t^u_{ji} + t^b_{ji}\right) = -\frac{\partial\tau^u_{ji}}{\partial x_j}\,, \tag{23}$$

and *filtered magnetic induction equation*

$$\frac{\partial\bar B_i}{\partial t} + \frac{\partial}{\partial x_j}\left(\tilde u_j\bar B_i - \tilde u_i\bar B_j\right) - \frac{1}{\mathrm{Re_m}}\,\frac{\partial^2\bar B}{\partial x_j^2} = -\frac{\partial\tau^b_{ji}}{\partial x_j}\,, \tag{24}$$

$$\frac{\partial\bar B_j}{\partial x_j} = 0\,, \tag{25}$$

since $\overline{\eta B_j} - \bar\eta\bar B_j = 0$ and $\bar\sigma_{ij} - \tilde\sigma_{ij} = 0$, where

$$\tilde\sigma_{ij} = 2\tilde\mu\tilde S_{ij} - \frac{2}{3}\,\tilde\mu\tilde S_{kk}\delta_{ij} + \tilde\zeta\tilde S_{kk}\delta_{ij}\,,$$

$$\bar\sigma_{ij} = 2\overline{\mu S_{ij}} - \frac{2}{3}\,\overline{\mu S_{kk}\delta_{ij}} + \overline{\zeta S_{kk}\delta_{ij}}\,.$$

In numerical computations, one usually neglects the last term by assuming the volume viscosity coefficient ζ to be equal to zero.

On the right-hand side of equations (23), (24), the terms denote the influence of subgrid-scale terms on the filtered part:

$$\tau^u_{ij} = \bar\rho\left(\widetilde{u_iu_j} - \tilde u_i\tilde u_j\right) - \frac{1}{\mathrm{M}_\mathrm{a}^2}\left(\overline{B_iB_j} - \bar B_i\bar B_j\right), \tag{26}$$

$$\tau^b_{ij} = \left(\overline{u_iB_j} - \tilde u_i\bar B_j\right) - \left(\overline{B_iu_j} - \bar B_i\tilde u_j\right). \tag{27}$$

A significant simplification should be noted when using the Favre type filtering. Indeed, the conventional filtering results in the following form of the continuity and momentum equations, respectively:

$$\frac{\partial\bar\rho}{\partial t} + \frac{\partial\bar\rho\bar u_j}{\partial x_j} = -\frac{\partial}{\partial x_j}\left(\overline{\rho u_j} - \bar\rho\bar u_j\right), \tag{28}$$

$$\frac{\partial\bar\rho\bar u_i}{\partial t} + \frac{\partial}{\partial x_j}\left(\bar\rho\bar u_i\bar u_j + \bar p\delta_{ij} - \bar\sigma_{ij} + \frac{\bar B^2}{8\pi}\,\delta_{ij} - \frac{1}{4\pi}\,\bar B_j\bar B_i\right) = -\frac{\partial}{\partial x_j}\left(\overline{\rho u_ju_i} - \bar\rho\bar u_i\bar u_j\right) + \frac{1}{4\pi}\,\frac{\partial}{\partial x_j}\left(\overline{B_jB_i} - \bar B_i\bar B_j\right) - \frac{\partial}{\partial t}\left(\overline{\rho u_i} - \bar\rho\bar u_i\right). \tag{29}$$

It is seen that additional terms in equations (28) and (29) arise due to making allowance for the mass transfer, in comparison with the Favre-filtered equations, which is the principal advantage of the density-weighted filtering for compressible fluids.

Let us consider in more detail the above-introduced equations (22)–(24). As the small-scale velocity (the same is also true for other characteristics of motion of an electrically charged fluid) $u'' = u - \tilde u$ is unknown, it must be estimated using the large-scale velocity obtained by the filtering procedure. In principle, there is no functional dependence between the small-scale (u'') and large-scale ($\tilde u$) velocities, so any estimate of u'' will be plagued with errors. As a rule, to assess this error, the DNS results are used, and here the analysis is performed for relatively low Reynolds numbers because of computational restrictions.

The influence of the subgrid-scale terms that appear on the right-hand side of MHD equations (23), (24) on the filtered part of the equations is described by the SGS terms. Taking into account compressibility leads to a complication of the subgrid-scale stress tensor τ^u_{ij} in the Navier–Stokes equation, the tensor related to the appearance of the filtered density, in comparison with an incompressible flow. However, the magnetic tensor of SGS stresses, τ^b_{ij}, arising in the magnetic induction equation, keeps the form as for an incompressible MHD flow. Nevertheless, these subgrid-scale closures should be extended over the compressible MHD turbulence. In Section 3, we will conserve the traditional names for subgrid-scale closures, bearing in mind that these

subgrid-scale models are extended and generalized to the case of compressible turbulent MHD flows.

Let us write out nonlinear terms in the momentum conservation equation in the form

$$\bar{\rho}\widetilde{u_j u_i} = \bar{\rho}(\tilde{u}_i + u_i'')\widetilde{(\tilde{u}_j + u_j'')} = \bar{\rho}\left(\widetilde{\tilde{u}_i\tilde{u}_j} + \widetilde{\tilde{u}_i u_j''} + \widetilde{\tilde{u}_j u_i''} + \widetilde{u_i'' u_j''}\right), \tag{30}$$

$$\overline{B_j B_i} = \overline{(\bar{B}_i + B_i')(\bar{B}_j + B_j')} = \overline{\bar{B}_i\bar{B}_j} + \overline{\bar{B}_i B_j'} + \overline{\bar{B}_j B_i'} + \overline{B_i' B_j'}. \tag{31}$$

Because the nonlinear terms must be expressed through large-scale variables, we write them as

$$\frac{\partial}{\partial x_j}\bar{\rho}\widetilde{u_j u_i} = \frac{\partial}{\partial x_j}\bar{\rho}\tilde{u}_i\tilde{u}_j + \frac{\partial}{\partial x_j}\left(\bar{\rho}\widetilde{u_j u_i} - \bar{\rho}\tilde{u}_i\tilde{u}_j\right) = \frac{\partial}{\partial x_j}\bar{\rho}\tilde{u}_i\tilde{u}_j + \frac{\partial}{\partial x_j}t_{ji}^u, \tag{32}$$

$$\frac{\partial}{\partial x_j}\overline{B_j B_i} = \frac{\partial}{\partial x_j}\bar{B}_i\bar{B}_j + \frac{\partial}{\partial x_j}\left(\overline{B_j B_i} - \bar{B}_i\bar{B}_j\right) = \frac{\partial}{\partial x_j}\bar{B}_i\bar{B}_j + \frac{\partial}{\partial x_j}t_{ji}^b, \tag{33}$$

where t_{ji}^u and t_{ji}^b are the hydrodynamic and magnetic parts, respectively, of the turbulent stress tensor τ_{ji}^u on the right-hand side of equation (23).

In a similar way, the tensor τ_{ij}^b arises in the filtered magnetic induction equation (24), which has the form

$$\tau_{ij}^b = \left(\overline{u_i B_j} - \tilde{u}_i\bar{B}_j\right) - \left(\overline{B_i u_j} - \bar{B}_i\tilde{u}_j\right). \tag{34}$$

Any subgrid-scale tensor can be resolved into three parts [97]; for example, for the tensor τ_{ij}^u we have

$$\begin{aligned}\tau_{ij}^u &= \bar{\rho}\left(\widetilde{u_i u_j} - \tilde{u}_i\tilde{u}_j\right) - \frac{1}{\mathrm{M}_a^2}\left(\overline{B_i B_j} - \bar{B}_i\bar{B}_j\right)\\ &= \underbrace{\bar{\rho}\left(\widetilde{\tilde{u}_i\tilde{u}_j} - \tilde{u}_i\tilde{u}_j\right) - \frac{1}{\mathrm{M}_a^2}\left(\overline{\bar{B}_i\bar{B}_j} - \bar{B}_i\bar{B}_j\right)}_{\text{Leonard term}}\\ &+ \underbrace{\bar{\rho}\left(\widetilde{\tilde{u}_i u_j''} + \widetilde{\tilde{u}_j u_i''}\right) - \frac{1}{\mathrm{M}_a^2}\left(\overline{\bar{B}_i B_j'} + \overline{\bar{B}_j B_i'}\right)}_{\text{Cross term}}\\ &+ \underbrace{\bar{\rho}\left(\widetilde{u_i'' u_j''}\right) - \frac{1}{\mathrm{M}_a^2}\left(\overline{B_i' B_j'}\right)}_{\text{Reynolds–Maxwell term}} = L_{ij} + C_{ij} + R_{ij}.\end{aligned} \tag{35}$$

The Leonard term L_{ij} on the right-hand side of equation (35) is responsible for the energy redistribution between large-scale and small-scale values of both velocity and the magnetic field [36]. The cross term C_{ij} includes both the direct energy transfer cascade and the energy backscatter (i.e., from small to large scales, for example, when several small eddies merge into one large eddy). Finally, the Reynolds–Maxwell term R_{ij} accounts for the energy dissipation (outscatter) at small scales (corresponding to large wave numbers). Generally speaking, there are two approaches in LES simulations of subgrid-scale stresses. The first relies on the idea of similarity of scales, where the first Leonard term L_{ij} dominates, i.e., the SGS tensors are proportional to the Leonard stress tensor: $\tau_{ij} \propto L_{ij}$. The second approach is based on the idea of eddy viscosity, which is focused on the Reynolds–Maxwell term R_{ij} and assumes the proportionality: $\tau_{ij} \propto R_{ij}$.

Thus, a filtered system of MHD equations comprise unknown turbulent tensors τ_{ij}^u and τ_{ij}^b. In order to determine them, it is necessary to utilize the special turbulent closures (parametrizations) based on large-scale values of quantities characterizing a turbulent MHD flow. It is the subgrid-scale SGS models that link the tensors τ_{ij}^u and τ_{ij}^b with the quantities $\tilde{u}_i$ and $\bar{B}_i$. The main purpose of any subgrid-scale parametrization in the LES method consists in providing an adequate description of the energy change for a large-scale motion; here, essentially, the Richardson turbulent cascade is simulated.

2.4 Filtered equations of magnetic hydrodynamics for a heat-conducting plasma

The system of filtered MHD equations describing a heat-conducting fluid that is used in large eddy simulations to model three-dimensional compressible turbulence is taken down in the following form [58, 62]:

$$\frac{\partial\bar{\rho}}{\partial t} + \frac{\partial\bar{\rho}\tilde{u}_j}{\partial x_j} = 0, \tag{36}$$

$$\frac{\partial\bar{\rho}\tilde{u}_i}{\partial t} + \frac{\partial}{\partial x_j}\left(\bar{\rho}\tilde{u}_i\tilde{u}_j + \bar{p}\delta_{ij} - \frac{1}{\mathrm{Re}}\tilde{\sigma}_{ij} + \frac{\bar{B}^2}{2\mathrm{M}_a^2}\delta_{ij} - \frac{1}{\mathrm{M}_a^2}\bar{B}_j\bar{B}_i\right) = -\frac{\partial\tau_{ji}^u}{\partial x_j}, \tag{37}$$

$$\frac{\partial\bar{B}_i}{\partial t} + \frac{\partial}{\partial x_j}(\tilde{u}_j\bar{B}_i - \tilde{u}_i\bar{B}_j) - \frac{1}{\mathrm{Re_m}}\frac{\partial^2\bar{B}_i}{\partial x_j^2} = -\frac{\partial\tau_{ji}^b}{\partial x_j}, \tag{38}$$

$$\begin{aligned}&\frac{\partial}{\partial t}\left(\bar{\rho}\tilde{E} + \frac{\bar{B}^2}{2\mathrm{M}_a^2}\right) + \frac{\partial}{\partial x_j}\left((\bar{\rho}\tilde{E} + \bar{P})\tilde{u}_j + \frac{1}{\mathrm{Pr\,Re\,M}_s^2(\gamma-1)}\tilde{q}_j\right.\\ &\left.- \frac{1}{\mathrm{Re}}\tilde{\sigma}_{ij}\tilde{u}_i - \frac{1}{\mathrm{M}_a^2}\bar{B}_j\bar{B}_i\tilde{u}_i\right) - \frac{\partial}{\partial x_j}\left(\frac{\eta}{\mathrm{Re_m\,M}_a^2}\bar{B}_i\left(\frac{\partial\bar{B}_i}{\partial x_j} - \frac{\partial\bar{B}_j}{\partial x_i}\right)\right)\\ &= -\frac{\partial}{\partial x_j}\left(\frac{1}{(\gamma-1)\mathrm{M}_s^2}Q_j + \frac{1}{2}J_j + \frac{1}{\mathrm{M}_a^2}V_j - \frac{1}{\mathrm{M}_a^2}G_j\right),\end{aligned} \tag{39}$$

$$\frac{\partial\bar{B}_i}{\partial x_i} = 0, \tag{40}$$

where

$$\tilde{q}_j = -\tilde{\psi}\frac{\partial\tilde{T}}{\partial x_j}.$$

The dimensionless filtered equation of state that is used to close the system of equations is written down as

$$\bar{p} = \frac{\tilde{T}\bar{\rho}}{\gamma\mathrm{M}_s^2}. \tag{41}$$

The total energy equation for MHD case has the form (39), since the following relationships are fulfilled (for clarity, we write them down in the dimensional form):

$$\begin{aligned}\overline{pu_j} &= \overline{\rho RTu_j} = \bar{\rho}R\widetilde{Tu_j} = \bar{\rho}R\tilde{T}\tilde{u}_j + R\bar{\rho}\left(\widetilde{u_jT} - \tilde{u}_j\tilde{T}\right),\\ \overline{\rho Eu_j} &= \bar{\rho}C_v\tilde{T}\tilde{u}_j + C_v\bar{\rho}\left(\widetilde{u_jT} - \tilde{u}_j\tilde{T}\right)\\ &+ \frac{1}{2}\bar{\rho}\tilde{u}_j\widetilde{u_k u_k} + \frac{1}{2}\bar{\rho}\left(\widetilde{u_j u_k u_k} - \tilde{u}_j\widetilde{u_k u_k}\right)\\ &= \bar{\rho}\tilde{E}\tilde{u}_j + C_v\bar{\rho}\left(\widetilde{u_jT} - \tilde{u}_j\tilde{T}\right) + \frac{1}{2}\bar{\rho}\left(\widetilde{u_j u_k u_k} - \tilde{u}_j\widetilde{u_k u_k}\right).\end{aligned}$$

In this derivation, the Mayer equation $C_p - C_v = R$, which relates specific heat capacities at constant pressure (C_p) and constant volume (C_v) with the molar gas constant R, is also taken into account. Considering that $\gamma = C_p/C_v$, we can write down the desired relation as $C_p = \gamma R/(\gamma - 1)$.

The influence of small-scale turbulence on the filtered part of MHD equations is determined through the following SGS terms on the right-hand side of equations (37)–(39): the subgrid-scale stress tensor τ_{ij}^u, the subgrid-scale magnetic stress tensor τ_{ij}^b, the subgrid-scale heat flux Q_j, the subgrid-scale turbulent diffusion J_j, the subgrid-scale magnetic energy flux V_j, and the subgrid-scale interaction energy of the magnetic stress and velocity G_j. These quantities are defined as

$$\tau_{ij}^u = \bar{\rho}\left(\widetilde{u_i u_j} - \tilde{u}_i\tilde{u}_j\right) - \frac{1}{\mathrm{M}_\mathrm{a}^2}\left(\overline{B_i B_j} - \bar{B}_i\bar{B}_j\right), \tag{42}$$

$$\tau_{ij}^b = \left(\overline{u_i B_j} - \tilde{u}_i\bar{B}_j\right) - \left(\overline{B_i u_j} - \bar{B}_i\tilde{u}_j\right), \tag{43}$$

$$Q_j = \bar{\rho}\left(\widetilde{u_j T} - \tilde{u}_j\tilde{T}\right), \tag{44}$$

$$J_j = \bar{\rho}\left(\widetilde{u_j u_k u_k} - \tilde{u}_j\widetilde{u_k u_k}\right), \tag{45}$$

$$V_j = \left(\overline{B_k B_k u_j} - \overline{B_k B_k}\tilde{u}_j\right), \tag{46}$$

$$G_j = \left(\overline{u_k B_k B_j} - \tilde{u}_k\bar{B}_k\bar{B}_j\right). \tag{47}$$

Paper [47] presented a detailed study of the contribution from nonlinear diffusion terms to the momentum and energy conservation equations in neutral fluid dynamics, and *a priori* tests using DNS data obtained from calculations of a mixed layer at Mach numbers in the range of 0.2–1.2 were performed. It was also shown that the diffusion term can be neglected, i.e., $\bar{\sigma}_{ij} - \tilde{\sigma}_{ij} = 0$ and $\bar{q}_j - \tilde{q}_j = 0$. In our papers [57–68, 94–96], we also neglect the diffusion terms related to the magnetic energy in equation (39). As found in paper [49], the subgrid-scale diffusion of viscosity, defined as $D_j = \widetilde{\sigma_{ij}u_i} - \tilde{\sigma}_{ij}\tilde{u}_i$, is a small parameter in the total energy equation, and amounts to only about 5% of the divergence of the subgrid-scale heat flux Q_j, so in calculations we neglect this SGS term D_j in Eqn (39).

3. Subgrid-scale modeling of small-scale turbulence

As noted in Section 2, the filtering operation is applied to exclude small-scale turbulence. The resulting system of filtered equations turns out to be nonclosed, since it includes terms describing nonlinear interactions of large eddies with small-scale turbulence. The parametrization of such interactions is called the subgrid-scale (SGS) model and makes up the most important ingredient of large eddy simulations. All subgrid-scale models are subdivided into functional and structural models [98]. The functional models express the influence of subgrid scales on large scales. Widespread parametrizations based on the eddy viscosity belong to functional models. This influence is usually described by the energy transfer. The structural models are constructed in such a way that the subgrid-scale stress tensor is approximated by the formal replacement of an unknown (small-scale) parameter by the known (filtered) quantity. The structural models include closings based on the scale similarity idea [98].

First, let us discuss the tensors τ_{ij}^u and τ_{ij}^b. To close the system of equations, it is necessary to find such parametrizations for τ_{ij}^u and τ_{ij}^b that would relate these tensors with known large-scale values of the flow characteristics. To guarantee the nonnegativity of subgrid-scale energy, the turbulent subgrid-scale tensors should satisfy the realizable conditions. The necessary and sufficient condition of nonnegative energy is provided by a positive value of the semidefinite form for the turbulent tensor τ_{ij}; therefore, the following relations are satisfied [47]:

$$\begin{aligned} &\tau_{ii} \geqslant 0 && \text{for} \quad i \in \{1,2,3\}, \\ &|\tau_{ij}| \leqslant \sqrt{\tau_{ii}\tau_{jj}} && \text{for} \quad i,j \in \{1,2,3\}, \\ &\det(\tau_{ij}) \geqslant 0. \end{aligned} \tag{48}$$

We assume that the turbulent tensor τ_{ij}^u is connected with the strain rate tensor and viscosity (the eddy viscosity model), while τ_{ij}^b is connected with dissipation due to resistance (i.e., this dissipation is expressed via the generalized Ohm law and equals ηj [104], where j is the electric current density) as follows:

$$\tau_{ij}^u - \frac{1}{3}\tau_{kk}^u\delta_{ij} = -2\nu_t\left(\tilde{S}_{ij} - \frac{1}{3}\tilde{S}_{kk}\delta_{ij}\right), \tag{49}$$

$$\tau_{ij}^b - \frac{1}{3}\tau_{kk}^b\delta_{ij} = -2\eta_t\bar{J}_{ij}. \tag{50}$$

Here,

$$\tilde{S}_{ij} = \frac{1}{2}\left(\frac{\partial\tilde{u}_i}{\partial x_j} + \frac{\partial\tilde{u}_j}{\partial x_i}\right)$$

is the large-scale strain rate tensor,

$$\bar{J}_{ij} = \frac{1}{2}\left(\frac{\partial\bar{B}_i}{\partial x_j} - \frac{\partial\bar{B}_j}{\partial x_i}\right)$$

is the large-scale magnetic rotation tensor, and ν_t and η_t are scalar turbulent functions depending on the spatial coordinates and time.

On the right-hand side of equations (49) and (50), symmetric terms containing the magnetic strain tensor $\bar{S}_{ij}^b = (\partial\bar{B}_i/\partial x_j + \partial\bar{B}_j/\partial x_i)/2$ and the eddy tensor $\tilde{J}_{ij}^u = (\partial\tilde{u}_i/\partial x_j - \partial\tilde{u}_j/\partial x_i)/2$, respectively, are omitted since their role is insignificant [53]. It should be noted that the main goal of the subgrid-scale modeling is not to fully reconstruct the information lost due to filtering, but to simulate the effect of small-scale dynamics on the large-scale energy distribution.

Sometimes, the term $\tau_{kk}^u\delta_{ij}/3$ is neglected by connecting it with the thermodynamic pressure $\nabla(p + (2/3)K\delta_{ij})$ [46], where $K = (\tau_{11} + \tau_{22} + \tau_{33})/2$ is the subgrid-scale turbulent kinetic energy. A more general case is considered in papers [57, 58, 60–65, 67] that takes into account the isotropic term (the subgrid-scale term in formula (50) is equal to zero, since J_{ij} vanishes in this case).

The subgrid-scale isotropic term can be found from the realizability conditions (48). Using these inequalities, it is possible to write the following relation for the subgrid-scale stress tensor τ_{ij}:

$$\tau_{12}^2 + \tau_{13}^2 + \tau_{23}^2 \leqslant \tau_{11}\tau_{22} + \tau_{11}\tau_{33} + \tau_{22}\tau_{33}. \tag{51}$$

Substituting relevant values from formula (49) into this expression, the isotropic term can be estimated as [105]

$$K \geqslant \frac{1}{2}\sqrt{3}\left(\nu_t|\tilde{S}^u|\right), \tag{52}$$

where $|\tilde{S}^u| = (2\tilde{S}_{ij}^u\tilde{S}_{ij}^u)^{1/2}$.

Thus, by assuming different closures and parametrizing ν_t, we obtain the anisotropic part of the subgrid-scale term in

Eqn (49), and the isotropic part from Eqn (52). In the next section, we present some subgrid-scale models for compressible MHD turbulence.

3.1 Smagorinsky model for compressible MHD turbulence

The Smagorinsky model represents a model of the eddy viscosity in which the subgrid scales are assumed to be isotropic and in equilibrium with the large-scale flow [106]. An extended Smagorinsky model for compressible MHD turbulence has the form [57, 60, 61, 63]

$$\tau^u_{ij} - \frac{1}{3}\,\tau^u_{kk}\delta_{ij} = -2C_1\bar{\rho}\bar{\Delta}^2|\tilde{S}^u|\left(\tilde{S}_{ij} - \frac{1}{3}\,\tilde{S}_{kk}\delta_{ij}\right), \tag{53}$$

$$\tau^b_{ij} = -2D_1\bar{\Delta}^2|\bar{j}|\bar{J}_{ij}\,. \tag{54}$$

Here, $\bar{j}$ is the large-scale electric current density. The quantity η_t is an analog of the velocity shear that is present in Eqn (53) for ν_t, which is replaced here by the shear in the magnetic field (54) (which is the electric current density [104]).

Inequality (52) makes it possible to construct a subgrid-scale model for the turbulent kinetic energy K, corresponding to the eddy viscosity model [47]. By substituting the turbulent viscosity from formula (53) into (52), we arrive at

$$K \geqslant \frac{1}{2}\,\sqrt{3}\,C_1\bar{\rho}\bar{\Delta}^2|\tilde{S}^u|^2\,. \tag{55}$$

From here, we obtain the subgrid-scale closure for the isotropic term in the form [47]

$$\tau^u_{kk} = 2Y_1\bar{\rho}\bar{\Delta}^2|\tilde{S}^u|^2\,, \tag{56}$$

where Y_1 is the constant that ensures a transition from inequality (55) to equality (56) and getting into the domain of definition of the turbulent kinetic energy, i.e., the fulfilment of condition (55).

For other subgrid-scale models that will be presented below, isotropic terms can be specified in a similar way.

The Smagorinsky model extended to the MHD case provides sufficient dissipation and diffusion, which, in addition, stabilize numerical calculations [57]. The nonuniversality of C_1, Y_1, and D_1 constants has to do with shortcomings of this model. Indeed, by specifying certain positive or negative values of the constants, the energy backscatter or direct energy transfer cascade, respectively, cannot be described.

3.2 Kolmogorov model for compressible MHD turbulence

If the filter pass-band is in the inertia interval of fully developed turbulence, the nonlinear interaction between the large-scale kinetic and magnetic energies can be assumed to be much smaller than the dissipation energy, so the subgrid-scale kinetic and magnetic energies can be thought to depend only on time [51]. It is also assumed that the coefficient responsible for dimensionality is equal to unity [53]. These parametrizations are based on the Kolmogorov scaling. The extended Kolmogorov model for compressible MHD turbulence takes the form [57, 60, 61, 63]

$$\tau^u_{ij} - \frac{1}{3}\,\tau^u_{kk}\delta_{ij} = -2C_2\bar{\rho}\bar{\Delta}^{4/3}\left(\tilde{S}_{ij} - \frac{1}{3}\,\tilde{S}_{kk}\delta_{ij}\right), \tag{57}$$

$$\tau^b_{ij} = -2D_2\bar{\Delta}^{4/3}\bar{J}_{ij}\,, \tag{58}$$

$$\tau^u_{kk} = 2Y_2\bar{\rho}\bar{\Delta}^{4/3}|\tilde{S}^u|\,. \tag{59}$$

The constants used in one model are different from those used in other methods of equation closure. All shortcomings related to constants in the Smagorinsky model persist in the Kolmogorov model.

3.3 Model based on cross-helicity

The cross-helicity between the velocity field and magnetic field is defined as follows: $H^c = \int_V(\mathbf{uB})\,\mathrm{d}V$. In the case of MHD turbulence, one finds the characteristic turbulent velocity and magnetic field, and the cross-helicity is related to the exchange between the kinetic and magnetic energies due to the Lorentz force [52]. The cross-helicity characterizes the energy exchange between the large and small scales in the LES method. Papers [57, 60, 61] proposed a parametrization based on the cross-helicity in the compressible MHD turbulence:

$$\tau^u_{ij} - \frac{1}{3}\,\tau^u_{kk}\delta_{ij} = -2C_3\bar{\rho}\bar{\Delta}^2|\tilde{f}|\left(\tilde{S}_{ij} - \frac{1}{3}\,\tilde{S}_{kk}\delta_{ij}\right), \tag{60}$$

$$\tau^b_{ij} = -2D_3\bar{\Delta}^2\,\mathrm{sgn}\,(\bar{j}\tilde{\omega})|\bar{j}\tilde{\omega}|^{1/2}\bar{J}_{ij}\,, \tag{61}$$

$$\tau^u_{kk} = 2Y_3\bar{\rho}\bar{\Delta}^2|\tilde{f}|\,|\tilde{S}^u|\,. \tag{62}$$

Here, the following notation was introduced:

$$\tilde{f} = |\tilde{S}_{ij}\bar{S}^b_{ij}|^{1/2}\,,$$

$$\bar{S}^b_{ij} = \frac{1}{2}\left(\frac{\partial\bar{B}_i}{\partial x_j} + \frac{\partial\bar{B}_j}{\partial x_i}\right), \qquad \tilde{S}_{ij} = \frac{1}{2}\left(\frac{\partial\tilde{u}_i}{\partial x_j} + \frac{\partial\tilde{u}_j}{\partial x_i}\right),$$

and $\tilde{\omega} = \nabla\times\tilde{\mathbf{u}}$ is the large-scale vorticity.

In the cross-helicity model, only the magnetic diffusion η_t can change sign [in formula (61) the function sgn (.) defines the sign of the argument], since in the MHD turbulence only the magnetic energy is responsible for the energy transfer process from small (i.e., subgrid) to large scales [52].

3.4 Scale-similarity model for compressible MHD turbulence

The scale-similarity model is not identical to the eddy viscosity model. Thus, the unknown turbulence tensors are modeled assuming that they are proportional to the Leonard term. The theory of this approach relies on the idea of turbulence universality at moderate scales, i.e., under the assumption that the most energy-capacious subgrid-scale components in the energy transfer cascade from large to small scales can be estimated with a sufficient accuracy from the smallest large-scale eddies obtained after the filtering operation. This method is relatively simple. However, it does not provide the necessary energy dissipation rate in the neutral fluid dynamics. The scale-similarity model was proposed in paper [107] and then explored in Ref. [108]. The scale-similarity model was generalized to the case of compressible MHD turbulence in papers [60, 67]:

$$\tau^u_{ij} = \bar{\rho}\left(\widetilde{\tilde{u}_i\tilde{u}_j} - \tilde{\bar{u}}_i\tilde{\bar{u}}_j\right) - \frac{1}{\mathrm{M}_a^2}\left(\overline{\bar{B}_i\bar{B}_j} - \bar{\bar{B}}_i\bar{\bar{B}}_j\right), \tag{63}$$

$$\tau^b_{ij} = \left(\overline{\tilde{u}_i\bar{B}_j} - \tilde{\bar{u}}_i\bar{\bar{B}}_j\right) - \left(\overline{\bar{B}_i\tilde{u}_j} - \bar{\bar{B}}_i\tilde{\bar{u}}_j\right). \tag{64}$$

Thus, the scale-similarity model (63), (64), unlike other models, is fully defined in the LES method by using filtered variables of the turbulent motion.

3.5 Mixed model for compressible MHD turbulence

In the hydrodynamic case, paper [42] has suggested joining two different approaches — the scale-similarity model and the eddy viscosity model — and in paper [109] the dynamic form of the mixed model was used for the first time, where the model constant was determined dynamically at each time step. The extended mixed model for compressible MHD turbulence is written out in the following form [60]:

$$\tau_{ij}^u - \frac{1}{3}\,\tau_{kk}^u\delta_{ij} = -2C_5\bar{\rho}\bar{\Delta}^2|\tilde{S}^u|\left(\tilde{S}_{ij} - \frac{\delta_{ij}}{3}\,\tilde{S}_{kk}\right) + \bar{\rho}\left(\widetilde{\tilde{u}_i\tilde{u}_j} - \tilde{\tilde{u}}_i\tilde{\tilde{u}}_j\right) - \frac{1}{\mathrm{M}_\mathrm{a}^2}\left(\overline{\bar{B}_i\bar{B}_j} - \bar{\bar{B}}_i\bar{\bar{B}}_j\right), \tag{65}$$

$$\tau_{ij}^b = -2D_5\bar{\Delta}^2|\bar{j}|\bar{J}_{ij} + \left(\overline{\tilde{u}_i\bar{B}_j} - \tilde{\tilde{u}}_i\bar{\bar{B}}_j\right) - \left(\overline{\bar{B}_i\tilde{u}_j} - \bar{\bar{B}}_i\tilde{\tilde{u}}_j\right), \tag{66}$$

$$\tau_{kk}^u = 2Y_5\bar{\rho}\bar{\Delta}^2|\tilde{S}^u|^2. \tag{67}$$

In expressions (65), (66), the mixed model is represented as a combination of two models: the scale-similarity model, and the Smagorinsky model for compressible MHD turbulence.

3.6 Dynamical constant determination procedure

To remove the problem related to the choice of model constants in subgrid-scale closures, a dynamical procedure was proposed [110, 111] that determines the value of constants at each step. To this end, an additional test filter is used, with the test filter width being larger than that of the main filter. In other words, dynamical subgrid-scale models imply the invariance of constants, which are present in closures, with respect to the filtering width [110]. One and the same subgrid-scale model is assumed to be applicable to both lower and higher spatial resolution. From the solution on a fine mesh, it is possible to derive the solution on a more coarse mesh using additional test spatial filtering and to estimate turbulent stresses for it. The generalization of the dynamical procedure for compressible MHD turbulence can be presented as follows [57].

Let T_{ij}^u and T_{ij}^b be the test subgrid-scale tensors which are produced by the test filtering for τ_{ij}^u and τ_{ij}^b, respectively:

$$T_{ij}^u = \hat{\tau}_{ij}^u + L_{ij}^u, \tag{68}$$

$$T_{ij}^b = \hat{\tau}_{ij}^b + L_{ij}^b, \tag{69}$$

where the Leonard tensors are defined as

$$L_{ij}^u = \frac{\widehat{\overline{\rho u_i}\,\overline{\rho u_j}}}{\bar{\rho}} - \frac{\widehat{\overline{\rho u_i}}\,\widehat{\overline{\rho u_j}}}{\hat{\bar{\rho}}} - \frac{1}{\mathrm{M}_\mathrm{a}^2}\left(\widehat{\bar{B}_i\bar{B}_j} - \hat{\bar{B}}_i\hat{\bar{B}}_j\right), \tag{70}$$

$$L_{ij}^b = \left(\frac{\widehat{\overline{\rho u_i}\,\bar{B}_j}}{\bar{\rho}} - \frac{\widehat{\overline{\rho u_i}}\,\hat{\bar{B}}_j}{\hat{\bar{\rho}}}\right) - \left(\frac{\widehat{\bar{B}_i\,\overline{\rho u_j}}}{\bar{\rho}} - \frac{\hat{\bar{B}}_i\,\widehat{\overline{\rho u_j}}}{\hat{\bar{\rho}}}\right). \tag{71}$$

Here, the 'hat' mark $\widehat{\ }$ over a variable denotes its test filtering. The Leonard tensors can be derived from the large-scale values of velocity and the magnetic field induction. Equations (70) and (71) link the initial subgrid-scale and test tensors.

The turbulent viscosity and magnetic diffusion can be denoted as follows: $\nu_t = C_s\alpha_{ij}^u$ (for τ_{ij}^u), $\acute{\nu}_t = Y_s\alpha^u$ (for τ_{kk}^u), and $\eta_t = D_s\varphi_{ij}^B$ (for τ_{ij}^b), where $s = 1, 2, 3\ldots$.

To specify the constants, we can apply the least-square method for minimizing the error from the functionals [112]:

$$Z^u = \left\langle\left(T_{ij}^u - \hat{\tau}_{ij}^u - L_{ij}^u\right)^2\right\rangle,$$

$$Z^b = \left\langle\left(T_{ij}^b - \hat{\tau}_{ij}^b - L_{ij}^b\right)^2\right\rangle.$$

The angular brackets stand for the spatial averaging.

The constants are determined dynamically at each time step using formulas [57]

$$C_s = \frac{\langle L_{ij}^u M_{ij}^u\rangle}{\langle M_{ij}^u M_{ij}^u\rangle}, \tag{72}$$

$$Y_s = \frac{\langle L_{kk}^u\rangle}{\left\langle\hat{\alpha}^u|\hat{\tilde{S}}^u| - \alpha^u\widehat{|\tilde{S}^u|}\right\rangle}, \tag{73}$$

$$D_s = \frac{\langle L_{ij}^b m_{ij}^B\rangle}{\langle m_{ij}^B m_{lk}^B\rangle}, \tag{74}$$

where

$$M_{ij}^u = \hat{\alpha}_{ij}^u\left(\hat{\tilde{S}}_{ij}^u - \frac{\delta_{ij}}{3}\,\hat{\tilde{S}}_{kk}\right) - \widehat{\left[\alpha_{ij}^u\left(\tilde{S}_{ij}^u - \frac{\delta_{ij}}{3}\,\tilde{S}_{kk}\right)\right]},$$

$$m_{ij}^B = \hat{\varphi}_B\hat{\bar{J}}_{ij} - \widehat{\varphi_B\bar{J}_{ij}}.$$

Here, $\widehat{[\,.\,]}$ means that the test filtering operation relates to the whole expression in the square brackets.

Notice that Favre-filtered variables of the problem in the original equations should also be Favre-averaged when the test filtering is applied. The notation $\hat{\tilde{u}}$ is recognized here as $\hat{\tilde{u}} = \widehat{\overline{\rho u}}/\hat{\bar{\rho}}$. The characteristic test filter pass-band, as a rule, in most papers is taken to be twice as high: $\hat{\Delta} = 2\bar{\Delta}$.

It is important to note that constant values may also be negative, which corresponds to the inverse energy transfer cascade (backscatter), i.e., to the energy increase for large-scale flow. To avoid numerical instability, it is necessary to restrict the constant values so as to provide a nonnegative value of the full viscosity (turbulent plus molecular).

3.7 Parametrization of subgrid-scale terms for heat-conducting plasma

When closing the complete system of compressible MHD equations without assuming a polytropic or adiabatic character of this process, the number of terms to be parametrized drastically increases.

The presence of an energy equation in the system of MHD equations (36)–(39) strongly complicates solving the problem by the LES method. Unlike the momentum and magnetic induction equations, fundamentally new SGS terms emerge in the filtered total energy equation, which need be parametrized.

Consider first the subgrid-scale heat flux $Q_j = \bar{\rho}\left(\widetilde{u_jT} - \tilde{u}_j\tilde{T}\right)$. To parametrize this SGS term, the so-called eddy diffusion model is used in the form

$$Q_j = -C_s\,\frac{\bar{\Delta}^2\bar{\rho}|\tilde{S}^u|}{\mathrm{Pr}_\mathrm{T}}\,\frac{\partial\tilde{T}}{\partial x_j}, \tag{75}$$

where C_s is the coefficient determined earlier in the extended Smagorinsky model for the MHD case. The constant C_s is dynamically calculated from formula (72). In expression (75), Pr_T is the turbulent Prandtl number which is also calculated using the dynamical procedure as follows:

$$\mathrm{Pr}_\mathrm{T} = C_s\,\frac{\langle\Upsilon_k\Upsilon_k\rangle}{\langle\Phi_j\Upsilon_j\rangle}. \tag{76}$$

In formula (76), the following notations have been introduced:

$$\Upsilon_j = -\hat{\Delta}^2 \hat{\bar{\rho}}\, |\hat{\tilde{S}}^u|\, \frac{\partial \hat{\tilde{T}}}{\partial x_j} + \widehat{\bar{\Delta}^2 \bar{\rho} |\tilde{S}^u|} \frac{\partial \tilde{T}}{\partial x_j}, \tag{77}$$

$$\Phi_j = \frac{\widehat{\overline{\rho u_j}}\,\widehat{\overline{\rho T}}}{\bar{\rho}} - \frac{\widehat{\overline{\rho u_j}}\,\widehat{\overline{\rho T}}}{\hat{\bar{\rho}}}\,. \tag{78}$$

A nondynamical formulation for Q_j was first proposed in paper [113] to solve the Rayleigh–Benard problem. The dynamical variant of the eddy diffusion model for subgrid-scale thermal flux was demonstrated in paper [43] for LES. The given model (75), based on the eddy diffusion, is similar to the determination of the molecular heat flux; however, the molecular viscosity and Prandtl number were replaced by the dynamical eddy viscosity and turbulent Prandtl number, respectively.

Consider the quantity J_j describing the subgrid-scale turbulent diffusion. The model for $J_j = \bar{\rho}\big(\widetilde{u_j u_k} u_k - \tilde{u}_j \widetilde{u_k u_k}\big)$ was proposed in paper [114]; it can be obtained by analogy with the Reynolds averaging of the Navier–Stokes equations and by assuming $\tilde{u}_i \simeq \tilde{\tilde{u}}_i$. Then, we find for J_j the following expression:

$$J_j \simeq \tilde{u}_k \tau^u_{jk}\,, \tag{79}$$

where the subgrid-scale tensor τ^u_{jk} was set up above.

To finally close the complete system of equations for compressible MHD equations, there is a need to parametrize the SGS terms in energy equation (39), arising due to the magnetic field. To obtain these subgrid-scale models, use is made of the theory relying on the generalized central moments [111]. In papers [58, 62], this approach was extended and applied to the MHD case. The second-order correlation moments read as follows:

$$\varphi(B_i, B_k) = \overline{B_i B_k} - \bar{B}_i \bar{B}_k\,, \tag{80}$$

$$\varphi(u_i, B_k) = \overline{u_i B_k} - \tilde{u}_i \bar{B}_k\,. \tag{81}$$

The third-order correlation moments are given by

$$\varphi(B_i, B_k, u_j) = \big(\overline{B_i B_k u_j} - \bar{B}_i \bar{B}_k \tilde{u}_j\big) - \tilde{u}_j \varphi(B_i, B_k) - \bar{B}_k \varphi(u_j, B_i) - \bar{B}_i \varphi(u_j, B_k)\,. \tag{82}$$

Let us change the subscripts in the above formula:

$$\phi(B_k, B_k, u_j) = \big(\overline{B_k B_k u_j} - \bar{B}_k \bar{B}_k \tilde{u}_j\big) - \tilde{u}_j \phi(B_k, B_k) - \bar{B}_k \phi(u_j, B_k) - \bar{B}_k \phi(u_j, B_k)\,. \tag{83}$$

Using the notations of the subgrid-scale magnetic energy flux (46), we can write

$$\begin{aligned} V_j &= \overline{B_k B_k u_j} - \overline{B_k B_k} \tilde{u}_j \\ &= \overline{B_k B_k u_j} - \bar{B}_k \bar{B}_k \tilde{u}_j - \overline{B_k B_k} \tilde{u}_j + \bar{B}_k \bar{B}_k \tilde{u}_j\,, \end{aligned} \tag{84}$$

from which the following equation can be obtained:

$$V_j = \varphi(B_k, B_k, u_j) + 2\bar{B}_k \varphi(u_j, B_k)\,. \tag{85}$$

The SGS tensor G_j can be expressed in a similar way. Using formulas (82) and (47), we finally arrive at

$$G_j = \varphi(B_j, B_k, u_k) + \bar{B}_k \varphi(u_k, B_j) + \tilde{u}_k \varphi(B_j, B_k) + \bar{B}_j \varphi(u_k, B_k)\,. \tag{86}$$

Below, we will assume that the triple correlation $\varphi(B_j, B_k, u_k)$ in equation (86) can be neglected. The correlation $\varphi(B_j, B_k)$ is not taken into account when simulating the SGS tensor (42) in the momentum equation, because the magnetic moments show much weaker correlation compared with the velocity moments. As shown in paper [53], the model coefficient C_b in the magnetic part of Eqn (42), obtained using the dynamical procedure, is much smaller than C_s, namely, $C_b/C_s \sim 10^{-3}$. The second-order moment $\varphi(u_k, B_k)$ in expression (86) describes correlations in the direction where the velocity vector is collinear with the magnetic field vector and, hence, the Lorentz force is zero along this direction. Thus, it is reasonable to neglect the last term in formula (86). Therefore, the sum of the subgrid-scale tensors V_j and G_j can be represented in the form

$$\frac{1}{2}\, V_j - G_j \simeq \frac{1}{2}\big(2\bar{B}_k \varphi(u_j, B_k)\big) - \bar{B}_k \varphi(u_k, B_j)\,. \tag{87}$$

The subgrid-scale magnetic stress tensor can be expressed as

$$\tau^b_{ij} = \big(\overline{u_i B_j} - \tilde{u}_i \bar{B}_j\big) - \big(\overline{B_i u_j} - \bar{B}_i \tilde{u}_j\big) = \varphi(u_i, B_j) - \varphi(u_j, B_i)\,, \tag{88}$$

which suggests the following subgrid-scale closure for the SGS terms in the total energy equation (39), which arise in electrically conductive fluid due to the presence of a magnetic field, namely, for fluxes of the subgrid-scale magnetic energy V_j and subgrid-scale energy G_j of the magnetic tension interaction with velocity:

$$\frac{1}{2}\, V_j - G_j \simeq \bar{B}_k \tau^b_{jk}\,. \tag{89}$$

Thus, using the subgrid-scale parametrizations elaborated in papers [58, 62] for the system of filtered MHD equations, we obtain the closed system of the LES method for modeling compressible MHD turbulence in heat-conducting fluid.

3.8 Results of numerical simulations for polytropic plasma

In this section, we present the main results of simulations of compressible MHD flows by the LES method applying different subgrid-scale parametrizations. The analysis is carried out by comparing the LES results obtained with direct numerical simulations [60].

The LES method was realized in papers [57, 60, 61, 63] for the five subgrid-scale models formulated in Section 3.7. Different properties of compressible MHD turbulence at different similarity numbers were examined. Details of the numerical simulations, filtered equations, as well as the algorithm, boundary and initial conditions, numerical grid, and other aspects of compressible MHD simulations are discussed in paper [60].

In time integration, a modified explicit third-order in accuracy Runge–Kutta method (proposed by Williamson [115]) was utilized, which requires less random-access memory (RAM) compared with the standard low-storage Runge–Kutta method. In this modified Runge–Kutta

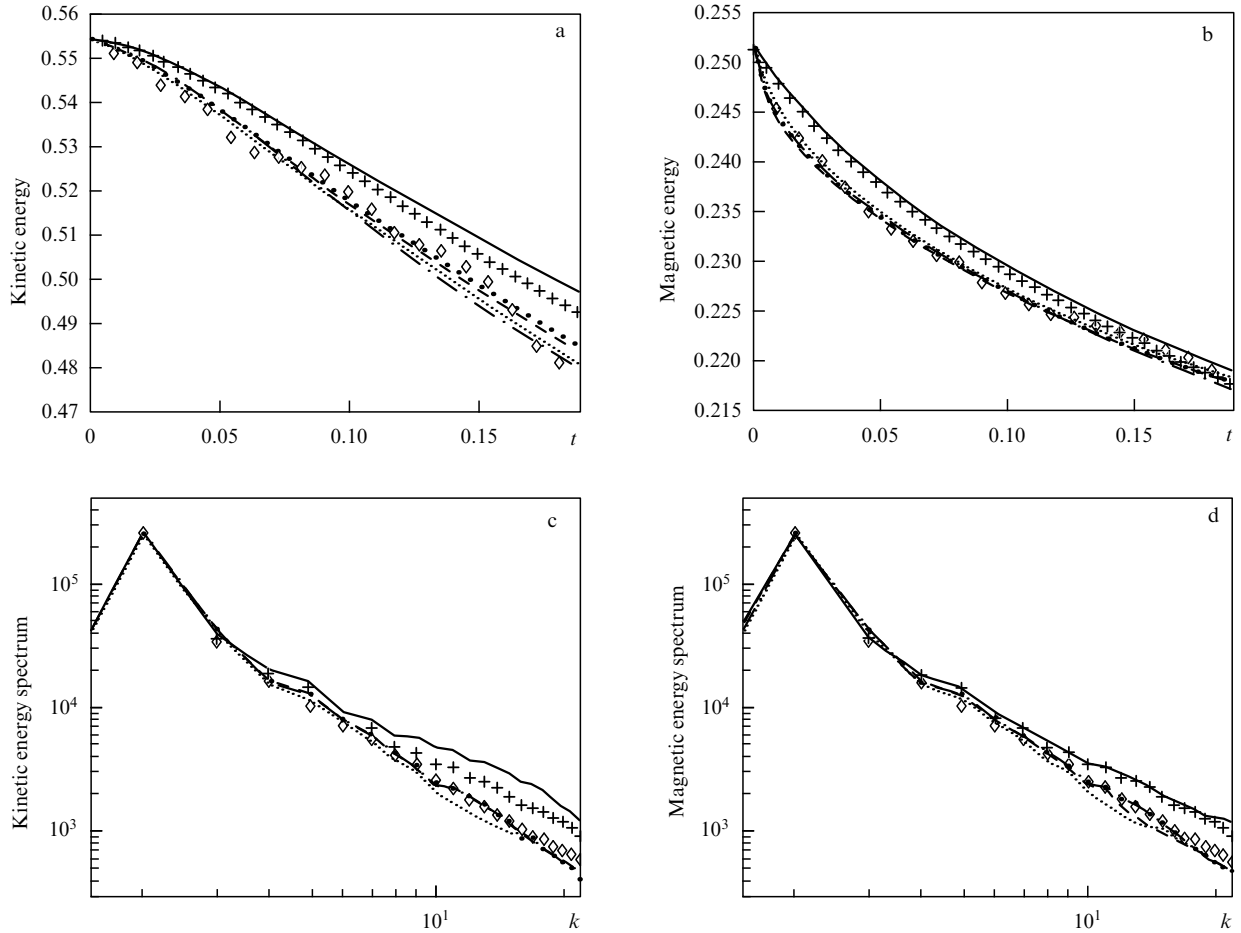

Figure 2. (a, b) Temporal dynamics of the kinetic (a) and magnetic (b) energies. (c, d) Spectra of the kinetic (c) and magnetic (d) energies. The solid lines correspond to the case where the subgrid-scale tensors τ_{ij}^{u} and τ_{ij}^{b} are omitted, i.e., LES is, in fact, DNS on the rough LES mesh; this case is presented here for a more complete analysis and understanding of the influence of subgrid-scale closures on simulations of MHD flows when comparing DNS results with those obtained for different SGS models. The dashed, dotted, black point, plus mark, and dashed-dotted lines correspond to the Smagorinsky model for MHD flows, the extended Kolmogorov model for magnetic hydrodynamics, the cross-helicity model, the scale-similarity model, and the mixed model for the MHD case, respectively. DNS results are shown by diamond lines.

method, only two sets of variables should be allocated in RAM. Such a numerical approach is applicable for arbitrary high order in accuracy, although not all Runge–Kutta schemes can be written in the modified form [115, 116]. The numerical code with fourth-order finite difference schemes is used for modeling compressible MHD turbulence. For most MHD problems [84, 117–119], different spectral methods (usually devised for an incompressible fluid) were utilized. However, use is made of the finite-difference approach in the present study, which, unlike the spectral method, is more effective when solving problems with complex geometry and with different boundary conditions; it also requires fewer computer resources and less computational time [103, 120].

A numerical code was designed and realized in papers [57, 60, 61, 63] to solve MHD equations written in the conservative form. However, nonlinear terms are written in the skew-symmetrical form:

$$\Psi_i^{\mathrm{d}} = \frac{\partial \rho u_i u_j}{\partial x_j}\,,$$
$$\Psi_i^{\mathrm{a}} = \rho u_j \frac{\partial u_i}{\partial x_j} + u_i \frac{\partial \rho u_j}{\partial x_j}\,, \tag{90}$$
$$\Psi_i^{\mathrm{s}} = \frac{1}{2}(\Psi_i^{\mathrm{d}} + \Psi_i^{\mathrm{a}})\,.$$

Expressions (90) demonstrate how the skew-symmetrical form Ψ_i^{s} can be obtained. The skew-symmetrical form represents, in fact, the result of taking an average between the divergent (Ψ_i^{d}) and convective (Ψ_i^{a}) forms of the nonlinear term. Although analytically all three forms — the skew-symmetrical, divergent and convective — are equivalent, the results of numerical simulations will be different. As shown in paper [121], the skew-symmetrical form provides more accurate results, since errors related to the discretization in the finite-difference simulations of turbulent flows decrease.

To resolve a turbulent flow into large-scale and small-scale eddies, the fourth-order in accuracy Gaussian filter is applied. In paper [101], optimal discrete forms of the cylinder filter and Gaussian filter for central difference schemes of various orders in accuracy were studied in detail. The one-dimensional filter (for the x-direction) is written out as follows:

$$\bar{\zeta}_i = \frac{\epsilon^4 - 4\epsilon^2}{1152}(\zeta_{i-2} + \zeta_{i+2}) + \frac{16\epsilon^2 - \epsilon^4}{288}(\zeta_{i-1} + \zeta_{i+1}) + \frac{\epsilon^4 - 20\epsilon^2 + 192}{192}\,\zeta_i\,, \tag{91}$$

where ζ_i is the characteristic of the fluid flow at point i, and ϵ is the parameter defined as the ratio of the mesh size to the

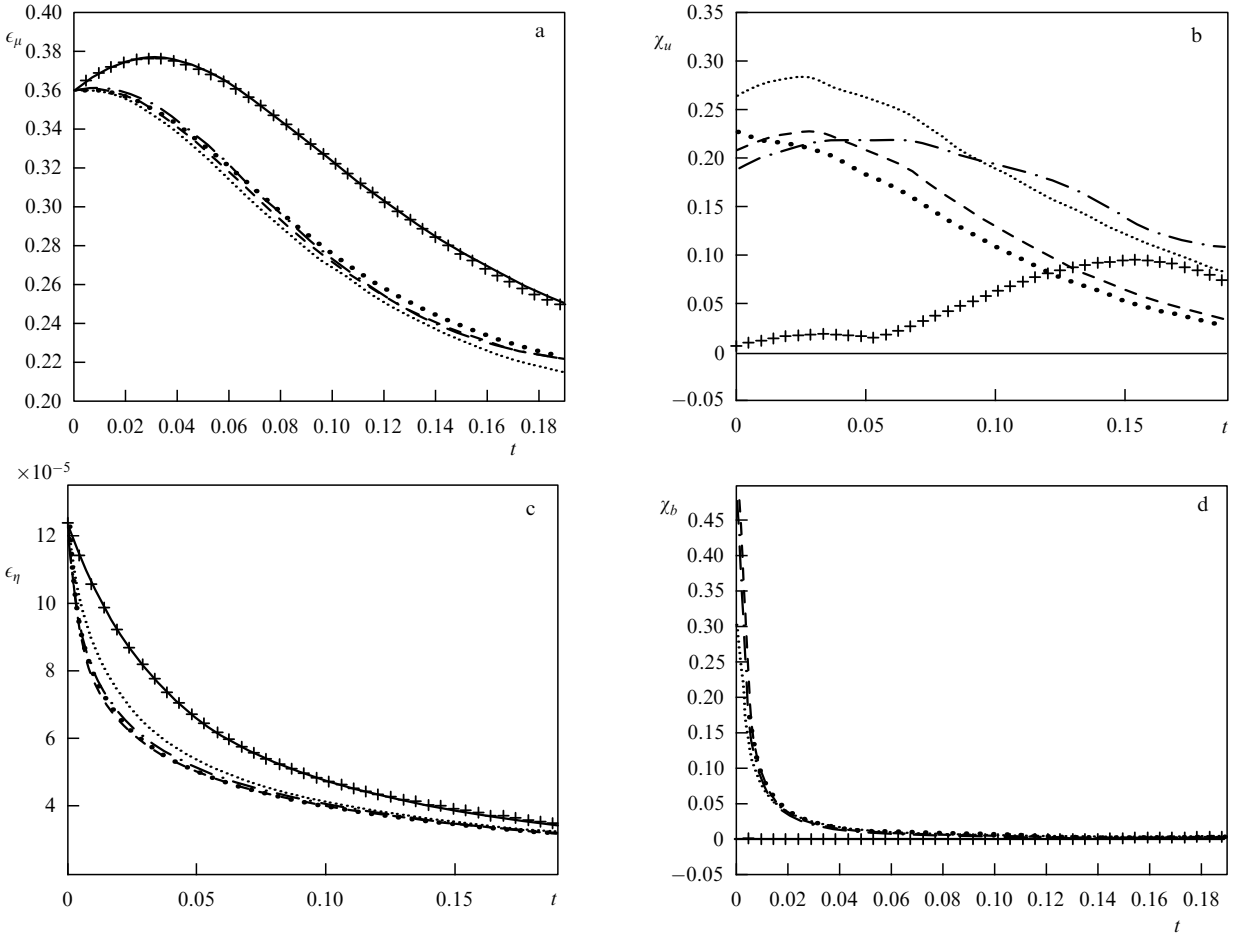

Figure 3. Temporal dynamics of energy dissipation (notation is the same as in Fig. 2).

cut-off lengthscale of the filter [101]. Constants in subgrid-scale models are specified using the dynamical procedure. For this purpose, an additional test filter twice as wide as the original pass-band is used. Because three-dimensional turbulent MHD flow is studied, formula (21) is applied in the three-dimensional filtering.

The LES results are being compared to the DNS calculated results, and the quality of LES is determined by the difference between the filtered DNS and LES results. The DNS and LES results were obtained using the grids with discretization densities of 256^3 and 64^3, respectively. The simulation domain was taken as a cube with the dimensions $2\pi \times 2\pi \times 2\pi$. The initial conditions for LES are found by filtering the DNS initial conditions. The initial conditions are chosen so as to provide the magnetic field solenoidity, i.e., so that the condition $\operatorname{div} \mathbf{B} = 0$ is fulfilled. The Courant–Friedrichs–Lewy (CFL) condition was involved in simulations to restrict the time step for maintaining stable calculations. Periodic boundary conditions were established at all boundaries of the calculation domain.

Figures 2a, b show the time evolution of the kinetic and magnetic energies. The main goal of the subgrid-scale closures is to adequately describe the energy dissipation of large-scale motion. As expected, the results obtained in the case without subgrid-scale models turn out to be the least precise as compared with the DNS data. As seen from Figs 2a and 2b, the Kolmogorov model demonstrates the least accurate results among other subgrid-scale models. An especially strong deviation is observed at the initial time intervals, as is seen in Fig. 2b for the magnetic energy, and in Fig. 2a for the kinetic energy. The scale-similarity model demonstrates the deficit of dissipation energy in both Fig. 2a and Fig. 2b, similarly to the case of hydrodynamic turbulence in a neutral fluid [122]. Other subgrid-scale parametrizations significantly improve the accuracy of calculations.

In the magnetic hydrodynamics of an electrically charged fluid, both the temporal dynamics of the magnetic and kinetic energies and the evolution of the magnetic field and velocity field cross-helicities are important. In this case, as for the kinetic and magnetic energies, the model without subgrid-scale parametrization and the scale-similarity model are less precise [60]. Other models provide better agreement with DNS results (Fig. 2c, d).

In Fig. 3a, shown is the molecular dissipation $\epsilon_\mu = 2\mu \tilde{S}_{ij}\tilde{S}_{ij}$, which is always positive, as a function of time. Figure 3b presents the time evolution of the subgrid-scale kinetic dissipation defined as $\chi_u = -\tau^u_{ij}\tilde{S}_{ij}$ and chosen such that the filtered kinetic energy decreases when $\chi_u > 0$, and increases when $\chi_u < 0$ (corresponds to the energy back-scatter). The value of χ_u determines the amount of energy transferred from the large-scale part to subgrid scales, and χ_u depends on the SGS model that is used to find the subgrid-scale tensor τ^u_{ij}. In Fig. 3b, the subgrid-scale dissipation for the case without SGS parametrization is absent, since here the subgrid-scale parametrization is not used. As seen from this figure, the subgrid-scale energy dissipation in the scale-similarity model until the time $t = 0.13$ is minimal; therefore, such a model does not provide adequately the kinetic

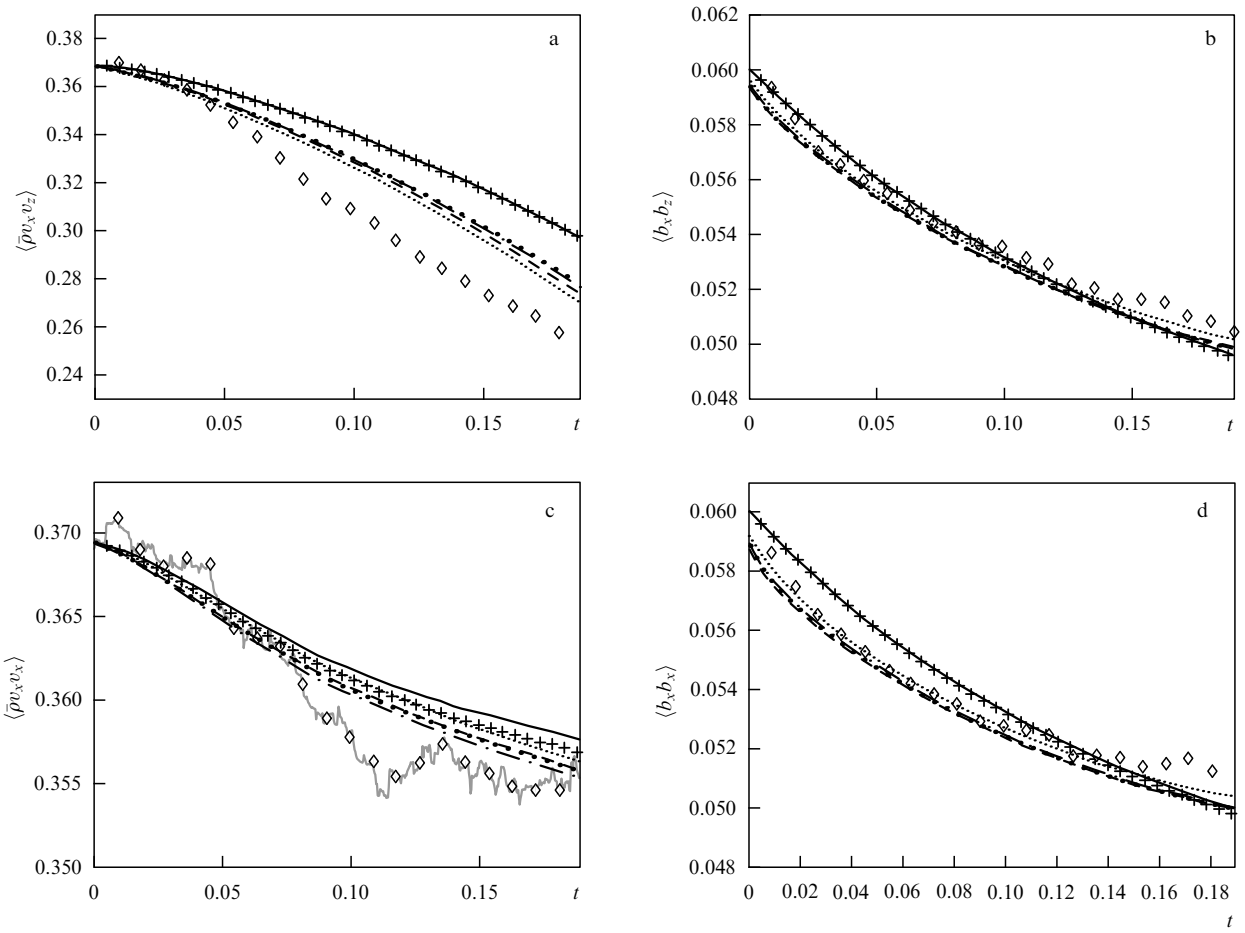

Figure 4. Temporal dynamics of turbulent stresses (notation is the same as in Fig. 2).

energy dissipation, and in Fig. 2a the scale-similarity model, like the case without subgrid-scale parametrizations, demonstrates the worst results. The deficit of the subgrid-scale dissipation is partially compensated by the fact that, as seen from Fig. 3a, molecular dissipations of the scale-similarity model have a somewhat higher value at the initial time interval, even without SGS closures, than other models. The highest value of the subgrid-scale kinetic energy is demonstrated by the Smagorinsky and mixed models.

The magnetic molecular dissipation of the turbulent field is found from the relationship $\epsilon_\eta = \eta|\bar{j}|^2$, and its temporal behavior is presented in Fig. 3c. The magnetic subgrid-scale dissipation (Fig. 3d) is defined as $\chi_b = -\tau^b_{ij}\bar{J}_{ij}$ and also represents a large-scale energy decrease due to the subgrid-scale effects, with the direct energy transfer cascade being observed for $\chi_b > 0$, and the energy backscatter for $\chi_b < 0$. As in the case of the kinetic energy, the molecular magnetic dissipation is somewhat larger for the scale-similarity model and for models without SGS parametrization, whereas the subgrid-scale magnetic energy is much smaller for the scale-similarity model than for other models (in the case without SGS closure it is, of course, equal to zero). These plots are in good agreement with the magnetic energy plot shown in Fig. 2b, where, after $t = 0.1$, the difference between DNS results and various SGS closures is insignificant, and in Fig. 3d, after $t = 0.1$, the subgrid-scale magnetic dissipation for all models is almost the same and is much smaller than at the initial stage of calculations.

Let us define the fluctuating part of the velocity as $v_i = \tilde{u}_i - \langle \bar{\rho}\tilde{u}_i \rangle / \langle \bar{\rho} \rangle$, and the fluctuating part of a magnetic field as $b_i = \tilde{B}_i - \langle \tilde{B}_i \rangle$, and let us compare the results of the subgrid-scale models with DNS results for turbulent stresses. The angle brackets $\langle\,.\,\rangle$ denote spatial averaging. Figures 4c and 4a show the time evolution of $\langle \bar{\rho} v_x v_x \rangle$ and turbulent stress tensor components $\langle \bar{\rho} v_x v_z \rangle$, respectively. Clearly, the turbulent tension in DNS dissipates more strongly, with $\langle \bar{\rho} v_x v_z \rangle$ demonstrating strong oscillations (shown in Fig. 4c by the gray line for clarity). Similarly to the energy, the results of calculations without applying subgrid-scale parametrization demonstrate maximum deviation from DNS results. Shown in Figs 4b, 4d are the magnetic turbulent stresses $\langle b_x b_z \rangle$ and $\langle b_x b_x \rangle$, respectively; the dissipation in DNS calculations with increasing time is slightly smaller than in LES. After $t = 0.15$, the Smagorinsky model turns out to be the least dissipative for magnetic turbulent stresses, even smaller than in the case without an SGS closure.

To understand the structure of a turbulent MHD flow, its statistical properties, and the intermittence of the motion considered, the skewness and flatness of turbulent flows that characterize the anisotropy of the considered fluid flow are important parameters. The skewness and flatness for the velocity components are defined as

$$Su_j = \frac{\langle u_j^3 \rangle}{\left(\langle u_j^2 \rangle\right)^{3/2}}\,, \qquad Ku_j = \frac{\langle u_j^4 \rangle}{\left(\langle u_j^2 \rangle\right)^{2}}\,, \tag{92}$$

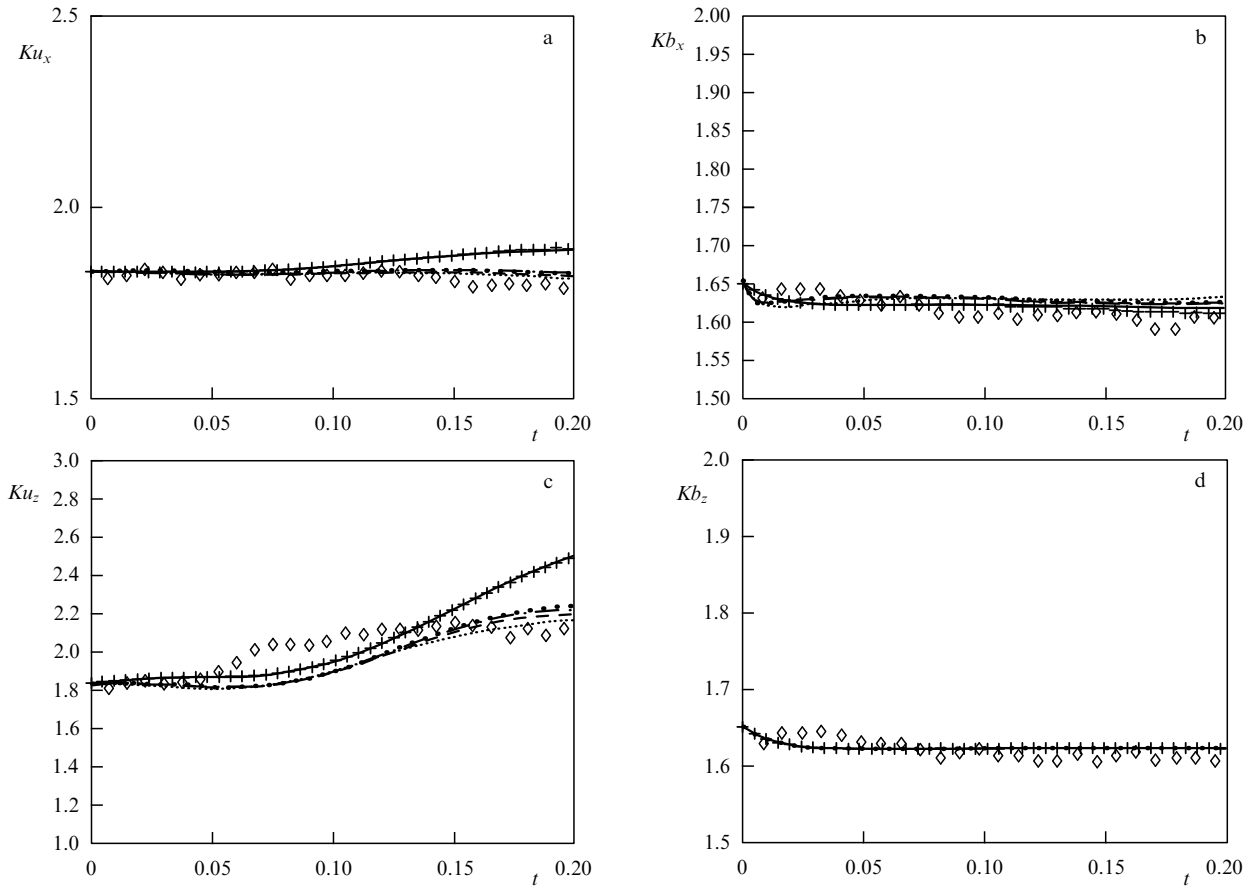

Figure 5. Temporal dynamics of flatness (notation is the same as in Fig. 2).

respectively. The skewness and flatness for the magnetic field have the corresponding forms

$$Sb_j = \frac{\langle B_j^3 \rangle}{\left(\langle B_j^2 \rangle\right)^{3/2}}\,, \qquad Kb_j = \frac{\langle B_j^4 \rangle}{\left(\langle B_j^2 \rangle\right)^{2}}\,, \tag{93}$$

respectively.

Figure 5 displays a comparison of different subgrid-scale LES models with DNS for flatness. Whereas for the magnetic field the results demonstrate almost no dispersion and all models virtually coincide with DNS results, the choice of the subfilter-scale parametrization for the velocity is more significant. Figure 6 presents the time evolution of the skewness. It is interesting to note that the skewness of magnetic fields, Sb_x and Sb_y (Fig. 6b, d), and velocities, Su_x and Su_z (Fig. 6a, c), for the scale-similarity model and for the case disregarding SGS closure, oppositely, turn out to be closer to DNS results.

Paper [63] investigates in detail the skewness, the flatness of the velocity components and the magnetic field components at different Reynolds numbers, the sonic Mach number, and the magnetic Reynolds number. It is shown that the Smagorinsky model for the MHD case and the model based on cross-helicity between the velocity and magnetic field are the most suitable for the study of flatness and skewness of the components of the velocity and the magnetic field. Numerical results indicate that the velocity flatness and skewness are more susceptible to the subgrid-scale parametrization choice than analogous characteristics of a magnetic field. As a result, the LES method was shown to provide adequate results and can be applied to study characteristics of the intermittency (for example, the structure functions of different moments of the velocity and magnetic field) of compressible MHD flows at different similarity numbers [63].

An important test for the LES method involves analyzing the spectral distribution of the kinetic and magnetic energies, which characterizes the energy redistribution as a function of the wave vector k (i.e., depending on scale). In addition, the spectrum allows the subgrid-scale closure effects to be assessed in compressible MHD flow simulations. Figure 2c, d presents the spectra of kinetic and magnetic energies, respectively. It can be noticed that on large scales (corresponding to small wave vectors) all plots almost coincide, and there is virtually no difference among results calculated with different subgrid-scale models. This means that the largest turbulent scales are almost independent of the SGS parametrizations. Differences arise mainly on small scales (at high k numbers). Generally, the energy spectrum confirms the earlier results for subgrid-scale closures. The DNS spectrum is consistent with the Smagorinsky modes, Kolmogorov model, the mixed model and cross-helicity based model, especially with the last two subgrid-scale models. Moreover, it is seen that in simulations utilizing the scale-similarity model and ignoring subgrid-scale terms, insufficient energy dissipation is obtained, i.e., these models are characterized by the energy accumulation at large wave vectors due to ineffective dissipation. These conclusions drawn from the energy spectrum confirm the results obtained from the temporal dynamics of kinetic and magnetic energies.

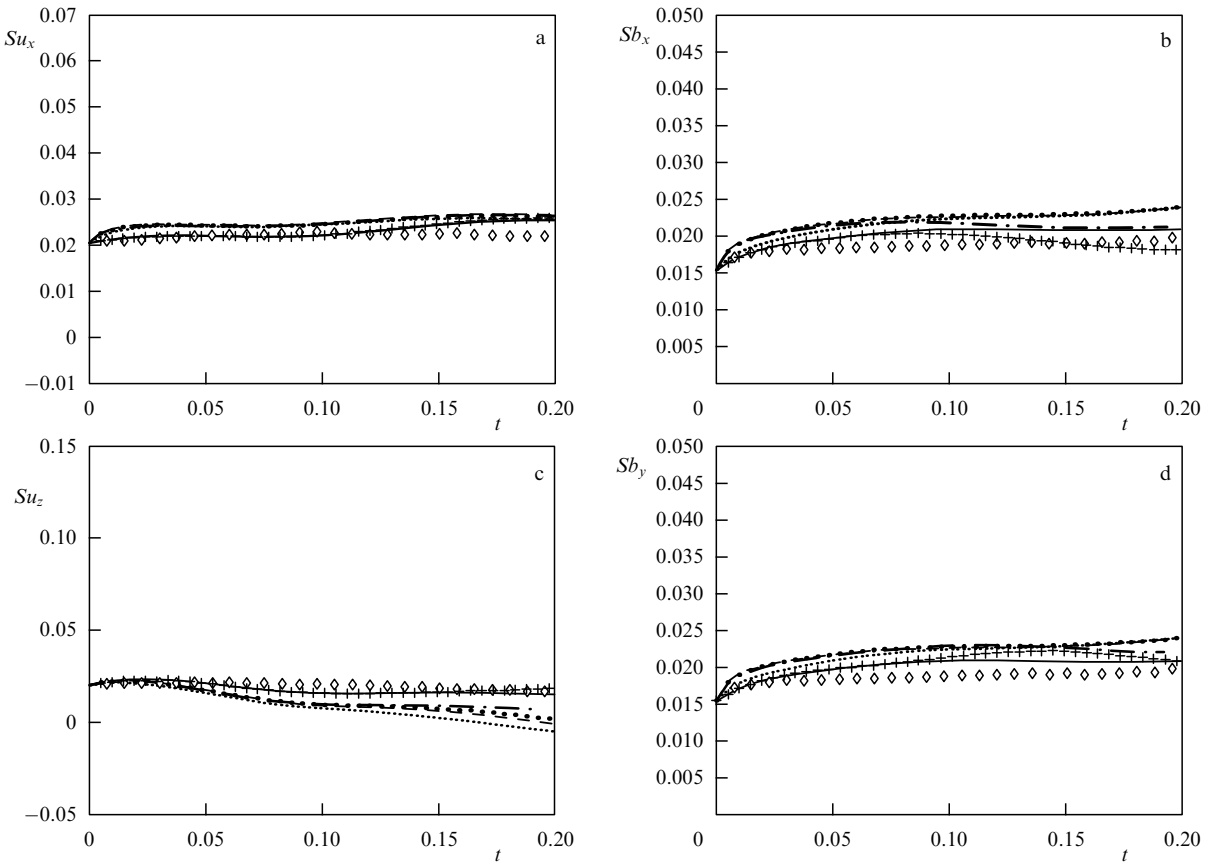

Figure 6. Temporal dynamics of skewness (notation is the same as in Fig. 2).

As shown in paper [60], when the magnetic Reynolds number Re_m decreases, the difference among subgrid-scale models diminishes for the magnetic energy, and all models considered demonstrate good agreement with DNS results at small Re_m. With a rising Reynolds number, the role of subgrid-scale closures in simulations of compressible MHD turbulence increases, and the rate of magnetic energy dissipation decreases. The Smagorinsky model, Kolmogorov model, and cross-helicity model demonstrate the best results for the magnetic energy evolution. The same behavior is evidenced for the cross-helicity: the role of subgrid-scale parameters increases with rising Re_m. When decreasing a magnetic Reynolds number, LES results show a large difference in the kinetic energy behavior for different SGS parametrizations. The scale-similarity model demonstrates the worst outcomes, while other SGS closures increase the accuracy of simulations [60]. The temporal dynamics of turbulent stresses, both magnetic and kinetic, are affected more strongly by the SGS parametrization in LES simulations of MHD turbulence with increasing Re_m. The role of anisotropy in simulations and discrepancy between LES and DNS results for anisotropy become stronger with decreasing a magnetic Reynolds number. It should be emphasized that the kinetic energy decreases more sharply, and the magnetic energy, in contrast, decreases more slowly with an increase in magnetic Reynolds number Re_m. Similar results were reported in paper [83], where the influence of Re_m on two-dimensional MHD turbulence was studied by the DNS method.

As the Taylor's Reynolds number Re_λ changes, the results of simulations are qualitatively similar. This is because the similar initial conditions for the magnetic field and the velocity field did not change, so in the simulations the Taylor's Reynolds number only weakly affects the choice of subgrid-scale parametrization [60]. The subgrid-scale Smagorinsky, Kolmogorov, mixed, and velocity and magnetic field cross-helicity models demonstrate adequate results and good agreement with DNS results.

The Mach number M_s significantly affects the simulation results. As M_s increases, DNS and LES results for the kinetic energy strongly diverge. For kinetic energy, the Smagorinsky model and the cross-helicity model demonstrate the best agreement with DNS results at different Mach numbers [60]. Conversely, magnetic energy is observed to diminish discrepancy between calculated results with increasing M_s. It should be noted that the magnetic energy more rapidly tends to a constant value with decreasing Mach number. For the cross-helicity of the magnetic field and velocity, the Smagorinsky model shows the best results for both high and low Mach numbers. The skewness of velocity components calculated in LES is in better agreement with DNS results as M_s increases. The choice of SGS parametrization barely affects the skewness of the magnetic field components. With increasing a Mach number, turbulent stresses in LES are in better agreement with DNS results [60].

In general, the subgrid-scale models have the least effect on the temporal evolution of the flatness and skewness (the model without subgrid-scale closures also demonstrates good agreement with DNS results) [60, 63]. This is due to the anisotropy and intermittency being properties of large-scale structures, while discrepancies among SGS models and models without subgrid-scale closures arise on small scales of the turbulent flow.

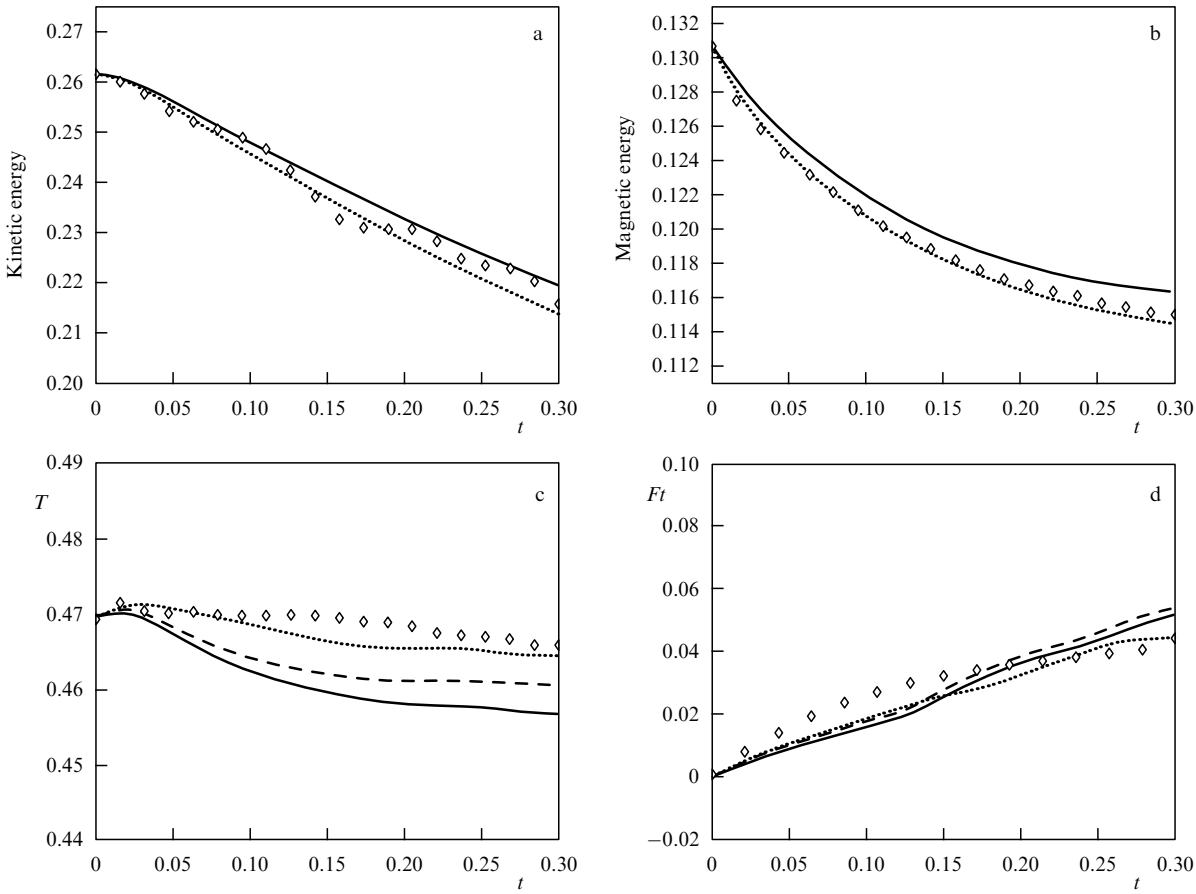

Figure 7. Temporal evolution of the kinetic energy (a), the magnetic energy (b), and the temperature (c) for $M_s = 0.38$. Time evolution of the parameter Ft for $M_s = 0.38$ (d). Diamonds show the DNS results, solid lines indicate the LES results without subgrid-scale closures, dotted lines show LES results with all SGS parametrizations, and dashed lines mark LES results without SGS parametrizations in the energy equation.

On the whole, the best results are obtained with the Smagorinsky model for the MHD case and with the model based on the cross-helicity of the magnetic field and velocity field [60]. The scale-similarity model does not provide sufficient kinetic or magnetic energy dissipation, and this model should be used only along with the eddy viscosity models (for example, the Smagorinsky model), which is the basic idea of the mixed model.

3.9 Results of numerical simulations of a heat-conducting plasma

Results of LES simulations of compressible MHD turbulence in heat-conducting plasma at different Mach numbers are presented in papers [58, 62]. The obtained numerical LES results are compared with direct numerical simulations of heat-conducting plasma.

Numerical methods, algorithms, diagrams, and the filtering function for resolving turbulence into small-scale and large-scale parts, which are utilized in LES and DNS of compressible MHD flows, are described in detail in paper [62], where the extended Smagorinsky model for magnetohydrodynamics was used in subgrid-scale parametrization of tensors τ^u_{ij} and τ^b_{ij}. Because the compressibility effects and temporal dynamics of the temperature, as determined from the total energy equation, depend nontrivially on the Mach number, paper [62] reported on three cases considered: the Mach number is $M_s = 0.38$, i.e., a mildly compressible flow; the Mach number is $M_s = 0.65$, i.e., the compressibility plays a significant role, and $M_s = 1.45$, which corresponds to the appearance of strong discontinuities in a substantially compressible flow.

The temporal dynamics of the kinetic and magnetic energy for flows with Mach number $M_s = 0.38$ is presented in Figs 7a and 7b, respectively. For a deeper understanding of the subgrid-scale model effects on the energy equation, the SGS terms are omitted in the total energy equation, and only subgrid-scale tensors in the momentum equation and the magnetic induction equation are evaluated.

As seen from Fig. 7a, b, taking account of the subgrid-scale parametrizations for kinetic and magnetic energies brings the LES curve closer to the DNS curve; consequently, the accuracy of simulations increases. The subgrid-scale closures in the total energy equation do not, in fact, affect the time evolution of the kinetic and magnetic energies. The plots suggest that the curves for the case that includes all parametrizations coincide with curves corresponding to parametrizations in magnetic induction and momentum equations only. A similar behavior is observed for cross-helicity between the magnetic field and velocity [62]. Subgrid-scale models for SGS tensors (42) and (43) noticeably increase the accuracy of simulations. As in the case of the magnetic and kinetic energies, the subgrid-scale parametrizations in the energy equation do not affect the time evolution of the cross-helicity.

Figure 7c demonstrates the temporal behavior of mean temperature. Unlike the magnetic and kinetic energy

dynamics, the inclusion of SGS parametrizations in the total energy equation significantly affects the results of numerical simulations. As seen from Fig. 7c, the most accurate results for the mean temperature are achieved when all subgrid-scale closures are taken into account in the complete system of filtered MHD equations. When all SGS parametrizations are neglected, the largest deviations from DNS results are obtained.

In paper [63], the influence of different parametrizations and similarity numbers on the skewness, flatness of the components of the magnetic field, and velocities is considered in detail. Whereas previous paper [62] focused on the temperature behavior (in other words, on the total energy equation) especially, as shown above, because the subgrid-scale terms in the energy equation have almost no effect on the calculation accuracy of the kinetic and magnetic energies. The temperature asymmetry weakly grows with time, and discrepancies among plots for all LES cases are small. This fact implies that the anisotropy (basically, the property of large-scale structures) and discrepancies between SGS closures and the model without subgrid-scale parametrizations mainly arise on small scales of a turbulent flow [62].

To better understand the behavior of temperature and its fluctuations at different Mach numbers depending on the SGS closures, let us define the parameter characterizing the temperature fluctuations as follows:

$$Ft = \left[\left\langle (T - \langle T \rangle)^2 \right\rangle\right]^{1/2} . \tag{94}$$

The parameter Ft is plotted in Fig. 7d as a function of time. More accurate results of numerical simulations are obtained for LES taking into account all subgrid-scale closures, which shows once again the importance of the subgrid-scale models in the total energy equation [62].

It should be noted that, as the Mach number M_s increases, the influence of viscosity and the role of nonlinear effects enhance, which leads to strengthening oscillations and fluctuations of characteristics of a turbulent flow [62].

It was ascertained that taking account of the subgrid-scale terms in the total energy equation has almost no effect on the kinetic and magnetic energies even at very high Mach numbers, while for the temperature (and, correspondingly, for the internal energy) the inclusion of SGS models in the total energy equation is an important condition to increase the calculation accuracy of thermodynamic variables [58, 62]. With increasing a Mach number, the kinetic energy and temperature oscillations grow. Generally, the LES method, including explicit density-weighted filtering, demonstrates good results in modeling electrically charged and heat-conducting plasmas in compressible magnetohydrodynamic turbulence at various Mach numbers.

4. Study of the local interstellar medium turbulence using subgrid-scale modeling

In this section, we present an MHD model for the local interstellar medium and the characteristic quantities that are utilized in the numerical modeling of compressible MHD turbulence using large eddy simulations.

The interstellar medium includes matter and the fields observed in the space between stars inside galaxies. Only comparatively recently was it recognized that stars do not exist in a vacuum and that the outer space is not completely transparent. The presence of an absorbing rarefied medium was convincingly revealed less than 100 years ago, in the first half of the 20th century, by comparing the observed properties of remote star clusters at different distances. The interstellar medium in our Galaxy, in the proximity of the Solar System, is referred to as the local interstellar medium. The Galactic interstellar medium strongly affects the Solar System. The parameters of this gas significantly determine the structure of the heliosphere, i.e., the region filled with the solar wind.

A strongly ionized gas under cosmic conditions undergoes continuous irregular motion. Even in regular flows (for example, differential rotations, solar/stellar wind outflow, accretion), fluctuations are present. The gas velocity then represents a random field, with its magnitude and direction changing chaotically. Abundance of turbulence under cosmic conditions, namely in the interstellar medium, is ubiquitous mainly because the Reynolds numbers are typically extremely high due to the huge sizes of most of the space objects.

Around sufficiently powerful energy sources, when the flow velocity exceeds the propagation speed of any linear perturbations in the medium considered (i.e., the sound and Alfvénic velocities), turbulence becomes supersonic. The analysis of observational data [90] suggests power-law spectra for velocity and density fluctuations, close to the Kolmogorov–Obukhov law [123–126]. Large-scale motions of gas and the stellar subsystem, as well as active phenomena in stars and stellar clusters, compose the main sources of energy and momentum of MHD turbulence in the interstellar medium [127]. The results obtained by satellites were unexpected, since Kolmogorov-like spectrum $k^{-5/3}$ was theoretically derived for an incompressible fluid, whereas the interstellar turbulence is magnetohydrodynamic and essentially compressible. Therefore, the main issue consists in understanding the reasons why the Kolmogorov spectrum for density and kinetic energy fluctuations is produced in the local interstellar turbulence. The solution to this problem is significantly complicated because the interstellar medium cannot be directly observed and probed in experiments; numerical simulations of MHD turbulence on space scales are limited by modern computational capacities of computers, since these processes are characterized by very high Reynolds numbers and, hence, very high numbers of degrees of freedom of the turbulent motion. For such flows in the local interstellar medium, it is convenient to apply the LES method described above for compressible MHD turbulence. In paper [94], the interstellar turbulence was studied for the first time by the LES method, which allowed new results on the density and energy fluctuation spectra of the MHD turbulence to be obtained.

Statistically homogeneous isotropic plasma in the local interstellar medium is described by the one-fluid MHD model for polytropic plasma [94].

Quantities that arise after normalization when reducing the original equations to the dimensionless form are due to large-scale plasma motions. In addition, there are turbulent velocities, the Mach and Reynolds numbers that depend locally on small-scale structures and relatively high frequency fluctuations. The large-scale flow, or steady mean background flow, leads, as a rule, to a constant Mach number, while fluctuating local eddies change the Mach number that depends on the local properties of small-scale turbulent pulsations.

Let us define the sound velocity for the small-scale turbulent flows as

$$\breve{c}_{\mathrm{s}} = \sqrt{\gamma}\,\rho^{(\gamma-1)/2}\,, \tag{95}$$

and the hydrodynamic turbulence Mach number as

$$\breve{\mathrm{M}}_{\mathrm{s}} = \frac{\sqrt{\langle |u|^2 \rangle}}{\breve{c}_{\mathrm{s}}}\,. \tag{96}$$

The fluctuating Alfvén velocity is $\breve{u}_{\mathrm{a}} = \breve{B}/\sqrt{4\pi\breve{\rho}}$; therefore, the turbulent Alfvén Mach number is written out as

$$\breve{\mathrm{M}}_{\mathrm{a}} = \frac{\sqrt{\langle |u|^2 \rangle}}{\breve{u}_{\mathrm{a}}}\,. \tag{97}$$

Here, $u_{\mathrm{rms}} = \sqrt{\langle |u|^2 \rangle}$ is the rms velocity. The turbulent Reynolds number and plasma parameter $\breve{\beta}$ are defined in a similar way. Notice that the evolution study of the local values of these quantities is important for understanding fluctuations of characteristics of turbulent MHD flows in the local interstellar medium.

To study compressible turbulence in the local interstellar medium, three-dimensional numerical simulation of decaying MHD turbulence is carried out. Numerical methods, schemes, and algorithms are described in detail in papers [64, 94]. In the study of the local interstellar turbulence, the LES method is applied to solve the system of compressible MHD turbulence equations (22)–(24); the extended Smagorinsky model for the MHD case, which, as shown in Section 3, demonstrated sufficiently accurate results at different similarity numbers, was utilized for subgrid-scale parametrization. The initial isotropic turbulent spectra for the kinetic and magnetic energies are defined in the Fourier domain and are chosen to be close to the spectrum k^{-2} with random amplitudes and phases along all three directions. The choice of exactly this spectrum as the initial conditions is due to the velocity perturbations in the Fourier domain being analogous to perturbations in the developed turbulence, and thus it can be used to model the developed turbulence at the initial time [4, 128]. The choice of the k^{-2} spectrum (the Burgers turbulence spectrum) is also physically determined by its rapid convergence to the k^{-3} spectrum via direct energy transfer cascade in hydrodynamic turbulence [89]. In addition, discontinuous shocks will also have a similar energy spectrum (due to the Fourier transform of the step function), and the Fourier transformation of the discontinuous shocks will not alter this spectrum. Nevertheless, most of the distributions with the k^{-2} spectrum do not involve shocks [4, 129]. Then, using the inverse Fourier transform, the initial conditions for the velocity and magnetic field were obtained. The computational domain represents a three-dimensional cube with a linear size π. In LES, a mesh with discretization density of 64^3 was used. The initial hydrodynamic Reynolds number is $\mathrm{Re} \approx 1000$, and the magnetic Reynolds number is $\mathrm{Re_m} \approx 200$. The Re number is taken to be larger than $\mathrm{Re_m}$, since the ambipolar diffusion effects may arise in the interstellar medium, which enhances the magnetic diffusion and, hence, decreases the $\mathrm{Re_m}$ number [29]. Other parameters that were used in modeling turbulence in the local interstellar medium were taken to be as follows: the Alfvén Mach number and sonic Mach number are $\mathrm{M_a} \approx \mathrm{M_s} \approx 2.2$, the specific heat capacity ratio is $\gamma = 5/3$, the time step is $\mathrm{d}t = 0.3 \times 10^{-3}$. The periodic boundary conditions were respected at all boundaries of the computational domain. Small changes in the initial conditions do not affect the results of calculations. Similar conclusions about the insignificant influence of the initial parameters were attained in paper [79].

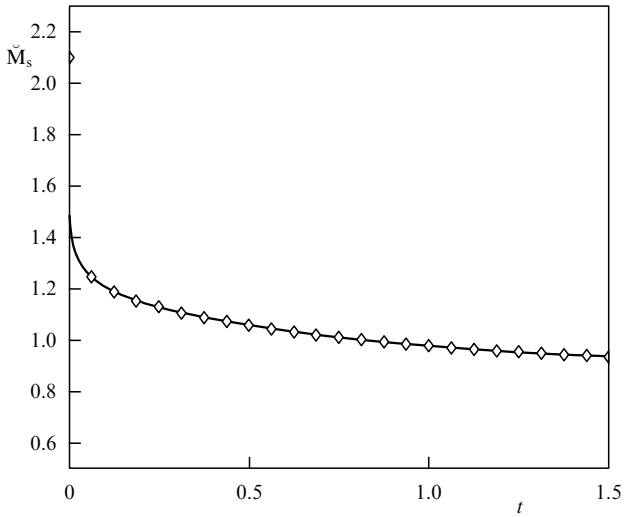

Figure 8. Decay of the small-scale turbulent Mach number $\breve{\mathrm{M}}_{\mathrm{s}}$ with time. The transition from supersonic regime $\breve{\mathrm{M}}_{\mathrm{s}} > 1$ to subsonic regime $\breve{\mathrm{M}}_{\mathrm{s}} < 1$ is seen.

4.1 Analysis of the results of simulations and theoretical interpretation

In this section, results of simulations of compressible MHD turbulence in the local interstellar medium by the large eddy simulation method are presented. Numerical results are analyzed and their theoretical justifications are given.

4.1.1 Compressibility properties of the medium. Compressible MHD turbulence evolves due to nonlinear interactions in which larger eddies transfer energy to smaller ones via direct turbulent energy cascades. MHD turbulence dissipates owing to the finite value of the Reynolds number and small-scale motion decay, because viscous shear stresses perform work. The time evolution of the hydrodynamic turbulence Mach number $\breve{\mathrm{M}}_{\mathrm{s}}$ is shown in Fig. 8. It is seen that the local small-scale Mach number decays from a supersonic value ($\breve{\mathrm{M}}_{\mathrm{s}} > 1$) to a subsonic value ($\breve{\mathrm{M}}_{\mathrm{s}} < 1$). This fact indicates that the turbulent cascade related to nonlinear interactions in combination with dissipative effects on small scales leads to the result that supersonic plasma fluctuations experience sufficiently strong decay to subsonic fluctuations in an electrically conducting flow, and turbulence becomes moderately compressible. In Fig. 9, the time evolution of the velocity divergence, $\operatorname{div}\mathbf{u} = \partial u_1/\partial x_1 + \partial u_2/\partial x_2 + \partial u_3/\partial x_3$, is plotted. In incompressible fluid, the condition $\operatorname{div}\mathbf{u} = 0$ is fulfilled according to the continuity equation. As seen from Fig. 9, the velocity divergence decays sufficiently fast and tends to zero (but does not vanish), i.e., an essentially compressible turbulent flow evolves into weakly compressible. This corresponds to conclusions and results followed from Fig. 8 for the local small-scale turbulent Mach number $\breve{\mathrm{M}}_{\mathrm{s}}$. Thus, a compressible MHD flow with a supersonic Mach number is transformed in the local interstellar medium into a subsonic flow of electrically conducting liquid, with an insignificant contribution of the solenoidal velocity component, i.e., with $\operatorname{div}\mathbf{u} \ll 1$.

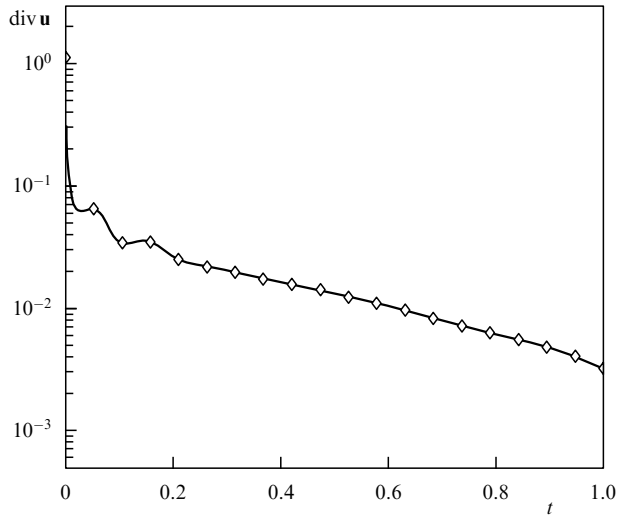

Figure 9. Temporal dynamics of the velocity divergence div **u**. The velocity divergence, which characterizes compressibility of the fluid, decays, and the flow becomes weakly compressible with time.

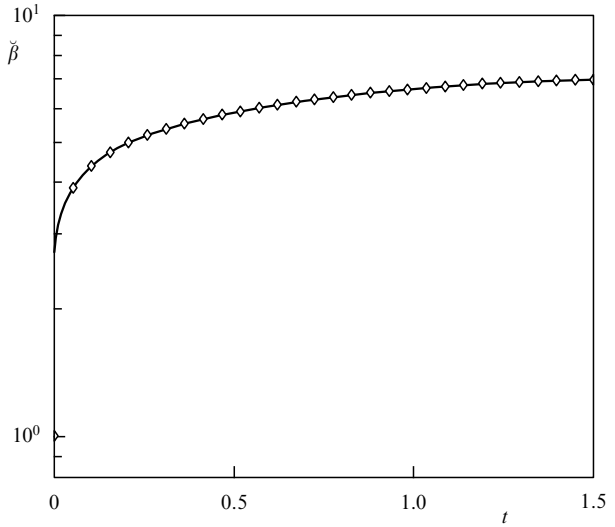

Figure 10. Time evolution of the turbulent plasma parameter $\breve{\beta}$ in compressible MHD turbulence. Initially strongly magnetized plasma becomes less magnetized with time.

The results obtained correspond to the conclusions derived from an asymptotic analysis and estimates made in paper [79], in which an essentially compressible MHD plasma was shown to evolve toward a moderately compressible flow with a velocity divergence decrease in the decaying turbulence, i.e., $\operatorname{div}\mathbf{u} \to 0$ (or $|iku_k| \ll 1$ in the Fourier space).

4.1.2 Dynamics of magnetized plasma. The evolution of an MHD plasma from an essentially compressible to moderately compressible flow in the interstellar medium not only transforms supersonic motion to subsonic motion, but also weakens the plasma magnetization. This can be seen from the time history of the turbulent plasma parameter $\breve{\beta}$ depicted in Fig. 10. The plasma beta-parameter is the ratio of the plasma pressure to the magnetic field pressure, defined as $\beta_0 = 8\pi p_0/B_0$. As evidenced from Fig. 10, the plasma pressure on the initial time interval does not exceed the magnetic pressure (i.e., $\breve{\beta} \leqslant 1$) in a strongly compressible MHD plasma. Later on, when essentially compressible plasma fluctuations decay (as is clearly seen in Figs 8 and 9), the plasma magnetization weakens and the plasma parameter goes up from a low value ($\breve{\beta} \leqslant 1$) to a high value ($\breve{\beta} > 1$). This suggests that the plasma pressure exceeds the magnetic energy. In the inertial turbulence interval, we can write out the relationship

$$kd \geqslant 1 > k_0\lambda_{\mathrm{mfp}}\,, \tag{98}$$

where d is the ion gyroradius, $k_0 \sim 1/L_0$, L_0 is the integral scale, and λ_{mfp} is a particle's mean free path. Physically, inequalities (98) mean that the plasma particles connected with the magnetic field lines are expelled from their gyroorbits due to the plasma pressure becoming dominate over the magnetic energy. This ultimately leads to weakening of the plasma magnetization and, hence, plasma fluctuations, and to a transition to the regime with $\breve{\beta} > 1$ and to a subsonic weakly compressible flow. The mode transformation is another factor that partially explains the MHD plasma transition from the strongly compressible to the weakly compressible state. The turbulent plasma parameter $\breve{\beta}$ can be written in the form

$$\breve{\beta} \simeq \frac{8\pi\breve{p}}{\breve{B}^2} \sim \frac{\breve{c}_{\mathrm{s}}^2}{\breve{u}_{\mathrm{a}}^2} \sim \frac{\breve{\mathrm{M}}_{\mathrm{a}}^2}{\breve{\mathrm{M}}_{\mathrm{s}}^2}\,. \tag{99}$$

As MHD plasma evolves into the regime with $\breve{\beta} > 1$, the Alfvén small-scale turbulent Mach number $\breve{\mathrm{M}}_{\mathrm{a}}$ decreases. The monotonic decrease of $\breve{\mathrm{M}}_{\mathrm{s}}$ (in accordance with Fig. 8) corresponds to a higher value of $\breve{\beta}$, i.e., the MHD flow becomes more and more weakly compressible. Also, the temporal dynamics of the compressible MHD flow suggest that the magnetosonic fluctuations decay faster than Alfvénic fluctuations (the Alfvénic modes, nevertheless, also decay due to dissipation). This conclusion coincides with the one previously predicted theoretically in papers [79, 93].

The gradual increase in the turbulent plasma parameter $\breve{\beta}$, in addition, changes the turbulent cascade rate in the subsonic regime of the compressible MHD plasma. The state of a turbulent flow with a high value of the plasma $\breve{\beta}$-parameter assumes that the Alfvénic shear modes propagate more slowly than acoustic waves. Thus, magnetohydrodynamic perturbations in the steady state are velocity-ordered as follows:

$$\breve{u} < \breve{u}_{\mathrm{a}} < \breve{c}_{\mathrm{s}}\,. \tag{100}$$

The time scales of nonlinear interactions for these inequalities can be written out as follows:

$$\tau_{\mathrm{s}} < \tau_{\mathrm{a}} < \tau_{\mathrm{NL}}\,, \tag{101}$$

where τ_{s}, τ_{a}, and τ_{NL} denote the magnetosonic timescale, the Alfvén timescale, and the timescale of one eddy turnover, respectively. Inequalities (101) imply that the nonlinear interaction time for Alfvénic modes increases in comparison with magnetosonic modes. Therefore, the plasma motion becomes weakly compressible on the Alfvén timescale. During the gradual transition to the weak compressibility regime, the compressible fast/slow magnetosonic modes are weakly connected with the Alfvénic modes [79]. Therefore, the Alfvénic shear modes (which are mainly incompressible) start gradually dominating in the cascade, while the compres-

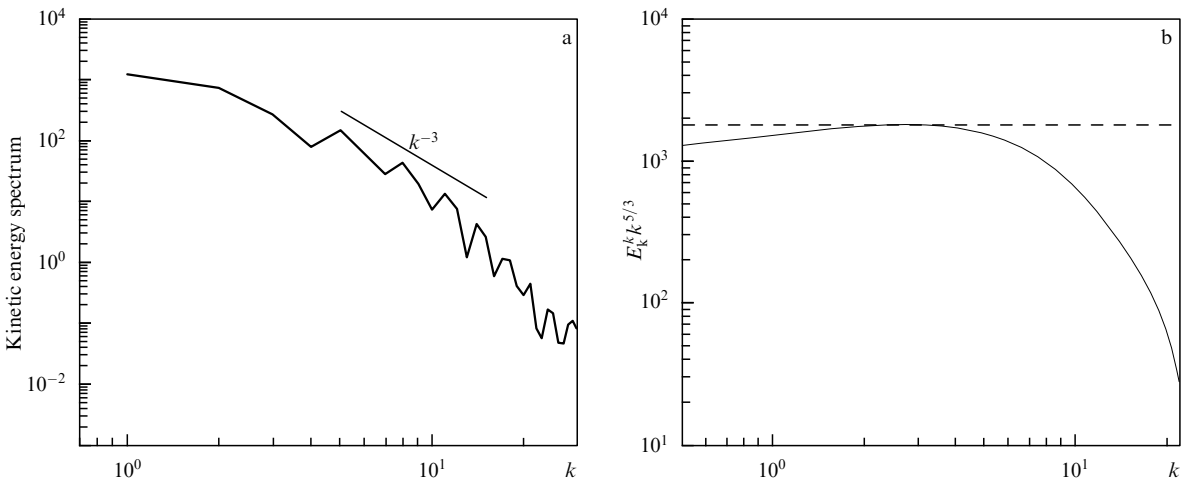

Figure 11. (a) Kinetic energy spectrum. (b) Normalized (multiplied by $k^{5/3}$), smoothed spectrum of the kinetic energy. It is seen that the power-law index of the spectrum is close to k^{-3} for most of the turbulent cascade. However, a clearly defined Kolmogorov-like inertial interval ($k^{-5/3}$) exists.

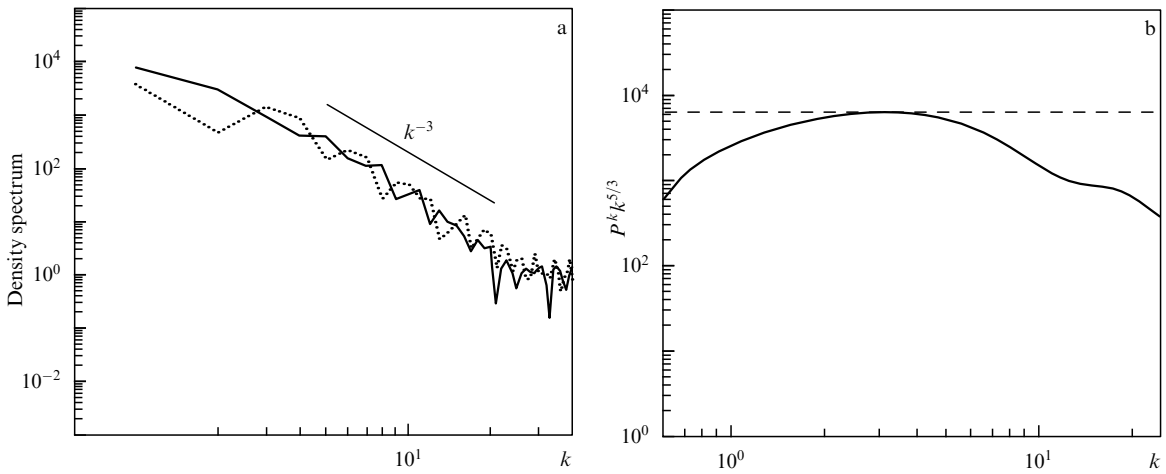

Figure 12. (a) Density spectrum (solid line) and density fluctuation spectrum (dashed line). (b) Normalized (multiplied by $k^{5/3}$), smoothed density fluctuation spectrum. Both plots in the (a) figure are close to the power-law k^{-3}. There is also a sharply cut Kolmogorov-like inertial interval ($k^{-5/3}$) for the density fluctuations, which is confirmed by observations.

sible fast/slow magnetosonic waves suppress nonlinear cascades by dissipating the longitudinal fluctuations, which leads to anisotropic MHD turbulence (the anisotropy effects will be considered in more detail below in Section 4.1.4). If the compressible plasma magnetization weakens, and the turbulent plasma pressure becomes highly dominant over the turbulent magnetic energy with time, perturbations are mostly unmagnetized, i.e., the situation is similar to the hydrodynamic case. Thus, the fluctuating magnetic field ultimately becomes sufficiently weak and has almost no effect on the turbulent energy dissipation rate.

4.1.3 Turbulence spectra in the local interstellar medium. Observations suggest that the density fluctuations in the local interstellar medium demonstrate a Kolmogorov-like spectrum in a wide range of turbulent scales [90, 91, 130]. In the interstellar plasma turbulence, the density fluctuations are random in both space and time. Similar results were obtained numerically in the frameworks of the 'almost incompressible' fluid approximation [89, 131].

Shown in Fig. 11a is the kinetic energy spectrum for $t = 1.45$ at the turbulent Mach number $\breve{\mathrm{M}}_{\mathrm{s}} < 1$ (the subsonic turbulence regime), which has a power index close to k^{-3} in a wide scale range, which corresponds to the dissipative turbulence interval. However, there is a clearly shaped inertial turbulence interval with the Kolmogorov spectrum varying as $k^{-5/3}$. In order to show the existence of such an interval and to determine at which wave numbers it emerges, we present in Fig. 11b the normalized (i.e., the product $E_{\mathrm{k}}^k k^{5/3}$ is plotted along the y-axis, where E_{k}^k is the kinetic energy in the Fourier space, and k is the wave vector), smoothed kinetic energy spectrum. It is seen that for $2 \leqslant k \leqslant 5$ there is an inertial interval with the Kolmogorov spectrum.

Figure 12a displays the density and density fluctuation spectra. Both plots in this figure demonstrate a power law in the Fourier space, namely, k^{-3}, which corresponds to the spectrum in the dissipative interval of the Kolmogorov turbulence in the direct energy transfer cascade regime for the decaying turbulence. The normalized smoothed spectrum of density fluctuations, $P^k k^{5/3}$, is presented in Fig. 12b. It is clearly seen that, as for the kinetic energy spectrum, there is an interval that can be approximated by the Kolmogorov spectrum $k^{-5/3}$, and essentially for the same wave numbers $2 \leqslant k \leqslant 5$. On the whole, the density fluctuation spectrum

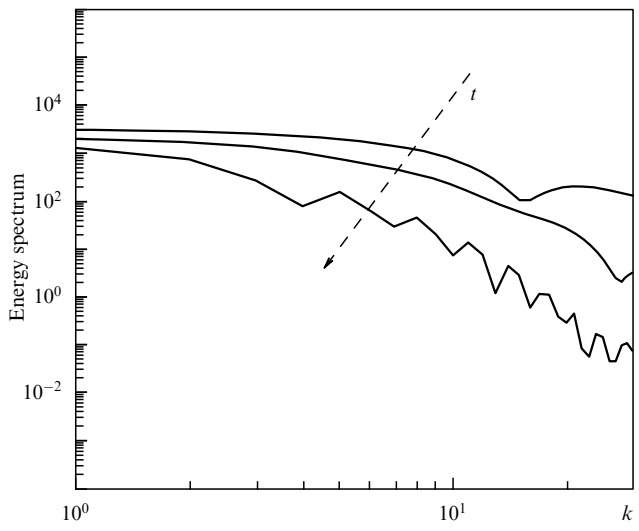

Figure 13. Energy spectrum change with time. The time arrow is shown by the dashed line.

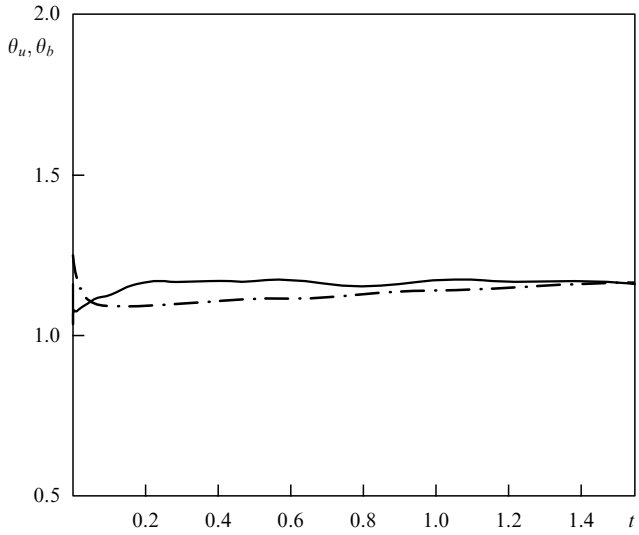

Figure 14. Time evolution of the anisotropy angle for velocity θ_u (solid line) and for magnetic field θ_b (dashed-dotted line).

demonstrates the same behavior in the Fourier domain as the kinetic energy spectrum (see Fig. 11). Thus, we can conclude that the density fluctuations make up a passive mixture in a moderately compressible subsonic turbulent flow. Theoretical models of turbulence, in addition, assume that any physical flow characteristic that passively propagates in the background turbulence field should demonstrate a similar spectrum [132].

The change in the total energy spectrum (the sum of the magnetic and kinetic energies) with time is presented in Fig. 13. It is seen that energy-containing large scales of turbulence diminish in the course of time. The spectrum amplitude also decreases, suggesting dissipation of the compressible flow considered. It is noticeable that the dissipation interval in the energy cascade widens, while the inertial interval becomes narrower, which corresponds to a decrease with time of the hydrodynamic Reynolds number in the decaying turbulence (the inertial turbulence interval is directly proportional to the Reynolds number).

4.1.4 Anisotropy properties of turbulence. The Kolmogorov turbulence model assumes that large and small scales are independent from each other, thus leading to flow isotropy on small scales [123, 124]. Kolmogorov assumed that, during the energy transfer from large to small scales, the information on its generation mechanism would be lost. If the number of steps in the energy cascade is large, all the information can be assumed to be lost. The smallest scales 'may know' only how much energy was acquired on these scales, and they can be expected to be isotropic, i.e., information on the possible anisotropy of the energy-containing large scales is lost. The interstellar turbulence is anisotropic, which was shown both theoretically and inferred from observations [88, 90]. Papers [64, 94] demonstrated that the large-scale flow in compressible MHD turbulence is anisotropic, unlike the small-scale flow. Numerical modeling [94] reveals a different behavior of the velocity components in the spectral cascade at small wave numbers k for x, y, and z components of the velocity field, as well as almost no differences at large Fourier modes, which means that anisotropic turbulence cascades arise predominantly on large scales. Thus, the large-scale developed turbulence in the local interstellar medium is anisotropic, which is confirmed by the results of independent studies [88, 89].

To estimate the degree of anisotropy and the symmetry of the flow, we make use of the Shebalin angle [133] (in other words, the anisotropy angle), which is defined as

$$\tan^2\theta_u = 2\,\frac{G^u_{xx} + G^u_{xy} + G^u_{xz}}{G^u_{yx} + G^u_{yy} + G^u_{yz}}\,, \tag{102}$$

$$\tan^2\theta_b = 2\,\frac{G^b_{xx} + G^b_{xy} + G^b_{xz}}{G^b_{yx} + G^b_{yy} + G^b_{yz}}\,, \tag{103}$$

where $G^u_{ij} = \langle \partial u_j/\partial x_i\rangle$, and $G^b_{ij} = \langle \partial B_j/\partial x_i\rangle$. For isotropic turbulence, one has $\theta = \arctan\sqrt{2} \approx 54^\circ \approx 1$ rad. Figure 14 presents the anisotropy angles θ_u (for velocity) and θ_b (for the magnetic field), characterizing the large-scale structures, as a function of time t. After the initial time interval, neither the velocity nor the magnetic field anisotropies really change, saturating at some level.

At low values of the plasma β-parameter, when the role of magnetic energy is significant, the anisotropy and symmetry breaking are mainly due to the magnetic field. At high values of β, when the role of the magnetic field is small, anisotropic turbulence cascades are observed due to the propagation of compressible acoustic modes, which hamper the spectral transfer in the local Fourier space. These modes in MHD turbulence may be excited either by large scales or by an external velocity of the background turbulence [88].

To summarize, the local interstellar gas was modeled using the LES method to solve the system of MHD equations governing compressible MHD turbulence in the local interstellar medium. Despite the local interstellar medium being characterized by supersonic flows with high large-scale Mach numbers, there are also evidenced subsonic fluctuations of weakly compressible components of the interstellar medium. It is these compressible subsonic fluctuations that are responsible for the appearance of a Kolmogorov type spectrum in the local interstellar turbulence, which is suggested by observations. It is shown that density fluctuations are a passive scalar in the velocity field of moderately

compressible MHD turbulence and demonstrate the Kolmogorov spectrum in the dissipative interval of the energy transfer cascade. This supports the hypothesis for the weakly compressible nature of the density fluctuations observed in the local interstellar medium. The power-law spectrum indexes for density and kinetic energy are almost the same and are close to k^{-3} for compressible decaying MHD turbulence. It is also demonstrated that the kinetic energy spectrum changes with time, which indicates the decrease in the energy-containing large scales and the inertial interval and the increase in the dissipation scale. The turbulent Mach number $\breve{\mathrm{M}}_{\mathrm{s}}$ is shown to significantly decrease from a supersonic regime of turbulence ($\breve{\mathrm{M}}_{\mathrm{s}} > 1$), in which the medium is strongly compressible, to a subsonic flow ($\breve{\mathrm{M}}_{\mathrm{s}} < 1$) with weak compressibility. This conclusion on the diminishing role of compressibility in turbulent fluctuations is confirmed by the time evolution of the velocity divergence, which tends to zero (but does not vanish). The plasma transition from an essentially compressible turbulent MHD flow to a mildly compressible flow in the local interstellar medium not only transforms supersonic motion into subsonic motion, but also weakens the plasma magnetization, since the plasma $\breve{\beta}$-parameter increases with time; thus, the role of magnetic energy decreases compared to that of the plasma pressure. The anisotropy of turbulent flows was also considered. It was shown that the large-scale flow exhibits anisotropic properties, whereas small-scale structures are isotropic.

Large eddy simulations of three-dimensional compressible MHD turbulence in the local interstellar medium allowed observational data to be interpreted and new insight into the spectra of a local interstellar gas turbulence to be gained [94].

5. Scale-invariant spectra of MHD turbulence

In the previous sections, we discussed the large eddy simulation method aimed at studying compressible MHD plasma turbulence and showed that it can be applied to explore homogeneous degenerating turbulence. Let us discuss whether the LES method is adequate when studying physical processes in compressible MHD turbulence driven by an external force. The fact of the matter is that for a numerical solution of the filtered equations of compressible MHD turbulence in the LES method, as well as of the original equations in DNS, finite-difference and finite-volume methods in the coordinate space appear to be the most adequate [78, 83, 134, 135]. Solving the original governing equations by finite-difference methods, in addition, enables natural studies of inhomogeneous and nonstationary turbulent flows. The traditional way of introducing an external force for compressible MHD flows relies on the experience of turbulence studies in incompressible fluids and is based on the spectral representation of the external force with a subsequent recalculation of the given force into the coordinate space [102, 103, 136]. Notice that in the magnetic hydrodynamics of a compressible fluid there are four types of waves: Alfvénic, slow magnetosonic, fast magnetosonic, and entropic [137, 138]. The spectra in the turbulence inertial interval can be determined in this case by a richer picture of interactions among these waves, and to describe such turbulence at different values of the similarity parameters, the traditional types of external force, based on the local spectral representations of the turbulence source, can strongly simplify the real picture of processes in compressible MHD plasma turbulence. The problem of adequacy of large eddy simulations in this case is reduced not only and not to a large extent to matching with direct numerical simulations (which was done in our papers [57–63, 94], but rather to the possibility of reproducing the scale-invariant Kolmogorov and Iroshnikov–Kraichnan spectra under the suitable physical conditions for their origination. This section is dedicated to highlighting this important aspect of large eddy simulations.

To study compressible MHD turbulence over the inertial interval, papers [65–68] proposed using a linear external force, recently suggested in incompressible neutral fluid dynamics [139–141]. The idea is to utilize a force that is directly proportional to the fluctuating velocity. This approach to the driving force definition was dubbed 'linear forcing'. In spite of evident merits, this method has not been widely applied to LES and DNS of turbulence. The main advantage of using such a force is that it acts on all scales in the coordinate space and so provides the production of turbulent kinetic energy and the adequacy of stationary solutions taking into account the nonlinear wave interactions accumulating in the space [65, 67].

5.1 Basics of the theory of scale-invariant MHD turbulence and methods of its modeling

Magnetohydrodynamic plasma turbulence, like hydrodynamic turbulence, possesses a property of scale invariance on the inertial interval [12, 13, 76, 117, 123–126, 142–157]. A fully developed turbulence is possible if the integral scale L and the dissipation scale d differ by several orders of magnitude ($L \gg d$). According to the phenomenological Kolmogorov theory, this state is characterized by two properties. First, the energy dissipation rate is independent of the viscosity of the fluid considered, i.e., it tends to a finite value in the zero-viscosity limit. Because the nonlinear interactions of eddies do not violate the energy conservation law, the dissipation rate ϵ should be equal to the energy transfer rate Π^0 to the system (i.e., $\Pi^0 = \epsilon$) either from an external source or from the largest energy-containing eddies with scale L. Second, the energy is not transported directly from the largest scale to the dissipative scale, but is transferred over the spectrum due to consecutive interactions between progressively smaller scales, i.e., an energy transfer cascade shows its worth. In this cascade, eddies with scale l decay into smaller eddies, but are reproduced by larger eddies, etc. According to the Kolmogorov theory, all scales are assumed to be in energy equilibrium; the energy dissipation rate for eddies of size l does not depend on the scale l and is equal to ϵ: $\Pi(l) = \Pi^0 = \epsilon$. If $\tau^*(l)$ is the characteristic time needed for an eddy with size l to transfer its energy $E(l)$, then one obtains

$$\Pi(l) \approx \frac{E(l)}{\tau^*(l)} \,. \tag{104}$$

Because the energy transport in a neutral fluid is due to the eddy deformation by its own motion, the transport time is equal to the eddy's turnover time τ_{nl}. Assuming the interactions to be local in the wave number space, this time can be written out as

$$\tau_{nl} \approx \frac{l}{u(l)} \,, \tag{105}$$

where $u(l)$ is the characteristic velocity dispersion inside the eddy. Using the relationship $E(l) \approx u^2(l)$, we get $E(l) \approx \epsilon^{2/3}$.

Taking into account that $k \approx 1/l$ and $E(l) \approx \int^k E_\kappa \, \mathrm{d}\kappa \approx kE_k$, we can write the following equation

$$\Pi_k \approx k^{5/2} E_k^{3/2} = \epsilon \,. \tag{106}$$

The scale-independence of the flow thus leads to the Kolmogorov spectrum:

$$E_k \approx \epsilon^{2/3} k^{-5/3} \,. \tag{107}$$

In an electrically conducting fluid placed in a homogeneous magnetic field, incompressible fluctuations appear as Alfvénic waves. The principal assumption of the Iroshnikov–Kraichnan theory is that the proper eddy deformations in the large-scale magnetic field are due to weaker interactions among propagating Alfvénic waves. The propagation of Alfvénic waves introduces an additional timescale, the Alfvén time $\tau_\mathrm{A} \approx l/V_\mathrm{A}$, where V_A is the Alfvén velocity, so the effective time $\tau^*(l)$ of energy transfer along the spectrum is no longer equal to the eddy turnover time $\tau_{nl} \approx l/u \approx l/b$, where b is the magnetic field fluctuation expressed in units of velocity. The time of coherent interactions is reduced to τ_A, and τ_A differs from the eddy turnover time by factor b/V_A. Thus, by treating consecutive collisions of wave packets as independent, one can show that

$$\tau^*(l) \approx \frac{\tau_{nl}}{\tau_\mathrm{A}} \, \tau_{nl} \approx \frac{V_\mathrm{A}}{b} \, \tau_{nl} \,, \tag{108}$$

and this time can be much longer than τ_{nl}. Substituting now the effective transfer time $\tau^*(l)$ instead of the eddy turnover time in equation (104) for the energy transfer rate Π, we obtain the relationship

$$\Pi_k \approx \frac{kE^2}{V_\mathrm{A}} = \frac{k^3 E_\mathrm{k}^2}{V_\mathrm{A}} \,. \tag{109}$$

Imposing the constancy condition on the energy dissipation rate ϵ yields

$$E(l) \approx (V_\mathrm{A} l \epsilon)^{1/2} \,. \tag{110}$$

Expression (110) leads to the Iroshnikov–Kraichnan spectrum:

$$E_k \approx (\epsilon V_\mathrm{A})^{1/2} k^{-3/2} \,. \tag{111}$$

In paper [158], the generalized formulas for the energy transfer cascade in the Elsasser variables $z = u \pm b$ [159] are derived. The Elsasser variables are sometimes convenient in MHD turbulence studies. This representation offers a more clear description of fluctuations propagating either along the large-scale magnetic field or in the opposite direction. The turnover time of a type z^+ or z^- eddy depends on the field amplitude of another type, i.e.,

$$\tau_{nl}^{\pm} \approx \frac{l}{z^{\mp}} \,. \tag{112}$$

By allowing the destruction of correlations, as assumed in the Iroshnikov–Kraichnan theory, the spectral fluxes Π^+ and Π^- must be equal:

$$\Pi_k^+ \approx \Pi_k^- \approx \frac{k^3 E_k^- E_k^+}{V_\mathrm{A}} \,. \tag{113}$$

This relationship leads again to the Iroshnikov–Kraichnan spectrum (proportional to $k^{-3/2}$) if the amplitudes are comparable in magnitude.

In paper [160], it was assumed that the nonlinear timescale $\tau_{nl}^{\pm} \approx (k z_k^{\mp})^{-1}$ is defined as the eddy turnover time, i.e., interactions are coherent, as in the Kolmogorov cascade. The spectral transfer rates are, thus, different:

$$\Pi_k^{\pm} \approx k^{5/2} \, \frac{E_k^- E_k^+}{(E_k^{\mp})^{1/2}} \approx \epsilon^{\pm} \,. \tag{114}$$

In this case, the condition that both fluxes be constant leads to the Kolmogorov spectra for both fields independently of the flux ratio $\epsilon^{\pm}$. In other words, the Kolmogorov spectrum is recovered in the Elsasser variables:

$$E_k^{\pm} \approx (\Pi^{\pm})^{4/3} (\Pi^{\mp})^{-2/3} k^{-5/3} \,. \tag{115}$$

The main difference between the two concurrent phenomenological theories ($-3/2$ and $-5/3$) consists in the choice of the characteristic timescale for the interaction time. The main assumption is that the Iroshnikov–Kraichnan hypothesis is valid in a strong magnetic field, whereas the phenomenological Kolmogorov theory for the MHD case (i.e., the assumption made in paper [160]) is applicable when fluctuations dominate the magnetic field (strong turbulence). Both phenomenological theories are developed by assuming isotropic turbulence, i.e., when there is no large-scale, permanent, mean magnetic field. The large-scale mean magnetic field usually suppresses energy transfer cascades along the magnetic field direction.

There are several physical reasons why correlations cannot be destroyed, as assumed in the Iroshnikov–Kraichnan model. The first is that when the large-scale magnetic field is present, the energy cascade is not isotropic in the wave-vector space, and for modes with wave vectors almost perpendicular to the magnetic field, the decay time of the Alfvén correlations becomes much longer than the nonlinear interaction time [13]. The second reason is that fluctuations are incompressible in most space physics problems, which can lead to direct interactions among compressible waves propagating in one direction. For example, the solar wind is not incompressible, isotropic, or homogeneous, and what is more it is an electrically conducting medium; most solar wind turbulence observations suggest spectral power indices very close to the Kolmogorov value, despite the fact that the spectrum with the power-law index $-3/2$ is expected in MHD turbulence. To resolve this issue, for example, paper [161] proposes applying a renorm-group analysis and shows that the scale-dependent 'local mean magnetic field' affects the Alfvénic fluctuations. By substituting the local mean magnetic field, defined as $k^{-1/3}$, into the energy cascade equation in the Elsasser variables [158], we recover a Kolmogorov type spectrum for MHD turbulence.

The possibilities of direct numerical simulations to determine the scale-invariant spectra of compressible MHD turbulence are restricted by the high Reynolds numbers needed to obtain a clearly determined turbulence inertial interval. Therefore, it is quite difficult to accurately measure the spectrum slopes in order to determine which of the phenomenological theories, Kolmogorov's or Iroshnikov–Kraichnan's, is valid. To address this issue, paper [65] proposed that the advantages of large eddy simulations be used.

The concept of isotropic homogeneous turbulence was formulated to study the universal statistical spectral properties. If energy is not supplied to a turbulent flow, after some time this flow becomes laminar due to contributions of viscosity and diffusion. To obtain results with high statistical significance, it is necessary to average sufficiently many realizations of the turbulent flow. In numerical simulations, it is much more effective to carry out one long calculation than to run many calculations with different initial conditions; therefore, the ensemble average is frequently substituted by the time average. In many space physics problems, statistically stationary (quasisteady) turbulence should be studied. The quasisteadiness implies that the energy and energy dissipation rate are about constant in time, and only small fluctuations around their mean values may arise. To sustain three-dimensional turbulence, external forces are invoked to inject energy into the system (energy forcing), and this energy compensates for losses due to energy dissipation on small scales. It should be noted that the driving force determination (by different methods) is, in fact, a technical problem and not a real physical issue. Most of the methods were developed for determining the driving force in neutral fluid turbulence studies and rely on introducing the external force into the Navier–Stokes equation for all modes in the wave number interval $|\mathbf{k}| = |k_{\mathrm{f}}|$ or inside the sphere $|\mathbf{k}| \leqslant k_{\mathrm{f}}$, where k_{f} is the limiting value of k. These intervals are bounded by the minimal wave numbers, such that the external force acts only on large scales of the flow, and thus the injected energy cascade arises, which is dissipated due to viscosity effects on small scales.

To determine the driving force, various methods are employed in turbulence modeling. Frequently, an approach is applied in which the driving force is expressed in the form

$$\hat{f}(\mathbf{k}, t) = \zeta \hat{\mathbf{u}}(\mathbf{k}, t)\,, \tag{116}$$

where the 'hat' symbol $\hat{}$ over a variable denotes the Fourier transformation. The coefficient ζ is chosen in the course of modeling such that the injected energy holds constant. In paper [162], the volume force was tapped in the form

$$\hat{f}(\mathbf{k}, t) = \frac{\epsilon \hat{\mathbf{u}}(\mathbf{k}, t)}{N \hat{\mathbf{u}}^2(\mathbf{k}, t)} \tag{117}$$

for each wave number $\mathbf{k}$ in the range $(0, k = k_0)$ containing N wave numbers, where ϵ is the dissipation rate. This formulation for the external force assumes that the energy delivered to the system is constant and is equal to the energy lost by dissipation. However, there is a problem with such a definition of the external force, since in that case it strongly correlates with the velocity field. Paper [163] utilized the same approach to define the driving force, but to ease the problem related to the correlation, this method was modified. The modification consisted in involving only $\acute{N} < N$ random wave numbers from a given interval to define the external force.

Paper [164] proposed using the stochastic force in the form

$$\hat{f}_i(\mathbf{k}, t) = \left(\delta_{ij} - \frac{k_i k_j}{k^2}\right) w_j(\mathbf{k}, t)\left[\Theta(\mathbf{k}) - \Theta(\mathbf{k} - \mathbf{k}_{\mathrm{f}})\right], \tag{118}$$

where w_j is the Ornstein–Uhlenbeck stochastic process, and Θ is the Heaviside function. However, as there is a certain timescale on which the force is correlated, the force–velocity correlation will significantly contribute to the total external forcing effect. In paper [165], this method of defining the external force was applied to study the subgrid-scale closures in the large eddy simulation method, but these simulations meet with difficulties in providing a constant driving force for different sizes of the computational domain.

Paper [166] reported using a stochastic scheme with a driving external force in the form

$$\hat{f}_i(\mathbf{k}, t) = A(\mathbf{k}, t) e_i^1 + B(\mathbf{k}, t) e_i^2\,. \tag{119}$$

Here, e_i^1 and e_i^2 are unitary orthogonal vectors perpendicular to $\mathbf{k}$, and functions A and B are random complex functions that depend on the force spectrum at the initial instant of time. Such an external force was applied in papers [78, 137, 167] to study compressible MHD turbulence, the evolution of different MHD waves (Alfvénic, slow and fast magnetosonic waves), and the magnetic reconnection.

When exploring supersonic turbulence in magnetized molecular clouds, paper [134] made use of a large-scale (at fixed wave numbers $k \leqslant 2$), isotropic, solenoidal, external force with zero helicity written in the form

$$f = \rho a - \langle \rho a \rangle\,, \tag{120}$$

where $a = u_0/\tau$ is the acceleration, and the angle brackets $\langle \ldots \rangle$ denote averaging over the entire computational domain. This driving force formulation allowed the sonic Mach number to be almost constant during the whole numerical computation process.

It is worth noting that there are different methods as well in which the kinetic energy for the lowest wave numbers is held constant. In the method applied in paper [168], the values of the $\hat{\mathbf{u}}$ Fourier coefficients held constant in the range $1 \leqslant k \leqslant 2$. This idea was later modified [169] so that the value of $|\hat{\mathbf{u}}(\mathbf{k}, t)|$ is kept constant for each mode from the range $1 \leqslant k < 2$, while their phases are evolving. However, it is difficult to associate this external force with some physical quantity. In paper [170], this method was applied with slight modifications, namely, by assuming that the energy is conserved within the range $|\mathbf{k}| \leqslant k_{\mathrm{f}}$, where k_{f} can be larger than two. Paper [171] utilizes the external force that keeps constant the total kinetic energy via the repetitive supply of the energy lost at each time step in the range $1 \leqslant k \leqslant 5$. Thus, the dissipated energy is transferred to large scales of the flow considered. Papers [172, 173] proposed a method in which the total energy is conserved on the first two wave number intervals ($1 \leqslant k < 2$ and $2 \leqslant k < 3$) as time passes. Paper [174] was concerned with other wave number intervals: $0.5 < k \leqslant 1.5$ and $1.5 < k \leqslant 2.5$. The ratio between energies on these wave number intervals was set so as to correspond to the scale-invariant Kolmogorov spectrum $k^{-5/3}$. This method was also utilized in papers [175, 176] in considering an isotropic external force.

Paper [177] compares the results of simulations based on stochastic turbulence excitation methods (118) with those using a deterministic external force written as follows: $\hat{f}(\mathbf{k}, t) = \hat{\mathbf{u}}(\mathbf{k}, t)\, g_k(t)/\tau$. The function $g_k(t)$ is expressed through the solutions of a differential equation for each wave number. Both these methods were shown to give consistent results; at the same time, the deterministic method demonstrated smaller statistical variations for most of the variables.

All the methods discussed above have been developed to solve the original governing equations in the wave number domain. However, it is frequently necessary to employ the finite-difference approach in the physical space, when modeling turbulent flows. This approach, unlike the spectral method in the wave number domain, is more effective for treating problems with complex geometry and different boundary conditions, and also requires less computational capacity and time. The driving force definition methods described above require knowledge of wave numbers and the Fourier transforms of physical variables describing the flow studied. Below, we will discuss another method for defining the external force in the physical space to study scale-invariant properties of compressible MHD turbulence, in which the driving force is independent of the Fourier transform.

5.2 Linear representation of the driving force in compressible MHD turbulence in physical space

In this section, we address the generalization of the theory of linear representation of the driving force to the case of compressible MHD turbulence. We will devise expressions for the external force entering the momentum equation and magnetic induction equation, which can be tapped to model MHD turbulence in physical space.

The governing equations of compressible MHD turbulence with external forcing can be written out in the form

$$\frac{\partial \rho}{\partial t} = -\frac{\partial \rho u_j}{\partial x_j}\,, \tag{121}$$

$$\frac{\partial \rho u_i}{\partial t} = -\frac{\partial}{\partial x_j}\left(\rho u_i u_j + p\delta_{ij} - \sigma_{ij} + \frac{B^2}{8\pi}\,\delta_{ij} - \frac{1}{4\pi}\,B_j B_i\right) + F_i^u\,, \tag{122}$$

$$\frac{\partial B_i}{\partial t} = -\frac{\partial}{\partial x_j}(u_j B_i - u_i B_j) + \eta\,\frac{\partial^2 B_i}{\partial x_j^2} + F_i^b\,, \tag{123}$$

$$\frac{\partial B_i}{\partial x_i} = 0\,. \tag{124}$$

Here, F_i^u and F_i^b are the external forces that maintain turbulence, since, in addition to decaying turbulence, it is often needed to study statistically stationary (quasistationary) turbulence. If energy is not supplied to a turbulent flow, after some time the flow becomes laminar due to viscosity and diffusion effects. To sustain three-dimensional turbulence, external forces are invoked to deliver energy into the system; this energy compensates for losses due to dissipation on small scales. The quasisteadiness implies that the amounts of the supplied energy and the dissipated energy are approximately constant in time, and that only small fluctuations around the mean values can emerge.

To model the hydrodynamic turbulence of an incompressible fluid with driving force in the physical space, so-called 'linear forcing' method has recently been developed and adopted [139, 140, 178]. The main idea of this approach consists in adding an external force that is proportional to the fluctuating velocity. The linear external force corresponds to turbulence with a driving force caused by a mean velocity gradient, i.e., the shear. This force emerges as one of the terms in the fluctuating velocity equation which corresponds to the energy generation term in the turbulent kinetic energy equation. Here, we will generalize this approach to the case of the compressible MHD flow of an electrically conducting fluid [65, 66].

The equation for fluctuating velocity in a turbulent compressible MHD flow is written out as

$$\rho\left[\frac{\partial \acute{u}_i}{\partial t} + U_j\,\frac{\partial \acute{u}_i}{\partial x_j}\right] = -\frac{\partial \acute{p}}{\partial x_j} + \frac{\partial \acute{\sigma}_{ij}}{\partial x_j} - \rho\acute{u}_j\,\frac{\partial U_i}{\partial x_j} - \left[\rho\acute{u}_j\,\frac{\partial \acute{u}_i}{\partial x_j} - \rho\left\langle \acute{u}_j\,\frac{\partial \acute{u}_i}{\partial x_j}\right\rangle\right] - \frac{\partial}{\partial x_j}\,\frac{\acute{B}^2}{8\pi} + \frac{1}{4\pi}\left[\Upsilon_j\,\frac{\partial \acute{B}_i}{\partial x_j} + \acute{B}_j\,\frac{\partial \Upsilon_i}{\partial x_j}\right] + \frac{1}{4\pi}\left[\acute{B}_j\,\frac{\partial \acute{B}_i}{\partial x_j} - \left\langle \acute{B}_j\,\frac{\partial \acute{B}_i}{\partial x_j}\right\rangle\right]. \tag{125}$$

Here, use has been made of the following, the so-called Reynolds, resolutions: $u_i = U_i + \acute{u}_i$, $B_i = \Upsilon_i + \acute{B}_i$, $p = P + \acute{p}$, $\sigma_{ij} = \Sigma_{ij} + \acute{\sigma}_{ij}$, where U_i, Υ_i, Σ_{ij}, and P are the mean values, and $\acute{u}_i$, $\acute{B}_i$, $\acute{\sigma}$, and $\acute{p}$ are the fluctuating variables.

The third term on the right-hand side of equation (125), $\rho\acute{u}_j(\partial U_i/\partial x_j)$, corresponds to the source in the turbulent kinetic energy equation. The turbulent kinetic energy equations can be derived as the difference between the statistically averaged equation, obtained from the scalar product of the velocity and nonaveraged momentum equations, and the scalar product of the velocity by the averaged momentum equation. In the symbolic form, the derivation of the turbulent kinetic energy equation can be written out as $\langle u \cdot \text{NS eq.}\rangle - U\langle\text{NS eq.}\rangle$, where NS eq. means the Navier–Stokes equation with the Lorentz force. Therefore, the turbulent kinetic energy equation takes the form

$$\frac{\partial}{\partial t}\left\langle\frac{1}{2}\,\rho\acute{u}^2\right\rangle + \frac{\partial}{\partial x_j}\left(\left\langle\frac{1}{2}\,\rho\acute{u}^2\right\rangle U_j + \left\langle\frac{1}{2}\,\rho\acute{u}^2\acute{u}_j\right\rangle - \langle\beta_{ij}\acute{u}_i\rangle\right) = -\left\langle\acute{u}_i\,\frac{\partial \acute{p}}{\partial x_i}\right\rangle + \left\langle\acute{u}_i\,\frac{\partial \acute{\sigma}_{ij}}{\partial x_j}\right\rangle - \langle\rho\acute{u}_i\acute{u}_j\rangle\,\frac{\partial U_i}{\partial x_j} - \left\langle\beta_{ij}\,\frac{\partial \acute{u}_i}{\partial x_j}\right\rangle, \tag{126}$$

where β_{ij} is the turbulent magnetic tensor:

$$\beta_{ij} = \frac{\acute{B}_i\acute{B}_j}{4\pi} - \frac{\acute{B}^2}{8\pi}\,\delta_{ij}\,. \tag{127}$$

The terms entered into equation (126) can be interpreted as follows: $\langle(1/2)\rho\acute{u}^2\rangle U_j$ is the turbulent kinetic energy flux related to the mean velocity; $\langle(1/2)\rho\acute{u}^2\acute{u}_j\rangle$ is the diffusion turbulent flux of the turbulent kinetic energy; $\langle\acute{u}_i(\partial\acute{\sigma}_{ij}/\partial x_j)\rangle$ is the viscous dissipation of the turbulent energy, and $\langle\acute{u}_i(\partial\acute{p}/\partial x_i)\rangle$ is the pressure–strain rate term (turbulent diffusion of the pressure via pressure and velocity correlations). The last terms on the left-hand and right-hand sides of Eqn (126) characterize the turbulent kinetic energy relation to the magnetic energy, i.e., the effect of the magnetic force work on the turbulent velocity. The term $\langle\rho\acute{u}_i\acute{u}_j(\partial U_i/\partial x_j)\rangle$ in Eqn (126) is the source of the turbulent kinetic energy per unit volume per unit time due to the interaction between Reynolds stresses and shear in the mean flow. In equation (125), this term is interpreted as the forcing term [139] proportional to the velocity. Thus, it is assumed that this term for isotropic homogeneous turbulence can represent the appropriate force to sustain a stationary turbulent flow with the force directly proportional to velocity (linear forcing):

$$F_i^u = \Theta\rho u_i\,. \tag{128}$$

Here, Θ is the coefficient that is determined from the kinetic energy balance for a stationary statistical state, taking into

account that the mean velocity gradient in homogeneous isotropic turbulence is equal to zero:

$$\Theta = \frac{1}{3\langle\rho\rangle u_{\rm rms}^2}\left[\left\langle u_j \frac{\partial}{\partial x_j} p\delta_{ij}\right\rangle + \varepsilon + \frac{1}{8\pi}\left\langle u_j \frac{\partial}{\partial x_j} B^2\delta_{ij}\right\rangle\right], \tag{129}$$

where $\varepsilon = -\langle u_j(\partial\sigma/\partial x_j)\rangle$ is the mean dissipation rate of the turbulent energy into heat. In expression (129), it is taken into account that $1/\langle\rho u^2\rangle = 1/(3\langle\rho\rangle u_{\rm rms}^2)$, since $u_{\rm rms}^2 = \langle\rho u^2\rangle/(3\langle\rho\rangle)$ is the mean-weighted averaging of the rms velocity. Notice that the term $\langle u_j(\partial p/\partial x_j)\rangle = -\langle p(\partial u_j/\partial x_j)\rangle$ in compressible homogeneous turbulence. It should be noted that the coefficient Θ in expression (128) can be either kept constant or recalculated in due course of simulations [140].

The functional representation of the external force $F_i^u = \Theta\rho u_i$ in the physical space is equivalent to the force representation in the spectral (Fourier) domain, which acts on all modes. This is, in fact, the sole distinction between the linear forcing and the standard spectral representation of the external force in the case where the energy is delivered into the system only on the interval of small wave numbers, i.e., into the integral turbulence scale.

In a similar way, we can find the external force F_i^b in the magnetic induction equation. The equation for the fluctuating part of the magnetic field in a compressible MHD flow can be written out as

$$\begin{aligned}\frac{\partial \acute{B}_i}{\partial t} + U_j\frac{\partial \acute{B}_i}{\partial x_j} &= \acute{B}_j\frac{\partial U_i}{\partial x_j} - \acute{B}_i\frac{\partial U_j}{\partial x_j} - \Upsilon_i\frac{\partial \acute{u}_j}{\partial x_j} + \eta\frac{\partial^2 \acute{B}_i}{\partial x_j^2}\\ &+ \left[\acute{B}_j\frac{\partial \acute{u}_i}{\partial x_j} - \left\langle \acute{B}_j\frac{\partial \acute{u}_i}{\partial x_j}\right\rangle\right] + \Upsilon_j\frac{\partial \acute{u}_i}{\partial x_j} - \acute{u}_j\frac{\partial \Upsilon_i}{\partial x_j}\\ &- \left[\acute{u}_j\frac{\partial \acute{B}_i}{\partial x_j} - \left\langle \acute{u}_j\frac{\partial \acute{B}_i}{\partial x_j}\right\rangle\right].\end{aligned} \tag{130}$$

In the last equation, the first term on the right-hand side, $\acute{B}_j(\partial U_i/\partial x_j)$, corresponds to the generation term in the turbulent magnetic energy equation. The turbulent magnetic energy equation has the form

$$\begin{aligned}&\frac{\partial}{\partial t}\left\langle\frac{\acute{B}^2}{8\pi}\right\rangle + \frac{\partial}{\partial x_j}\left[\left\langle\frac{\acute{B}^2}{8\pi}\right\rangle U_j + \left\langle\frac{\acute{B}^2}{8\pi}\acute{u}_j\right\rangle\right]\\ &= \frac{\langle\acute{B}_i\acute{B}_j\rangle}{4\pi}\frac{\partial U_i}{\partial x_j} + \left\langle\frac{\acute{B}_i\acute{B}_j}{4\pi}\frac{\partial \acute{u}_i}{\partial x_j}\right\rangle + \frac{\eta}{4\pi}\left\langle\acute{B}_i\frac{\partial^2\acute{B}_i}{\partial x_j^2}\right\rangle.\end{aligned} \tag{131}$$

Terms in the last equation describe the transport, generation, and dissipation of the turbulent magnetic energy in an electrically conducting gas. In equation (131), the term $\langle\acute{B}^2/8\pi\rangle U_j$ corresponds to advection of the turbulent magnetic energy, the term $\langle(\acute{B}^2/8\pi)\acute{u}_j\rangle$ to turbulent diffusion of the turbulent magnetic energy, the term $\langle(\acute{B}_i\acute{B}_j/4\pi)(\partial\acute{u}_i/\partial x_j)\rangle$ to the interaction of magnetic turbulent energy with fluctuating components of the mean shear, and the term $(\eta/4\pi)\langle\acute{B}_i(\partial^2\acute{B}_i/\partial x_j^2)\rangle$ to turbulent magnetic energy dissipation caused by magnetic diffusion. The first term on the right-hand side of equation (131), $(\langle\acute{B}_i\acute{B}_j\rangle/4\pi)(\partial U_i/\partial x_j)$, is interpreted as the magnetic energy generation due to interaction between the magnetic field and the mean shear. It should be noted that this term corresponds to the term $-\langle\rho\acute{u}_i\acute{u}_j(\partial U_i/\partial x_j)\rangle$ in the turbulent kinetic energy equation (126). Let us assume that the driving force in the magnetic induction equation is proportional to the magnetic field. Therefore, the force F_i^b can be defined as

$$F_i^b = \Psi B_i\,, \tag{132}$$

where Ψ is a coefficient. As when finding Θ above, to determine the coefficient Ψ we make use of the magnetic energy balance for a steady statistical state (i.e., we take into account that the time derivative is zero):

$$\Psi = \frac{\chi}{3B_{\rm rms}^2}\,, \tag{133}$$

where $\chi = \langle\eta B_i(\partial^2 B_i/\partial x_j^2)\rangle$ is the resistive dissipation of the turbulent magnetic energy in MHD turbulence, and $B_{\rm rms}^2 = \langle B^2\rangle/3$ is an rms magnetic field. Like the parameter Θ in Eqn (128), the coefficient Ψ in Eqn (132) during simulations of forced MHD turbulence can be either kept constant or recalculated at each time step.

Thus, we derived expressions for external forces in the momentum conservation equation (128) and in the magnetic energy equation (132) that will be used below for modeling three-dimensional compressible MHD turbulence in physical space.

5.3 Large eddy simulation method for forced compressible MHD turbulence

In this section, we formulate the LES method to model compressible MHD turbulence with external forcing as derived in Section 5.2. The filtered equations with external forcing can be written out as [65, 67, 68]

$$\frac{\partial\bar\rho}{\partial t} + \frac{\partial\bar\rho\tilde u_j}{\partial x_j} = 0\,, \tag{134}$$

$$\begin{aligned}\frac{\partial\bar\rho\tilde u_i}{\partial t} + \frac{\partial}{\partial x_j}\Bigg(&\bar\rho\tilde u_i\tilde u_j + \frac{\bar\rho^{\gamma}}{\gamma {\rm M}_{\rm s}^2}\delta_{ij} - \frac{1}{\rm Re}\tilde\sigma_{ij}\\ &+ \frac{\bar B^2}{2{\rm M}_{\rm a}^2}\delta_{ij} - \frac{1}{{\rm M}_{\rm a}^2}\bar B_j\bar B_i\Bigg) = -\frac{\partial\tau_{ji}^u}{\partial x_j} + \tilde F_i^u\,,\end{aligned} \tag{135}$$

$$\frac{\partial\bar B_i}{\partial t} + \frac{\partial}{\partial x_j}(\tilde u_j\bar B_i - \tilde u_i\bar B_j) - \frac{1}{{\rm Re}_{\rm m}}\frac{\partial^2\bar B_i}{\partial x_j^2} = -\frac{\partial\tau_{ji}^b}{\partial x_j} + \bar F_i^b\,, \tag{136}$$

$$\frac{\partial\bar B_j}{\partial x_j} = 0\,. \tag{137}$$

The first terms on the right-hand side of equations (135), (136) contain the subgrid-scale turbulent tensors τ_{ij}^u and τ_{ij}^b, which describe the influence of the subgrid-scale terms on the large-scale dynamics.

The right-hand parts of equations (135), (136) contain the external forces F_i^u and F_i^b, respectively, as determined using linear forcing to excite turbulence in Eqns (128) and (132), respectively, which in the dimensionless form can be given as follows:

$$\begin{aligned}\tilde F_i^u = &\frac{1}{3\langle\bar\rho\rangle\tilde u_{\rm rms}^2}\\ &\times\left[\tilde\varepsilon + \aleph + \frac{\langle\tilde u_j(\partial/\partial x_j)\bar\rho^{\gamma}\delta_{ij}\rangle}{\gamma{\rm M}_{\rm s}^2} + \frac{\langle\tilde u_j(\partial/\partial x_j)\bar B^2\delta_{ij}\rangle}{2{\rm M}_{\rm a}^2}\right]\bar\rho\tilde u_i\,,\end{aligned} \tag{138}$$

$$\bar F_i^b = \frac{\chi + \hbar}{3\bar B_{\rm rms}^2}\bar B_i\,, \tag{139}$$

where $\tilde\varepsilon = -\langle(\tilde u_j/{\rm Re})(\partial\tilde\sigma/\partial x_j)\rangle$. The term $\aleph = \langle\tilde u_j(\partial\tau_{ij}^u/\partial x_j)\rangle$ represents the SGS dissipation by which the energy, in fact, is

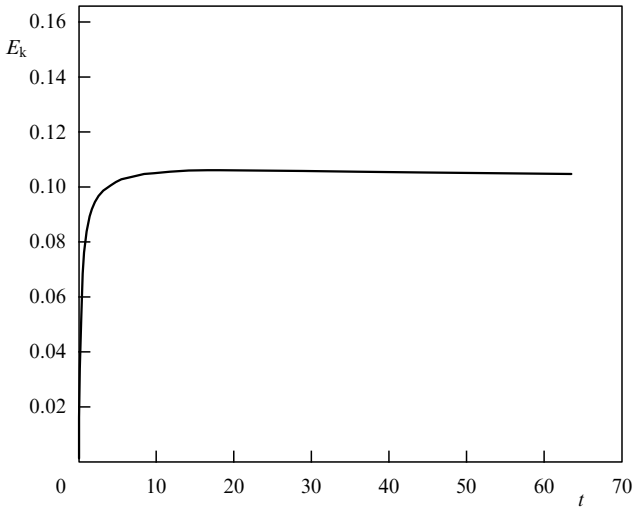

Figure 15. Time evolution of the kinetic energy for forced compressible MHD turbulence.

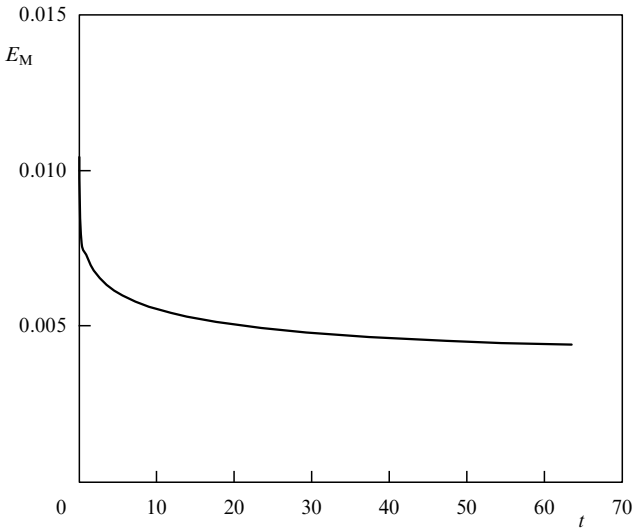

Figure 16. Time evolution of the magnetic energy for forced compressible MHD turbulence.

locally transferred from energetic large-scale eddies to small-scale motion. The term $\hbar = \langle \tilde{B}_i(\partial \tau^b_{ij}/\partial x_j)\rangle$ stands for the subgrid-scale magnetic energy dissipation.

It should be noted that, when applying the LES method to study compressible MHD turbulence with external forcing, an additional term arises, related to the subgrid-scale tensor, in the energy balance when defining the coefficient tapped to find the external force. However, if the eddy viscosity model (for example, the Smagorinsky model) and the dynamical procedure to find the model constants are used, the additional terms $\aleph$ and $\hbar$ can be omitted, since the values of these model constants are calculated self-consistently at each time step in the course of turbulence simulations. In the dynamical procedure, the model constant is obtained in such a way as to minimize (by the least-square method) the dependence of the turbulence statistics on the filter bandwidth $\bar{\Delta}$ [179], and, therefore, a suitable value of the dynamically determined constant is provided. If the scale-similarity model is used as the subgrid-scale parametrization, in which there are no model constants, the terms $\aleph$ and $\hbar$ should be included in the external force determination by the linear representation method.

Distinctions in the external force determination by the linear approach and in polytropic cases are due to the fact that, when considering a heat-conducting gas, the pressure is defined through the equation of state and depends on temperature [65], while in the polytropic case the pressure is assumed to be dependent on density as $p = \rho^\gamma$, where γ is the polytrope index.

5.4 Analysis of results of numerical simulations

Let us discuss the results of modeling of forced compressible MHD turbulence obtained for both a polytropic [65, 67] and a heat-conducting [65] electrically charged gas in the physical space. The initial isotropic turbulent spectrum for the kinetic and magnetic energies is determined in the Fourier space and is chosen to be close to the spectrum k^{-2} with random amplitude and phase along all three directions. For more detailed information on different aspects of three-dimensional simulations of forced MHD turbulence, see paper [65].

Figures 15 and 16 display the time evolution of the kinetic (E_k) and magnetic (E_M) energies, respectively, for the case

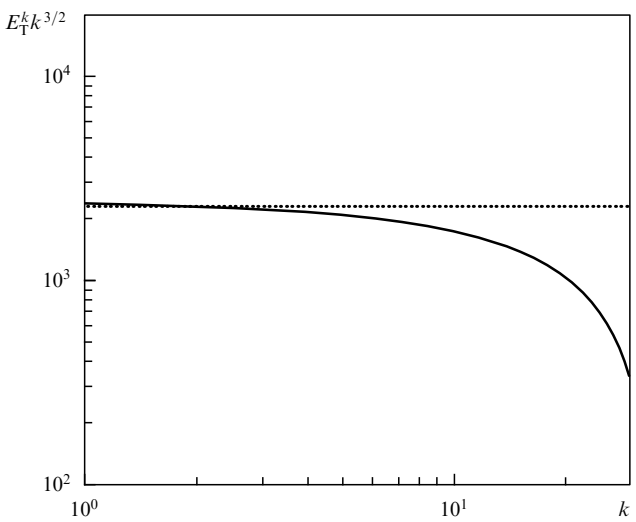

Figure 17. Normalized smoothed spectrum of the total energy multiplied by $k^{3/2}$ for the case of $E_k < E_M$.

where, at the initial instant of time, the magnetic energy exceeds the kinetic energy: $E_k < E_M$. Notice that a rapid growth in the kinetic energy and a simultaneous sharp decrease in the magnetic field strength are observed. Then, both the kinetic and magnetic energies take constant values. Paper [65] also presents the time evolution of the mean density, which suggests that density fluctuations arise until a statistically stationary regime of compressible MHD turbulence is established. After that, the mean density fluctuations become negligibly small. The normalized smoothed spectrum of the total energy E_T^k (multiplied by $k^{3/2}$) is shown in Fig. 17. Analyzing the properties of the inertial interval is one of the principal tasks in studies of scale-invariant spectra of MHD turbulence. The properties of the inertial interval are determined by averaging the statistics over the time period during which statistically stationary turbulence is realized [154]. The total energy spectrum is obtained after averaging the total energy $E_T = E_M + E_k$ in the statistically stationary turbulence regime. As seen from Fig. 17, there is a sharply defined inertial interval of MHD turbulence with the

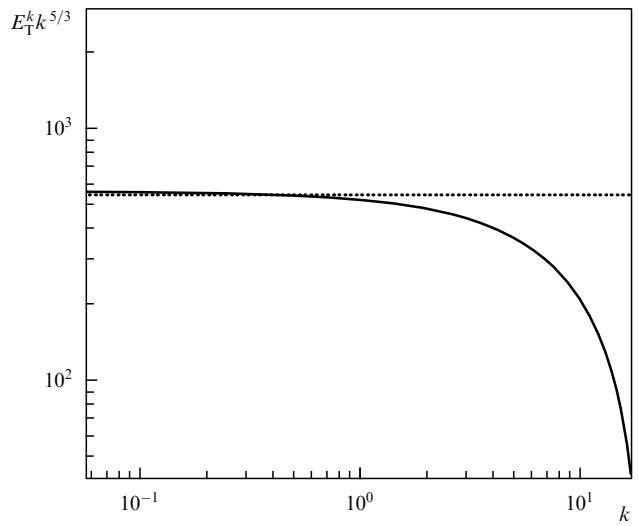

Figure 18. Normalized smoothed spectrum of the total energy multiplied by $k^{5/3}$ for the case of $E_k \gg E_M$.

Iroshnikov–Kraichnan spectrum varying as power-law $k^{-3/2}$, which is consistent with theoretical expectations. In this case, there are fluctuations in the form of Alfvénic waves in an electrically conducting fluid, and magnetic interactions play a significant role in the turbulent energy transfer cascade, which results in the Iroshnikov–Kraichnan $k^{-3/2}$ spectrum [144, 180].

If initially the kinetic energy is much larger than the magnetic energy, $E_k \gg E_M$, then, a statistically stationary turbulence is established after the initial time interval, when large fluctuations are observed, and the values of E_k and E_M are kept almost constant in time, i.e., a balance between dissipated energy and energy delivered into the system is observed [65]. In the case of MHD turbulence, when the kinetic energy is much higher than the magnetic one, i.e., nonlinear interactions are much more important than magnetic ones and the fluid is, in fact, hydrodynamic, the Kolmogorov spectrum with index $-5/3$ is observed. The normalized (multiplied by $k^{5/3}$) smoothed spectrum of the total energy is presented in Fig. 18. The total energy spectrum has been obtained after averaging the variables in the statistically stationary regime. Figure 18 suggests the Kolmogorov spectrum [123, 125]. This result is consistent with theoretical predictions. Moreover, the residual energy spectrum, which is determined as $E_R^k = |E_M^k - E_k^k|$, was investigated [65, 149]. This spectrum is of interest because it gives insight into the spectral interaction between the kinetic and magnetic energies and demonstrates a self-similar scaling. Paper [65] studies in depth the normalized smoothed spectrum of the residual energy $E_R^k \sim k^{-7/3}$ on the turbulence inertial interval, which was derived theoretically and confirmed numerically for incompressible MHD turbulence [119, 149]. It is seen that there are no significant differences in statistical properties on the inertial interval due to weak compressibility (this result has recently been obtained for compressible hydrodynamic turbulence in a neutral gas [181]). Therefore, this external force provides the correct result.

Thus, it is shown that the determination of the external driving force using the linear forcing to excite turbulence provides correct and adequate results in modeling compressible turbulent MHD flows and guarantees the detection of a statistically stationary turbulent regime. The expressions found are used to formulate the large eddy simulation method. The potential possibilities of the LES method to reproduce the physics of flows studied in the stationary regime for both polytropic and heat-conducting plasma have been addressed in Ref. [65]. It has been shown that, when the initial kinetic energy of the flow is much larger than the magnetic one, the Kolmogorov spectrum with power-law index $-5/3$ is observed, whereas if the initial magnetic energy is larger than the kinetic one, the Iroshnikov–Kraichnan spectrum with power-law $k^{-3/2}$ arises. Thus, the efficiency of the LES method for investigating the scale-invariant properties of compressible MHD turbulence has been demonstrated.

Several important remarks about the scale-similarity model are in order. As noted above, this model implies that large subgrid-scale eddies and small resolved scales possess a similarity property. For decaying turbulence — in both the MHD case and hydrodynamic case with a neutral fluid — the SGS models relied upon the eddy viscosity concept and/or mixed models demonstrated the most accurate results among the subgrid-scale closures. As is well known, the ability to dissipate energy appropriately is the most important feature of the subgrid-scale parametrizations. The general conclusion is that the scale-similarity model should be tapped along with the eddy viscosity model (for example, with the Smagorinsky parametrization, which is the key idea of the subgrid-scale mixed model) for degenerating turbulence. However, the scale-similarity model in *a priori* tests reproduces adequately the correlation between the model and the actual turbulent stress tensors, even if the flow is strongly anisotropic [122]. This suggests that the scale-similarity model correctly predicts the location of turbulent structures. Furthermore, despite this model being integrally dissipative, it is able to provide local generation of turbulence energy by imitating the energy backscatter from small to large eddies. This property turns out to be important in modeling anisotropic turbulent flows, when realizing the self-organization process of small-scale turbulence into coherent large-scale structures. One of the main advantages of the scale-similarity model is that this SGS parametrization, unlike eddy viscosity-based models, does not require entering special model constants. (Here, a second filter, broader than the main filter, can be utilized, thus resulting in the appearance of model constants [37, 182] which, in turn, can be found using a dynamic procedure; this, however, breaks the Galilean invariance [183].) Nevertheless, the insufficient dissipativity of the scale-similarity model leads to inaccurate results in the case of decaying hydrodynamic and MHD turbulences [48, 60]. The situation, however, cardinally changes when addressing scale-invariant properties of forced turbulence. In that case, the scale-similarity model can yield more accurate results than the closures based on the eddy viscosity. In forced turbulence, where an external force is introduced to inject energy into a turbulent flow (otherwise, the flow becomes in time laminar due to viscosity and diffusion effects), the subgrid-scale modeling should correctly provide the statistically stationary regime and not only guarantee an adequate energy dissipation rate, as in the case of degenerating turbulence. The scale-similarity model, which has a range of key merits mentioned above, can be applied to study the scaling properties of turbulent MHD flows. It can be expected that the results of modeling of forced compressible MHD turbulence by the LES method, in which the scale-similarity model is involved

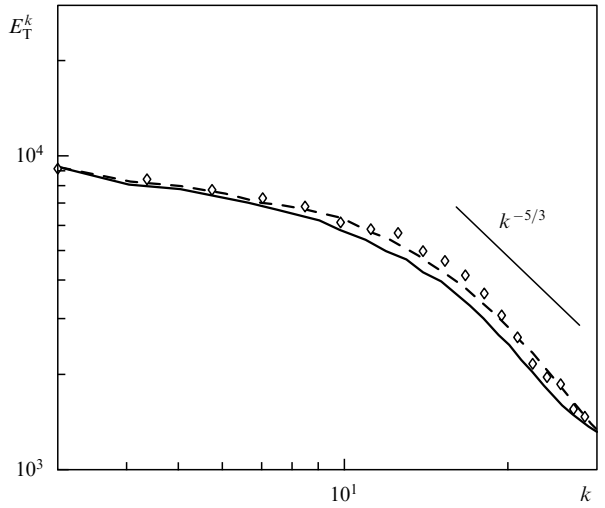

Figure 19. Spectrum of the total energy E_T^k. Diamonds show the DNS results, the solid line corresponds to the Smagorinsky model for compressible MHD turbulence, and the dashed line is in compliance with the scale-similarity model for compressible MHD turbulence.

as the subgrid-scale closure, will be accurate enough. Thus, such a parametrization, unlike decaying MHD turbulence, can be utilized as an independent subgrid-scale model. It should be noted that the Elsasser variables are frequently tapped in magnetohydrodynamics to write the MHD equations in a more symmetric form, and in this case it is especially important to provide a good correlation between the subgrid-scale and real turbulent tensors. For example, a strong correlation between all three components of the velocity fluctuations and the magnetic field fluctuations is actually observed in the solar wind, and it is shown that the total energy spectrum can depend on the level of correlations [146]. It is also possible that a good correlation plays an important role in problems where inhomogeneities of the turbulent flow are taken into account. Therefore, paper [67] carefully studies as well the efficiency of the scale-similarity model to model forced compressible MHD flows.

Figure 19 depicts the total energy spectrum for the case where $\mathrm{Re} > \mathrm{Re_M}$ and a Kolmogorov-like spectrum $k^{-5/3}$ is observed. As seen from this figure, the scale-similarity model provides even more accurate results than the Smagorinsky parametrization for MHD turbulence, i.e., results obtained with the scale-similarity model are in better agreement with DNS results [67]. Thus, this subgrid-scale model with linear forcing is able to correctly reproduce the scale-invariant properties of turbulent MHD flows. This makes the scale-similarity model a convenient subgrid-scale parametrization in studies of different nondecaying turbulent plasma flows, especially in astrophysical and space applications, taking into account this model's advantages, including, first of all, no need to define the model constants.

6. Conclusions

We have reviewed the state of the art and the latest achievements in computational studies of compressible turbulent space plasmas. The complexity of the governing MHD equations for compressible plasma requires developing methods that are alternatives to direct numerical simulations. The large eddy simulation method is an alternative to direct numerical simulations of complex turbulent flows. This method proved to be efficient in exploring the geophysical turbulence and the turbulence of engineering flows. The basic idea of the method is to take advantage of the filtering of the governing fluid dynamics equations with the subsequent parametrization of the universal part of the turbulent flow by subgrid-scale closures. This method is more favorable than alternative methods of turbulence studies. Unlike the Reynolds treatment, the LES method resolves large eddies and thus provides information on the statistical and spectral properties of the turbulent field. Unlike direct numerical simulations, LES allows one to study flows with higher similarity parameters than in DNS for present-day computational capacities of supercomputers, since the number of degrees of freedom of the turbulent motion is very high and the minimal number of the numerical grid nodes must be restrictively high for direct numerical simulations of turbulent flows with realistic Reynolds numbers. The last advantage is especially important for studying MHD turbulence in compressible plasma which is characterized by high Reynolds and Mach numbers.

We have described in detail the large eddy simulation method for studies of compressible magnetohydrodynamic plasma turbulence and have shown its applicability to the investigation of homogeneous degenerating turbulence. Possible parametrizations of subgrid-scale phenomena have been analyzed in detail. It is shown that in the case of polytropic plasmas the subgrid-scale models are designed by combining and generalizing the known subgrid-scale terms in compressible neutral fluid dynamics and in incompressible magnetized fluid. A theory is considered of subgrid-scale turbulent flows in a heat-conducting plasma for new subgrid-scale terms arising due to the presence of the magnetic field in the total energy equation. Also shown is that the extended Smagorinsky model and the model based on the cross-helicity of the magnetic field and velocity provide the most accurate numerical results in turbulence simulations of a polytropic gas. We discuss the modeling of compressible MHD turbulence of heat-conducting plasma at various Mach numbers and show that the LES method can be applied at small and moderate Mach numbers.

The efficiency of the LES method for solving important space plasma problems is demonstrated. The exploration of the three-dimensional dynamics of density fluctuations in MHD turbulence of the local interstellar medium by the LES method showed that there is a regime in which the originally strongly compressible fluctuations become in time weakly compressible, and the density fluctuation spectrum reproduces the kinetic energy spectrum. This corresponds to the density fluctuations being transferred by the MHD flow in the passive mixture regime. The temporal behavior of the properties of energy spectra obtained is analyzed. It is found that energy-containing large scales of turbulence diminishes with time, and the spectrum amplitude also declines. It is shown that the dissipation interval in the energy transfer cascade widens and the inertial interval narrows. The anisotropy properties of MHD turbulence in space plasma in the weakly compressible regime can be effectively studied by the proposed large eddy simulation method. It is demonstrated that the large-scale MHD flow is anisotropic, while the small-scale flow should be isotropic.

In this review, we also discussed the linear forcing to study compressible MHD plasma turbulence on the inertial interval. This method implies that the driving force is directly

proportional to the velocity in the momentum conservation equation. If the compressible MHD turbulence is considered, the governing MHD equations include the magnetic induction equation, and in that case the driving force is proportional to the magnetic field in the magnetic induction equation. Unlike the spectral representation of the driving force, linear forcing acts on all scales in the physical space and thus can more precisely reproduce the mode interactions in turbulent compressible MHD flows. In fact, the linear forcing corresponds to a forced turbulence caused by the mean velocity gradient, i.e., by the shear. The linear external force in the magnetic induction equation can be interpreted as the magnetic energy generation due to interactions between the magnetic field and the mean shear. We derive expressions for the external force that provide the statistically stationary turbulence regime. The equations found are used to formulate the large eddy simulation method. We highlighted the potential prospects of the large eddy simulation method to reproduce the physics of the flows in the stationary regime both for polytropic and heat-conducting plasmas. It is shown that, if the initial kinetic energy of the flow is much larger than the magnetic one, the Kolmogorov spectrum $k^{-5/3}$ is evidenced, and if the initial magnetic energy exceeds the kinetic one, the Iroshnikov–Kraichnan spectrum $k^{-3/2}$ is established. Thus, the efficiency of the LES method is demonstrated for the study of the scale-invariant properties of compressible MHD turbulence.

The results obtained can be utilized to study turbulent flows in various problems of space and astrophysical plasmas, in thermonuclear plasma, in problems of plasma aerodynamics, and in numerous engineering applications.

Acknowledgments

This work was financially supported by Program 22 entitled 'Fundamental Problems of Solar System Research and Exploration' of the Presidium of the Russian Academy of Sciences, by grants from the President of the Russian Federation (MK-1349.2011.2, MK-267.2014.5), by the Dynasty Foundation, and by grants from the Russian Foundation for Basic Research (08-08-00687-a, 11-02-00805-a, 13-05-90436, 14-02-31848).

References

1. Hawley J F, Gammie C F, Balbus S A *Astrophys. J.* **440** 742 (1995)
2. Balbus S A, Hawley J F, Stone J M *Astrophys. J.* **467** 76 (1996)
3. Schramkowski G P, Torkelsson U *Astron. Astrophys. Rev.* **7** 55 (1996)
4. Low M-M M et al. *Phys. Rev. Lett.* **80** 2754 (1998)
5. Boldyrev S, Nordlund Å, Padoan P *Astrophys. J.* **573** 678 (2002)
6. Kolesnichenko A V, Marov M Ya *Solar Syst. Res.* **41** 1 (2007); *Astron. Vestn.* **41** 3 (2007)
7. Zank G P *Space Sci. Rev.* **89** 413 (1999)
8. Kaplan S A *Interstellar Gas Dynamics* (Oxford: Pergamon Press, 1966); Translated from Russian: *Mezhzvezdnaya Gazodinamika* (Moscow: Gos. Izd. Fiz.-Mat. Lit., 1958)
9. Elmegreen B G, Scalo J *Annu. Rev. Astron. Astrophys.* **42** 211 (2004)
10. Zelenyi L M, Veselovsky I S (Eds) *Plazmennaya Geliogeofizika* (Plasma Heliogeophysics) (Moscow: Fizmatlit, 2008)
11. Priest E R *Solar Magneto-Hydrodynamics* (Dordrecht: D. Reidel Publ. Co., 1984); Translated into Russian: *Solnechnaya Magnitogidrodinamika* (Moscow: Mir, 1985)
12. Zhou Y, Matthaeus W H, Dmitruk P *Rev. Mod. Phys.* **76** 1015 (2004)
13. Mangeney A, Grappin R, Velli M, in *Advances in Solar System Magnetohydrodynamics* (Eds E R Priest, A W Hood) (Cambridge: Cambridge Univ. Press, 1991) p. 327
14. Petrosyan A et al. *Space Sci. Rev.* **156** 135 (2010)
15. Goldstein M L *Nature* **436** 782 (2005)
16. Usmanov A V et al. *Astrophys. J.* **727** 84 (2011)
17. Zelenyi L M, Milovanov A V *Phys. Usp.* **47** 749 (2004); *Usp. Fiz. Nauk* **174** 809 (2004)
18. Fortov V E et al. *Phys. Usp.* **47** 447 (2004); *Usp. Fiz. Nauk* **174** 495 (2004)
19. Budaev V P, Savin S P, Zelenyi L M *Phys. Usp.* **54** 875 (2011); *Usp. Fiz. Nauk* **181** 905 (2011)
20. Krause F, Rädler K-H *Phys. Earth Planet. Inter.* **20** 158 (1979)
21. Zel'dovich Ya B, Ruzmaikin A A, Sokoloff D D *Magnetic Fields in Astrophysics* (New York: Gordon and Breach, 1983)
22. Frick P, Stepanov R, Sokoloff D *Phys. Rev. E* **74** 066310 (2006)
23. Ruzmaikin A A, Shukurov A M, Sokoloff D D *Magnetic Fields of Galaxies* (Dordrecht: Kluwer Acad. Publ., 1988); Translated from Russian: *Magnitnye Polya Galaktik* (Moscow: Nauka, 1988)
24. Sokoloff D D, Frick P G *Astron. Rep.* **47** 511 (2003); *Astron. Zh.* **80** 556 (2003)
25. Berger T W et al. *Phys. Fluids* **12** 631 (2000)
26. Lee C, Kim J *Phys. Fluids* **14** 2523 (2002)
27. Lee D, Choi H *J. Fluid Mech.* **439** 367 (2001)
28. Satake S-I, Kunugi T, Smolentsev S *J. Turbulence* **3** 020 (2002)
29. Biskamp D *Magnetohydrodynamic Turbulence* (Cambridge, UK: Cambridge Univ. Press, 2003)
30. Yokoi N et al. *J. Turbulence* **9** 37 (2008)
31. Brandenburg A *Astrophys. J.* **550** 824 (2001)
32. Rogallo R S, Moin P *Annu. Rev. Fluid Mech.* **16** 99 (1984)
33. Reynolds O *Philos. Trans. R. Soc. Lond. A* **186** 123 (1895)
34. Frick P G *Turbulentnost': Modeli i Podkhody*. Kurs Lektsii (Turbulence: Models and Approaches. Lecture Notes) (Perm: PGTU, 1998)
35. Chkhetiany O G, Moiseev S S, Petrosyan A S, Sagdeev R Z *Phys. Scripta* **49** 214 (2004)
36. Esau I "An Introductory Essay" (Uppsala: Uppsala Univ., 2001)
37. Meneveau C, Katz J *Annu. Rev. Fluid Mech.* **32** 1 (2000)
38. Piomelli U *Prog. Aerospace Sci.* **35** 335 (1999)
39. Glazunov A V, Lykossov V N *Russ. J. Numer. Anal. Math. Modelling* **18** 279 (2003)
40. Deardorff J W *J. Fluid Mech.* **41** 453 (1970)
41. Lilly D K, in *IBM Scientific Computing Symp. on Environmental Sciences* (1967) number 320-1951, 195–210
42. Speziale G et al. *Phys. Fluids* **31** 940 (1988)
43. Moin P et al. *Phys. Fluids A* **3** 2746 (1991)
44. El-Hady N M, Zang T A, Piomelli U *Phys. Fluids* **6** 1299 (1994)
45. Zang T A, Dahlburg R B, Dahlburg J P *Phys. Fluids A* **4** 127 (1992)
46. Erlebacher G et al. *J. Fluid. Mech.* **238** 155 (1992)
47. Vreman B "Direct and large-eddy simulation of the compressible turbulent mixing layer", PhD Thesis (Netherlands: Univ. of Twente, 1995)
48. Vreman B, Geurts B, Kuerten H *Appl. Sci. Res.* **54** 191 (1995)
49. Martin P, Piomelli U, Candler G *Theor. Comput. Fluid Dyn.* **13** 361 (2000)
50. Yoshizawa A *Phys. Fluids* **30** 1089 (1987)
51. Agullo O et al. *Phys. Plasmas* **8** 3502 (2001)
52. Müller W-C, Carati D *Comput. Phys. Commun.* **147** 344 (2002)
53. Müller W-C, Carati D *Phys. Plasmas* **9** 824 (2002)
54. Zhou Y, Vahala G *J. Plasma Phys.* **45** 239 (1991)
55. Gomez T et al. *Phys. Fluids* **19** 032304 (2007)
56. Knaepen B, Moin P *Phys. Fluids* **16** 1255 (2004)
57. Chernyshov A A, Karelsky K V, Petrosyan A S *Phys. Plasmas* **13** 032304 (2006)
58. Chernyshov A A, Karelsky K V, Petrosyan A S *Phys. Plasmas* **13** 104501 (2006)
59. Chernyshov A A, Karelsky K V, Petrosyan A S *Russ. J. Numer. Anal. Math. Modelling* **21** 1 (2006)
60. Chernyshov A A, Karelsky K V, Petrosyan A S *Phys. Fluids* **19** 055106 (2007)
61. Chernyshov A A, Karelsky K V, Petrosyan A S *Flow Turbulence Combust.* **80** 21 (2008)
62. Chernyshov A A, Karelsky K V, Petrosyan A S *Phys. Fluids* **20** 085106 (2008)
63. Chernyshov A A, Karelsky K V, Petrosyan A S *Theor. Comput. Fluid Dyn.* **23** 451 (2009)
64. Chernyshov A A, Karelsky K V, Petrosyan A S *Phys. Scripta* **2010** (T142) 014029 (2010)
65. Chernyshov A A, Karelsky K V, Petrosyan A S *Phys. Plasmas* **17** 102307 (2010)
66. Chernyshov A A, Karelsky K V, Petrosyan A S *J. Phys. Conf. Ser.* **318** 072036 (2011)
67. Chernyshov A A, Karelsky K V, Petrosyan A S *Flow Turbulence Combust.* **89** 563 (2012)

68. Chernyshov A A, Karelsky K V, Petrosyan A S, arXiv:1311.1922
69. Balsara D *Astrophys. J. Suppl.* **132** 83 (2001)
70. Kulikovskii A G, Pogorelov N V, Semenov A Yu *Mathematical Aspects of Numerical Solution of Hyperbolic Systems* (Boca Raton: Chapman and Hall/CRC, 2001); Translated from Russian: *Matematicheskie Voprosy Chislennogo Resheniya Giperbolicheskikh Sistem Uravnenii* (Moscow: Fizmatlit, 2001)
71. Ustyugov S D, Andrianov A N, Center for Turbulence Research, Annual Research Briefs, 281 (2002)
72. Gilman P A, Glatzmaier G A *Astrophys. J. Suppl.* **45** 335 (1981)
73. Glatzmaier G A *J. Comput. Phys.* **55** 461 (1984)
74. Lantz S R, Fan Y *Astrophys. J. Suppl.* **121** 247 (1999)
75. Marsch E, in *Physics of the Inner Heliosphere II* (Eds R Schwenn, E Marsch) (Heidelberg: Springer-Verlag, 1991)
76. Goldstein M, Roberts D, Matthaueus W *Annu. Rev. Astron. Astrophys.* **33** 283 (1995)
77. Brandenburg A, Subramanian K *Phys. Rep.* **417** 1 (2005)
78. Cho J, Lazarian A *Mon. Not. R. Astron. Soc.* **345** 325 (2003)
79. Shaikh D, Zank G P *Nonlin. Processes Geophys.* **4** 351 (2007)
80. Picone J M, Dahlburg R B *Phys. Fluids B* **3** 29 (1991)
81. Dahlburg R B, Picone J M *Phys. Fluids B* **1** 2153 (1989)
82. Ghosh S, Matthaeus W H *Phys. Fluids B* **2** 1520 (1990)
83. Ladeinde F, Gaitonde D *Phys. Fluids* **16** 2097 (2004)
84. Orszag S, Tang C-M *J. Fluid Mech.* **90** 129 (1979)
85. Mininni P D, Pouquet A G, Montgomery D C *Phys. Rev. Lett.* **97** 244503 (2006)
86. Landau L D, Lifshitz E M *Electrodynamics of Continuous Media* (Oxford: Pergamon Press, 1984); Translated from Russian: *Elektrodinamika Sploshnykh Sred* (Moscow: Fizmatlit, 2005)
87. Dastgeer S, Zank G P *Astrophys. J.* **604** L125 (2004)
88. Dastgeer S, Zank G P *Nonlin. Processes Geophys.* **12** 139 (2005)
89. Dastgeer S, Zank G P *Astrophys. J.* **602** L29 (2004)
90. Armstrong J W, Rickett B J, Spangler S R *Astrophys. J.* **443** 209 (1995)
91. Spangler S *Space Sci. Rev.* **99** 261 (2001)
92. Zank G P, Matthaeus W H *Phys. Fluids A* **3** 69 (1991)
93. Zank G P, Matthaeus W H *Phys. Fluids A* **5** 257 (1993)
94. Chernyshov A A, Karelsky K V, Petrosyan A S *Astrophys. J.* **686** 1137 (2008)
95. Chernyshov A A, Karelsky K V, Petrosyan A S, in *Advances in Plasma Astrophysics* (IAU Symp., Vol. 274, Eds A Bonanno, E G dal Pino, A G Kosovichev) (Cambridge: Cambridge Univ. Press, 2011) p. 80
96. Chernyshov A A, Karelsky K V, Petrosyan A S *AIP Conf. Proc.* **1242** 197 (2010)
97. Leonard A *Adv. Geophys.* **18** 237 (1974)
98. Sagaut P *Large Eddy Simulation for Incompressible Flows: An Introduction* (Berlin: Springer, 2002)
99. Monin A S, Yaglom A M *Statistical Fluid Mechanics. Mechanics of Turbulence* (Cambridge, Mass.: MIT Press, 1971 – 1975); Translated from Russian: *Statisticheskaya Gidromekhanika. Mekhanika Turbulentnosti* (Moscow: Nauka, 1965 – 1967)
100. Favre A *J. Mecanique* **4** 361 (1965)
101. Sagaut P, Grohens R *Int. J. Numer. Mech. Fluids* **31** 1195 (1999)
102. Haugen N E L, Brandenburg A *Phys. Rev. E* **70** 026405 (2004)
103. Brandenburg A, in *Advances in Nonlinear Dynamos* (The Fluid Mechanics of Astrophysics and Geophysics, Vol. 9, Eds A Ferriz-Mas, M Núñez) (London: CRC Press, 2003) p. 269
104. Theobald M, Fox P, Sofia S *Phys. Plasmas* **1** 3016 (1994)
105. Vreman B, Geurts B, Kuerten H *J. Fluid Mech.* **278** 351 (1994)
106. Smagorinsky J *Mon. Weather Rev.* **91** 99 (1963)
107. Bardina J, Ferziger J H, Reynolds W C, in *AIAA 13th Fluid and Plasma Dynamics Conf., Snowmass, CO, USA, July 14 – 16, 1980*, p. 10
108. Liu S, Meneveau C, Katz J *J. Fluid Mech.* **275** 83 (1994)
109. Zang Y, Street R L, Koseff J R *Phys. Fluids A* **5** 3186 (1993)
110. Germano M et al. *Phys. Fluids A* **3** 1760 (1991)
111. Germano M *J. Fluid Mech.* **238** 325 (1992)
112. Lilly D *Phys. Fluids A* **4** 633 (1992)
113. Eidson T M *J. Fluid Mech.* **158** 245 (1985)
114. Knight D et al., AIAA Paper 98-0535 (1998)
115. Williamson J H *J. Comput. Phys.* **35** 48 (1980)
116. Brandenburg A, Dobler W *Comput. Phys. Commun.* **147** 471 (2002)
117. Müller W-C, Biskamp D *Phys. Rev. Lett.* **84** 475 (2000)
118. Knaepen B, Kassinos S, Carati D *J. Fluid Mech.* **513** 199 (2004)
119. Müller W-C, Grappin R *Phys. Rev. Lett.* **95** 114502 (2005)
120. Anderson J D (Jr.) *Computational Fluid Dynamics: The Basics with Applications* (New York: McGraw-Hill, 1995)
121. Park N, Yoo J, Choi H *J. Comput. Phys.* **198** 580 (2004)
122. Ferziger J, in *Simulation and Modeling of Turbulent Flows* (Eds T Gatski, Y Hussami, J Lumley) (New York: Oxford Univ. Press, 1996) p. 109
123. Kolmogorov A N *Proc. R. Soc. Lond. A* **434** 9 (1991); *Dokl. Akad. Nauk SSSR* **30** 299 (1941)
124. Kolmogorov A N *Dokl. Akad. Nauk SSSR* **31** 19 (1941)
125. Kolmogorov A N *Dokl. Akad. Nauk SSSR* **32** 16 (1941)
126. Obukhov A M *Dokl. Akad. Nauk SSSR* **32** 19 (1941)
127. Low M-M M *Astrophys. Space Sci.* **289** 323 (2004)
128. Porter D H, Pouquet A, Woodward P R *Theor. Comput. Fluid Dyn.* **4** 13 (1992)
129. Low M-M M *Astrophys. J.* **524** 169 (1999)
130. Armstrong J W, Cordes J M, Rickett B J *Nature* **291** 561 (1981)
131. Montgomery D, Brown M R, Matthaeus W H *J. Geophys. Res.* **92** 282 (1987)
132. Lesieur M *Turbulence in Fluids* (Dordrecht: Kluwer Acad. Publ., 1990)
133. Shebalin J V, Matthaeus W H, Montgomery D J *Plasma Phys.* **29** 525 (1983)
134. Kritsuk A G et al. *J. Phys. Conf. Ser.* **180** 012020 (2009)
135. Kitsionas S et al. *Astron. Astrophys.* **508** 541 (2009)
136. Lee H et al. *Astrophys. J.* **594** 627 (2003)
137. Cho J, Lazarian A *Theor. Comput. Fluid Dyn.* **19** 127 (2005)
138. Sridhar S *Astron. Nachrichten* **331** 93 (2010)
139. Lundgren T S, Center for Turbulence Research: Annual Research Briefs (2003) p. 461
140. Rosales C, Meneveau C *Phys. Fluids* **17** 095106 (2005)
141. De Stefano G, Vasilyev O V *J. Fluid Mech.* **646** 453 (2010)
142. Frisch U *Turbulence: The Legacy of A.N. Kolmogorov* (Cambridge: Cambridge Univ. Press, 1995); Translated into Russian: *Turbulentnost'. Nasledie A.N. Kolmogorova* (Moscow: Fazis, 1998)
143. Obukhov A M *Izv. Akad. Nauk SSSR Ser. Geograf. Geofiz.* **5** 4 (1941)
144. Iroshnikov P S *Sov. Astron.* **7** 566 (1964); *Astron. Zh.* **40** 742 (1963)
145. Kraichnan R H *Phys. Fluids* **8** 1385 (1965)
146. Grappin R, Leorat J, Pouquet A *Astron. Astrophys.* **126** 51 (1983)
147. Verma M K, Bhattacharjee J K *Europhys. Lett.* **31** 195 (1995)
148. Müller W, Biskamp D *Lecture Notes Phys.* **614** 3 (2003)
149. Müller W-C, Grappin R *Plasma Phys. Control. Fusion* **45** B91 (2004)
150. Müller W-C, Biskamp D *Phys. Rev. Lett.* **83** 2195 (1999)
151. Perez J C et al. *Phys. Rev. X* **2** 041005 (2012)
152. Carbone V, Pouquet A *Lecture Notes Phys.* **778** 71 (2009)
153. Hatori T *J. Phys. Soc. Jpn.* **53** 2539 (1984)
154. Biskamp D, Müller W *Phys. Plasmas* **7** 4889 (2000)
155. Wisniewski M, Kissmann R, Spanier F *J. Plasma Phys.* **79** 597 (2013)
156. Zybin K P et al. *JETP* **105** 455 (2007); *Zh. Eksp. Teor. Fiz.* **132** 510 (2007)
157. Zybin K P et al. *JETP* **107** 879 (2008); *Zh. Eksp. Teor. Fiz.* **134** 1024 (2008)
158. Dobrowolny M, Mangeney A, Veltri P *Phys. Rev. Lett.* **45** 144 (1980)
159. Elsasser W M *Phys. Rev.* **79** 183 (1950)
160. Marsch E, in *Reviews in Modern Astronomy* (Ed. G Klare) (Berlin: Springer, 1990)
161. Verma M K *Phys. Plasmas* **6** 1455 (1999)
162. Ghosal S et al. *J. Fluid Mech.* **286** 229 (1995)
163. Carati D, Ghosal S, Moin P *Phys. Fluids* **7** 606 (1995)
164. Eswaran V, Pope S B *Comput. Fluids* **16** 257 (1988)
165. Fureby C et al. *Phys. Fluids* **9** 1416 (1997)
166. Alvelius K *Phys. Fluids* **11** 1880 (1999)
167. Kowal G et al. *Astrophys. J.* **700** 63 (2009)
168. Siggia E D, Patterson G S *J. Fluid Mech.* **86** 567 (1978)
169. Chasnov J R *Phys. Fluids* **3** 188 (1991)
170. Sullivan N P, Mahalingam S, Kerr R M *Phys. Fluids* **6** 1612 (1994)
171. Seror C et al. *Phys. Fluids* **13** 476 (2001)
172. She Z S, Jackson E, Orzag S A, in *New Perspectives in Turbulence* (Ed. L Sirovich) (Berlin: Springer-Verlag, 1991)
173. She Z-S et al. *Phys. Rev. Lett.* **70** 3251 (1993)
174. Wang L et al. *J. Fluid Mech.* **309** 113 (1996)
175. Chen S, Shan X *Comput. Phys.* **6** 643 (1992)
176. Mosheni K et al. *Phys. Fluids* **15** 524 (2003)
177. Overholt M R, Pope S B *Comput. Fluids* **27** 11 (1998)
178. Brandenburg A, Petrosyan A *Astron. Nachrichten* **333** 195 (2012)
179. Pope S B *New J. Phys.* **6** 35 (2004)
180. Kraichnan R H *Phys. Fluids* **8** 1385 (1965)
181. Benzi R et al. *Phys. Rev. Lett.* **100** 234503 (2008)
182. Morinishi Y, Vasilyev O V *Phys. Fluids* **13** 3400 (2001)
183. Speziale G *J. Fluid Mech.* **156** 55 (1985)